AD NUMBER

ADB137561

NEW LIMITATION CHANGE

TO

Approved for public release, distribution unlimited

FROM

Distribution authorized to DoD and DoD contractors only; Administrative/Operational Use; Dec 88. Other requests shall be referred to Air Force Engineering Service Center, Attn: YE, Tyndall AFB, FL 32403-6001. This document contains export-controlled

AUTHORITY

STINFO Program Manager, AFRL/MLQP, Tyndall AFB, FL 32403-5323 via DTIC 55, Control No. 912721, dated 06/06/2000.

ESL-TR-88-01
VOLUME II

NORTH FIELD TEST REPORT: MAT INSTRUMENTATION, FINITE-ELEMENT ANALYSIS, AND MAT ANCHORING SYSTEM RELIABILITY STUDY, VOLUME II

DR C.J. COE, D.L. READ, DR J.A. MYERS

THE BDM CORPORATION
7915 JONES BRANCH DRIVE
MCLEAN VA 22102

DECEMBER 1988

FINAL REPORT

JUNE 1987 — NOVEMBER 1988

ENGINEERING AND SERVICES PROGRAM OFFICE
AIR FORCE ENGINEERING & SERVICES CENTER
TYNDALL AIR FORCE BASE, FLORIDA 32403

NOTICE

Please do not request copies of this report from HQ AFESC/RD (Engineering and Services Laboratory). Additional copies may be purchased from:

Defense Technical Information Center
Cameron Station
Alexandria, Virginia 22314

REPORT DOCUMENTATION PAGE

1a. REPORT SECURITY CLASSIFICATION Unclassified	1b. RESTRICTIVE MARKINGS None Admin. or Operational Use
2a. SECURITY CLASSIFICATION AUTHORITY	3. DISTRIBUTION / AVAILABILITY OF REPORT Distribution ~~limited~~ to DOD and DOD contractors only; ~~this report documents test and evaluation.~~ ~~Distribution limitation applied~~ December 1988.
2b. DECLASSIFICATION / DOWNGRADING SCHEDULE	
4. PERFORMING ORGANIZATION REPORT NUMBER(S) BDM/TYN-87-0311-TR	5. MONITORING ORGANIZATION REPORT NUMBER(S) RRR-TR-88-04
6a. NAME OF PERFORMING ORGANIZATION The BDM Corporation 6b. OFFICE SYMBOL (If applicable)	7a. NAME OF MONITORING ORGANIZATION Air Force Engineering and Services Center Engineering and Services Program Office
6c. ADDRESS (City, State, and ZIP Code) The BDM Corporation 7915 Jones Branch Drive McLean, Virginia 22102	7b. ADDRESS (City, State, and ZIP Code) Headquarters Air Force Engineering and Services Center Tyndall Air Force Base, Florida 32403-6001
8a. NAME OF FUNDING / SPONSORING ORGANIZATION Air Force Engineering and Services Center 8b. OFFICE SYMBOL (If applicable) YE	9. PROCUREMENT INSTRUMENT IDENTIFICATION NUMBER F08635-84-C-0185
8c. ADDRESS (City, State, and ZIP Code) Headquarters Air Force Engineering and Services Center Tyndall Air Force Base, Florida 32403-6001	10 SOURCE OF FUNDING NUMBERS PROGRAM ELEMENT NO. / PROJECT NO. / TASK NO. / WORK UNIT ACCESSION NO.

11. TITLE (Include Security Classification)
North Field Test Report - Volume II, Mat Instrumentation, Finite-Element Analysis, and Mat Anchoring System Reliability Study

12. PERSONAL AUTHOR(S)
Coe, Dr. C.J., Read, David L., Myers Dr. J.A.

13a. TYPE OF REPORT	13b. TIME COVERED	14. DATE OF REPORT (Year, Month, Day)	15. PAGE COUNT
Final	FROM 6/24/87 TO 11/30/88	December 30, 1988	128

16. SUPPLEMENTARY NOTATION
Subject to export control laws. Availability of this report is specified on the reverse of the front cover.

17. COSATI CODES			18. SUBJECT TERMS (Continue on reverse if necessary and identify by block number)
FIELD	GROUP	SUB-GROUP	anchor bolts, → bolt loads, → bow waves, → rapid runway repair, instrumentation, → mat strain, → shear stress, trafficking event finite-element analysis strain gages, fiberglass mats.

19. ABSTRACT (Continue on reverse if necessary and identify by block number)

As part of the USAF's program for developing systems and procedures to rapidly repair bomb-damaged runways, the Air Force Engineering and Services Center conducted the North Field '87 Rapid Runway Repair Test. This volume of the North Field '87 Test Report documents the design and installation of an instrumentation system to monitor mat response to F-15 and F-16 aircraft ground operations; data acquisition, processing, and reduction, finite-element modelling of the mat system; a comparison of predicted and actual mat response; and anchoring system reliability study.

20. DISTRIBUTION / AVAILABILITY OF ABSTRACT ☐ UNCLASSIFIED/UNLIMITED ☒ SAME AS RPT. ☐ DTIC USERS	21. ABSTRACT SECURITY CLASSIFICATION Unclassified
22a. NAME OF RESPONSIBLE INDIVIDUAL Mr. Perry E. Dukes	22b. TELEPHONE (Include Area Code) (904) 283-6203 22c. OFFICE SYMBOL YER

DD FORM 1473, 84 MAR 83 APR edition may be used until exhausted. All other editions are obsolete.

3. Distribution/Availability of Report (concluded)

Other requests for this document must be referred to the Air Force Engineering and Services Center (~~AFESC~~/YE), Tyndall Air Force Base, Florida 32403-6001.

PREFACE

This report was prepared by The BDM Corporation, 7915 Jones Branch Drive, McLean, Virginia 22102, under Contract F08635-84-C-0185, for the Air Force Engineering and Services Center, Engineering and Services Program Office, Tyndall Air Force Base, Florida.

This report summarizes work done between July 1987 and November 1988. Mr. Perry E. Dukes (AFESC/YER) was the Project Officer. Distribution ~~limited~~ authority to DOD and DOD contractors only; ~~this report document test and evaluation~~. ~~Distribution limitation applied~~ December 1988. Other requests for this document must be referred to the Air Force Engineering and Services Center (~~AFESC/YER~~), Tyndall Air Force Base, Florida 32403-6001. attn: YE

WARNING: This document contains technical data whose export is restricted by the Arms Export Control Act (Title 22, the U.S.C., Sec 2751 et seq.) or Executive Order 12470. Violations of these export laws are subject to severe criminal penalties.

DESTRUCTION NOTICE: Destroy by any method that will prevent disclosure of contents or reconstruction of the document.

This technical report has been reviewed and is approved for publication.

Perry E. Dukes

PERRY E. DUKES
Rapid Runway Repair
Test Manager

Guy A. Morgan

GUY A. MORGAN, Colonel, USAF
Director, Engineering and Services
Program Office

Accession For	
NTIS GRA&I	☐
DTIC TAB	☑
Unannounced	☐
Justification	
By	
Distribution/	
Availability Codes	
Dist	Avail and/or Special
D-16	

(The reverse of this page is blank.)

TABLE OF CONTENTS

TABLE OF CONTENTS
(Concluded)

LIST OF FIGURES

LIST OF FIGURES
(Concluded)

LIST OF TABLES

(The reverse of this page is blank.)

SECTION I

INTRODUCTION

As part of the U.S. Air Force's continuing program for developing systems and procedures to rapidly repair a runway in a postattack environment, the Air Force Engineering and Services Center (AFESC) conducted the North Field '87 Rapid Runway Repair (RRR) Test. The test was held at North Auxiliary Field, North, South Carolina between 24 August and 4 September 1987.

Part of the overall test involved the Development Test and Evaluation (DT&E) of the Folded Fiberglass Mat (FFGM) Crater Repair System under fighter aircraft (F-15 and F-16) trafficking. This volume discusses the mat instrumentation and finite-element modeling segments of the test. A more detailed discussion of the overall DT&E results is contained in Volume I of this report.

A. OBJECTIVES

The mat instrumentation and analysis phase of the North Field Test had three primary objectives.

1. To design an accurate, survivable mat instrumentation system to monitor the mat's response to F-15 and F-16 ground operations (touch-and-goes and fast and slow taxi runs).

2. The field installation of the instrumentation system and the documentation of anchor bolt loads and mat strains for at least 10 aircraft traffic events.

3. To develop a finite-element model of the mat system that accurately simulates mat response to fighter aircraft ground operations.

B. BACKGROUND

A conservative engineering analysis was performed on the FFGM System to define the limits of the stresses generated in the mat system as a result of aircraft traffic and to identify possible failure modes (Reference 1). Stress conditions were modeled for maximum aircraft loads resulting from braking, subgrade deflections, jet blast uplift, and bow waves. The response of the mat's panels, hinges, and anchor bolts were analyzed for these maximum load cases.

The engineering analysis indicated five possible modes by which the mat system may fail:

1. Mat panel failure by shear stress,

2. Mat panel failure by bearing stress (cargo aircraft only),

3. Hinge failure by axial stress (fighter aircraft only),

4. Anchor bolt pullout (anchor bolt with polymer plug), and

5. Anchor bolt bushing bending stress failure.

The analysis consistently assumed maximum loadings and evaluated the system under worst-case conditions. Actual operational trafficking may result in stresses as high as those used in the analysis. It was recommen that the analysis be used in conjunction with a testing program that subje the mat to actual operational trafficking.

C. SCOPE

This volume of the North Field '87 test report documents the design installation of an instrumentation system to monitor mat response to F-15 F-16 ground operations; data acquisition, processing, and reducti finite-element modeling of the mat system; and a comparison of predicted actual mat response. For the reader's convenience, figures and tables grouped at the back of the text.

SECTION II

MAT INSTRUMENTATION

A. INSTRUMENTATION SYSTEM DESIGN OVERVIEW

1. Requirements

Design requirements for the instrumentation system at North Field were extrapolated from the test objectives, operating environment, and assumed mat system behavior. Design requirements were the following:

a. The instrumentation system must operate in a severe environment (aircraft ground operations).

b. The mat system response (anchor bolt loads and mat strains) should be measured directly.

c. The accuracy and repeatability of instrumentation must be verified by field calibration tests.

d. The transducer system must be designed to monitor essential mat response with a maximum of 50 channels.

e. The instrumentation system would not alter or affect the mat response.

The requirement that the instrumentation system operate in a severe environment posed extensive design problems. Survival of the instrumentation components was considered; in addition, the system could not threaten the aircraft used in the test. The second design requirement of direct monitoring narrowed the consideration of candidate transducers. The field calibration requirements greatly increased the preparation time for the test and required considerable field testing time. The calibration tests provided some measure of the accuracy of the instrumentation system in the field and provided the key link between the observed transducer response in electrical units and the corresponding physical units (i.e., pounds and strain). The maximum channel number corresponded with the capabilities of the instrumentation van used in the test. The limited number of available channels required that the instrumentation system use an efficient layout for the transducers. Finally, the requirement for noninterference between the mat response and the measurement system greatly limited the transducer selection and the instrumentation protection design. The final design represented a balance of all design considerations.

2. Final System Configuration

The mat instrumentation system consisted of three segments: transducers, instrumentation cable, and data acquisition system (processing/recording equipment). Figure 1 shows the instrumentation system. Transducers convert a physical measurement (e.g., strain) to an electrical signal. The

instrumentation cable (a low-resistance, shielded, wire system) carries the electrical signal to the processing/recording equipment. Once received at the instrumentation van, the signal is processed and amplified by the conditioning amplifiers, then recorded in analog format by instrumentation tape recorders.

A detailed discussion of the mat instrumentation system, including system components, data acquisition, checkout and calibration testing, and field installation, is given in Appendix A of this report.

B. TEST EXECUTION

The test execution phase of the effort at North Field consisted of the calibration tests, system checkout, data acquisition setup, and data collection. Data collection involved only data associated with the instrumentation system.

1. Calibration and Checkout Tests

a. Instrumented Anchor Bolts

The calibration tests provided the conversion factor between the measured transducer signal and the corresponding physical load. After the instrumentation system was installed, horizontal and vertical calibration static load tests were conducted. Each bolt was loaded and unloaded (vertically and laterally), in 500-pound increments, to a maximum load of 2,000 pounds. A typical load-vs-signal curve from the field calibration tests is shown in Figure 2.

b. Mat Strain Gages

Static pull tests also were conducted directly on the folded fiberglass mat to test the response of the mat strain gages. Unlike the bolt calibration tests, the mat load tests were used only to check the general response of the mat transducers, since the mat strain is directly related to the mat stress by the Modulus of Elasticity. The test used a setup similar to the instrumented bolt calibration tests, except the lateral load was applied directly to the mat, and the active transducers were the mat strain gages. The 5,000-pound load cell and winch arrangement was joined directly to the mat by the connectors normally used to drag the mat. Each panel was loaded independently, and the strain gages in the loaded and adjacent panels were monitored. The load increment was again 500 pounds, to a maximum load of 2000 pounds. The mat connectors did not allow the load application directly in the horizontal plane of the mat and induced localized applied moment to the mat. Because of this out-of-plane loading, the gages near the connection exhibited a response typical of axial-moment applied load combinations. Gages located several feet from the loaded edge demonstrated linear load response characteristics (applied moment effects are localized). Gages on the opposite end of the loaded panel showed no indication of the applied load, including the 2000-pound maximum load. This response indicates that the force required to overcome the static frictional sliding resistance of the mat in this instance is greater than 2000 pounds. Also, mat gages in adjacent panels

registered strain in the same order of magnitude as the loaded panel, which implies that significant loads are transferred across the hinges.

2. Data Collection

From August 31 to September 3, 1987, the mat was trafficked with both F-15 and F-16 aircraft. Specific aircraft events were not established in advance, but general aircraft operations were followed, as discussed in Volume I. Trafficking operations included takeoffs, taxis, and touch-and-goes. Takeoffs and touch-and-goes were conducted westward. Taxis were bidirectional, with high-speed taxis (up to 80 knots) conducted westward and low-speed taxis (less than 40 knots) conducted eastward. During the final taxi event, a jet blast test was conducted. An F-15 trafficked over the mat, stopped approximately 50 feet West of the mat, and performed an 80-percent rpm engine runup that lasted approximately 8 seconds. At test completion, 108 passes had been conducted over the mat. The passes included 4 takeoffs, 48 taxis, and 56 touch-and-goes.

The minimum time between aircraft trafficking events was approximately 1 minute. Since the primary recording equipment used was analog tape recorders, the recorders were allowed to run continuously during aircraft trafficking. Instrumentation tape recorders required approximately 30 seconds to stabilize after the record cycle was activated. One-half second before each event, a calibration pulse was sent simultaneously to each channel. The calibration pulse is a square wave with a peak amplitude of 1 volt and is used as a reference waveform on each recorded channel. Complete change of the instrumentation setup (amplification range and calibration pulse) required several hours. Because of the extensive time required to alter the instrumentation setup and the importance of recording maximum anchor bolt loads and mat strains, the final instrumentation setup was configured with emphasis on observation of the large-load events (hard braking and airblast).

On the first day of aircraft trafficking, 14 events were monitored (10 nonbraking taxis and four touch-and-goes). All instrumented anchor bolts were operational, and their corresponding signal channels were recorded (28 channels). Nineteen of the original 20 mat gages were operational. The mat gages were not recorded since the instrumentation setup for them had not been completed before the test start. Two channels (in-plane horizontal channels from Bolts 4 and 10) were paralleled to the auxiliary observation van for recording on the digital oscilloscope. At the start of the test, relatively large magnitude noise was noticed on most instrumentation channels. The noise was attributed to improper shield grounding and/or equipment ground loop. Efforts throughout the test series to reduce the noise level were unsuccessful.

On the second day, 14 instrumented bolts and 17 mat strain gages were operational (the mat strain gage instrumentation having become operational by this time). The instrumentation setup was completed, and all 45 channels were recorded. Eighteen nonbraking taxis, six taxis with braking, and two takeoff events were recorded. During one braking event, the F-15 landing gear locked up on the mat, causing the wheel to slide on the mat surface. The in-plane horizontal channel from Bolt 4 and Mat Gage 3 were

monitored with the digital oscilloscope, in addition to the instrumentation tape recorders.

The next test day focused on low approaches and touch-and-go operations. Of the 76 third-day events, twenty-six touch-and-goes, four taxi's, and two takeoff events were conducted. All instrumented bolts and 14 mat gages were operational (42 channels). In-plane and out-of-plane horizontal loads on Bolt 10 were monitored with the digital oscilloscope. Several touch-and-go events included wheel spinup on the instrumented mat. The final test day involved 25 touch-and-goes, nine taxis (one with braking on Mat 1), and one jet blast event, described previously. At the beginning of the test day, 12 mat gages and all instrumented bolts were operational. Again, the digital oscilloscope recorded in-plane and out-of-plane horizontal loads on Bolt 10.

At the conclusion of the test series, 11 of the original 20 mat strain gages and all the instrumented bolt channels were operational. All inoperable gages were located on the east side of the mat. The cause of the mat gage failure was determined to be the instrumentation cable severing at the access hole in the mat. None of the gages failed because of mechanical damage to the gage itself, although several gages were located directly under the landing gears during tire spinup (Figure 3).

C. TEST RESULTS

1. Data Processing

The data processing phase of the study involved data digitization, filtering, curve fitting, waveform scaling, and video data analysis. The data collected included the anchor bolt calibration tests, mat static load tests, digital oscilloscope data, and data recorded by the instrumentation tape recorders. A least-squares fit was conducted on the bolt calibration data resulting in a typical load-signal curve shown in Figure 2. Data from the digital oscilloscope were downloaded to an IBM-AT-compatible computer, converted to standard ASCII format, filtered, and plotted. The low-pass filtering (time-series averaging) was used to attenuate signal noise. The filtering effort was effective, since the noise frequency spectrum was typically higher than the measured response frequency spectrum.

Thirty events were selected for data digitization, processing, and analysis (Table 1). The events were chosen to represent a spectrum of aircraft operations, to include braking taxis, takeoffs, touch-and-goes, and airblast. High-speed film and video were reviewed for each selected event to determine the position of the aircraft on the mat. The events were digitized at a rate of 5 ms/point for taxi and 2 ms/point for touch-and-goes, takeoffs, and airblast events. The digitized events were downloaded in ASCII format to an IBM-AT-compatible computer, filtered, plotted, and scaled.

2. Results Summary

A review of the test data revealed that several tape recorders used in the test did not operate properly. Of the four recorders used, one

recorder did not operate, and two other recorders worked intermittently. In addition, the time reference, IRIG, was recorded on only one tape recorder. The inoperable tape recorder was connected to 13 of the 20 mat strain gages. Also, the mat gages lost during the test were connected with an operational recorder. As a result, limited mat gage response was recorded successfully (two channels - five events). Table 2 represents a qualitative summary of the selected 30 events. The letter "V" stands for vertical anchor bolt load channel, and "H" is the horizontal load response. The number 1 in the table implies that a calibration pulse was present but was not a recognizable transducer signal; "2" and "3" stand for fair and good transducer signals, respectively. Blank entries represent channels on which no recognizable signal or calibration pulse was recorded. As shown, few mat strain gage channels were recorded. Most recorded signals were from the horizontal bolt channels on the east end of the mat.

Typical unfiltered horizontal bolt load response waveforms from Event 187 (F-15 aircraft, east 10- to 20-knot taxi with hard braking) are shown in Figure 4 and Appendix B. The large, square waveform near the zero time-reference mark is the calibration pulse. Since the IRIG signal is not recorded, the calibration pulse also provided a common time-reference point for other channels. Figure 4 shows the horizontal anchor bolt load measured by Bolt 6. The high-frequency signal throughout the waveform is the noise described previously. A low-pass filter (time-series averaging) was used to filter the high-frequency noise, and the resulting filtered waveform is shown in Figure 5. As shown in Figures 4 and 5, the bolt load response began with a sharp rise in the bolt load, a sinusoidal decay, and a residual load. The response is typical of braking events monitored at this test series. The peak horizontal load shown in Figure 4 was approximately 2250 pounds, with a residual load of 770 pounds. The duration of the dynamic load response was 0.1 second.

Table 3 shows the peak horizontal anchor bolt loads for the 30 events. As exhibited, the maximum horizontal anchor load occurs in the central panels or the panels the aircraft traverses (Bolts 3 through 12). The bolts in the outer panels (1, 2, 13, and 14) also exhibit relatively large horizontal loads. This correlates with the static horizontal mat-pull tests which showed that significant horizontal load is transferred across the hinges. In summary, the braking events from the F-15 aircraft indicate that the maximum horizontal load on the center panel bolts ranged from 2200 to 4300 pounds, with a duration of approximately 0.1 second. F-15 takeoffs with afterburner imposed a maximum horizontal bolt load of 3870 pounds (duration = 0.05 second). The maximum horizontal bolt load monitored for a touch-and-go event was approximately 1400 pounds. Finally, the maximum horizontal bolt load measured during the airblast (Event 216-Table 1) was 2650 pounds.

D. SUMMARY

A survivable mat instrumentation system was developed and implemented. Of the 48 original instrumentation channels, 39 were operational at the end of the test, to include all instrumented bolt channels and 11 of the original 20 mat strain gages. None of the mat gage inoperability was caused by mechanical damage to the gage, even though several gages were directly subjected to

aircraft tire spinup (Figure 3). Mat strain gage channel failure was attributed to instrumentation cable breakage at the mat access hole. The field implementation of the anchor bolt calibration tests was successful, and the calibration curves measured at the test site proved the instrumented bolt operability and established the load-signal relationships for the anchor load cell.

Excessive noise hampered data collection during aircraft operations. Horizontal anchor bolt response is documented in approximately 100 events. Maximum measured horizontal anchor bolt loads for various F-15 aircraft ground operations from 30 selected events are:

1.	Taxi with Hard Braking	4300 pounds
2.	Takeoff with Afterburner	3870 pounds
3.	Touch and Go without Afterburner	1400 pounds
4.	Airblast - 80-Percent Engine Runup (1- to 2-second duration)	2650 pounds

Residual loads were observed in the braking taxi events, with maximum measured residual loads approaching 1000 pounds. Maximum bolt loads measured for the F-16 ground operations are significantly less than the corresponding F-15 maximum anchor loads. The measured bolt loads are specific to the North Field Test; the bolt loads should only be extrapolated to other incidents in conjunction with the appropriate analysis (e.g., finite-element modeling).

SECTION III

FINITE-ELEMENT MODELING OF MAT REPAIR SYSTEM

A. ANALYSIS METHODOLOGY

The mat repair analysis consisted of two phases. The first phase was a detailed study of the ground reaction forces generated by F-15 and F-16 aircraft during ground operations. The aircraft dynamic analysis determined landing gear vertical and horizontal reaction forces for nonbraking and braking taxis. The dynamic models (TAXIG series) used were those that evaluate rough runway capabilities of the respective aircraft and were ideally suited for the landing gear reaction-force study.

The second phase is the finite-element modeling of the mat repair system. The goal of the finite-element analysis effort was to develop a mat system analytical model which could be used to evaluate anchor bolt loads and mat strains documented in the test series. The finite-element model included the two 30- by 54-foot mat sections, the hinges, the mat splice panel, and the anchor bolts.

The first analysis effort part involved the finite-element model development and model simulations without reference to the test results. The finite-element model development considered the finite-element code capabilities, computer system limitations, and the mat repair system modeling requirements. The model simulations conducted in this segment were static loads at incremental mat locations along the aircraft wheel tracks. This approach allowed mat system characteristics from the analytical model to be established without bias.

The second segment of the finite-element analysis began with the evaluation of mat system characteristics predicted by the analytical model. These characteristics were compared to mat system behavior documented in the test results. Major differences between the predicted and observed characteristics were resolved, and additional simulations were conducted to test the model refinements. Further field tests were conducted to support assumptions used in the revised finite-element model. In this segment, both static and dynamic simulations were conducted. The dynamic simulations involved dynamic moving loads and proved an early hypothesis that the horizontal response of the mat can be simulated accurately by a moving static load. Unresolved differences between predicted and actual test results are identified and discussed.

B. TAXIG SIMULATIONS

1. TAXIG Model Overview

TAXIG aircraft dynamic models were developed to evaluate aircraft rough runway capabilities. TAXIG F-15 and F-16 are comprehensive aircraft dynamic models simulating all types of aircraft ground operations (taxi, landing, and takeoff). Also, the models included nonlinear dynamic

characteristics (tire and landing gear nonlinear model), rigid and flexible body aircraft structure model, landing gear degree of freedoms, and aerodynamic loads (lift, drag, aerodynamic moment). Aircraft performance simulated by the models was based on the respective aircraft Technical Order (TO) specifications.

2. Analysis Description

F-15 and F-16 TAXIG models were exercised for nonbraking, light-, medium-, and heavy-braking taxis. The models assumed aircraft weights of 42,500 and 24,700 pounds for the F-15 and F-16, respectively. Aircraft servicing parameters (i.e., tire pressure, shock strut servicing, etc.) were assumed to be those specified in the maintenance TOs, and the aircraft were assumed to traverse a smooth surface. Table 4 shows the parameters used in the study. The aircraft weights and center-of-gravity locations were based on those used to evaluate the surface roughness safety limits for the test aircraft used at the North Field '87 Test. Rolling and braking horizontal resistance was expressed in terms of equivalent horizontal coefficients. The rolling resistance coefficient was based on the unbraked aircraft rollout specifications. Likewise, the braking coefficients again were found by matching aircraft braking rollout specifications from the aircraft TOs. Heavy braking was defined as the maximum average braking force that the aircraft can produce given optimum surface conditions. Medium and light braking are arbitrary terms, based on a percentage of the maximum average braking coefficient.

3. Simulation Results

Table 5 shows the results from the F-15 TAXIG simulations, and Table 6 shows the results for the F-16. As illustrated, the nose gear vertical load increased with increasing braking force. Also, the vertical landing gear Braking was done by the main landing gear. The maximum average horizontal braking force generated by the F-15 was approximately 6200 pounds per main landing gear, and 3300 pounds for the F-16.

C. MAT SYSTEM FINITE-ELEMENT MODEL

1. Finite-Element Analysis Overview

Finite-element modeling involves the discreditzation of continuous materials into a finite number of elements whose boundaries are defined by a limited set of nodes. The reduction from a continuous to a discrete system was done by assigning element shape functions which depend only on the functional value of the nodal variable. The shape functions allowed the determination of the functional relationship within the element regime given the nodal values. The approximate solution set was based on substituting the discreditized system into the governing partial differential equations, yielding a set of linear equations which could be readily solved. The accuracy of the approximate solution set was determined by the characteristics of the governing partial differential equations, the complexity of the shape functions used in the formulation, and the number of elements used to define

the continuum. For static problems, the formulation took the form of the following matrix equation:

$$[K](d) = (F) \quad (1)$$

For structural applications, [K] was the stiffness matrix, (d) was the unknown degree-of-freedom (DOF) displacements, and (F) was the applied force vector. The [K] and (F) were formulated using a "weak" (approximate) formulation of the problem. In the exact solution set, the partial differential equation was uniquely satisfied for every location within the problem regime. In the "weak" formulation, the solution requirements were relaxed by allowing the discreditized system to approximate the actual solution state and by using an energy minimization approach which averaged the error across the approximate solution state regime. The result of this approximate formulation is a systematic approach to the digitization process and the general solution of the approximate formulation.

The finite-element analysis for this study was conducted on a Micro VAX II computer system using Automatic Dynamic Incremental Nonlinear Analysis (ADINA), a general-purpose, finite-element analysis computer program. ADINA capabilities include linear and nonlinear material characterization (i.e., isotopic, orthotropic, nonlinear elastic, thermoelastic, etc.), numerous element types (i.e., truss, plane, solid, beam, isobeam, plate, shell, pipe, spring, fluid, etc.), frictional contact surfaces, static and dynamic simulations, and generalized load-input capability. In addition to the main program, the ADINA finite-element package included pre- and postdata processing programs, ADINA-IN and ADINA-PLOT. ADINA-IN minimized the input data requirements and included a node-renumbering scheme for minimizing the band width in the resulting stiffness matrix. ADINA used the data file created by ADINA-IN to formulate mass and stiffness matrices and the force vector. Next, ADINA solved for the unknown variables (matrix reduction for static problems, subspace iteration for mode shapes and natural frequencies, time integration for dynamic simulations, etc.). The output from ADINA was stored in a generic binary file called a portnole file. The final step in the code execution was the transition of the information presented in the porthole file to the desired output, which was done by the post-processor, ADINA-PLOT. Unfortunately, ADINA is not a memory-efficient code. Micro VAX limitations and ADINA memory requirements set the maximum allowable DOF's for two-dimensional linear analysis at approximately 6000.

2. Model Description

The first task in the finite-element study was the model development. The primary interest in this study was the transmission of lateral loads to the anchor bolts. For this analysis, it was assumed that lateral loads imposed on the mat are resisted by two force components. The first component is the lateral frictional resistance of the mat and the subgrade. The second component is the leading and trailing edge anchorage system. The second load-carrying system was modeled in this effort.

The mat was modeled as an isotropic, linear elastic material using plane stress elements. The two-dimensional, four-node, plane-stress elements

modeled in-plane mat response to horizontal loads. Figure 6 shows the finite-element grid developed for this analysis. The grid represents 1152 elements and approximate 2000 nodes. The largest element is 51 by 18 inches, and the smallest is 3 by 7 inches. The hinges were modeled with 3-inch wide elements of varying length. The connection panel was modeled as a uniform mat component by 12- by 18-inch and 3- by 12-inch elements in the center of the mat system. Anchor bolts were represented as fixed boundary conditions at the nodes marked with circles. The grid density was greatest in the area of the anchor bolts to ensure proper material characterization in the anchorage areas.

3. Preliminary Simulations

Preliminary simulations were conducted using the finite-element grid shown in Figure 6 and the assumed material properties shown in Table 7. Assumed material properties were used in this segment because actual material properties, discussed in the next subsection, were not yet available. The goal of this analysis segment was to identify predicted mat system characteristics, independent of test results. The primary relationship to be derived from this analysis was the anchor bolt load distribution as a function of load placement on the mat.

In structural applications, moving loads on structural systems generally are studied using influence functions. An example of an influence diagram is shown in Figure 7. The influence function is found by monitoring the reaction force of the left support for a unit moving load. The influence function shown in Figure 7 indicates that the reaction force at "A" varies linearly as a function of load location. This variation ranges from a maximum value equal to the applied load when the load is over the left support, to a minimum value of zero when the load is over the right support.

For the preliminary finite-element simulations, concentrated horizontal loads equal to 1000 pounds were applied sequentially to specific mat locations. The load application points corresponded to main gear tracks from the F-15 and F-16, assuming the aircraft traversed the mat centerline. Loads were placed at the mat edges, center point, and quarter points along each main gear track. Figure 8 shows the location of the concentrated load for one simulation conducted in this phase. As shown, the 1000-pound load was applied to the west end of the mat along the main gear track of an F-15. Table 8 shows the imposed anchor bolt loads for the load configuration in Figure 8. Table 8 lists the global bolt numbers, instrument bolt numbers (if applicable), and the node numbers from the finite-element grid (See Figure 9). As shown in Table 8, the maximum horizontal anchor bolt load occurred at the bolt closest to the concentrated load (East-13). In contrast, a load located along the same track in the center of the mat (Figure 10) produced the anchor bolt loads shown in Table 9. The anchor bolt loads in this case were more evenly distributed with the maximum horizontal load of 42 pounds (West-14, East-13, and East-14). The anchor bolt load distribution demonstrated that significant in-plane mat loads were transferred from panel to panel across the hinges.

The results from the individual simulations were combined into aircraft-specific influence tables. Table 10 shows the influence table for the F-15 aircraft. The numbers C, 25, 50, 75, and 100 are the location indicators for the F-15 main gear on the mat. Zero represents a main gear location on the east edge of the mat, and 100 represents a location on the west edge. Twenty-five and 75 indicate the quarter points and 50, the center location. For any anchor bolt, reading across a table row is the specific bolt-load influence function. For example, mat bolt number (Mat Bolt) W-1 (top row) shows a near-zero load when the aircraft main gear is at the east leading edge (0 location). The load then increases to a maximum load of approximately 41 pounds per thousand pounds of horizontal main gear load at centerspan (50 location), then decreases to 0 again when the aircraft main gear reaches the west trailing edge (100 location). Bolts closer to the wheel track (e.g., mat bolt W-14) exhibited a sudden increase in load, followed by an exponential decay.

4. Final Simulations

a. Supplemental Field Testing

This phase of the analysis compared the preliminary simulation and test results, supplemental field testing, static and dynamic simulations, and final analytical/test results. The preliminary analysis assumed that the imposed horizontal load on the mat was constant over the entire wheel track. Comparison between the influence functions shown in Table 10 and the measured peak bolt load ratios exhibited in Table 3 shows that the peak bolt loads measured in the field were more uniformly distributed. This finding indicates that, at the North Field Test, the imposed mat lateral loading occurred when the aircraft were in the central section of the mat. This hypothesis suggests that the aircraft lateral loads are transmitted to the mat only when the aircraft is traversing the crushed stone subgrade.

To test this hypothesis, simple static friction tests were conducted at the Small Crater Test Facility (Appendix C). An 8- by 18-inch mat section was tested for static frictional resistance against a crushed stone subgrade and a rough concrete underlying layer. Test results indicate that the static frictional coefficient between the mat and the rough concrete was approximately 0.37. The coefficient between the mat and crushed stone is estimated to be 0.13. The 0.37 frictional coefficient can be compared to the equivalent maximum average braking coefficient of 0.34 for the F-15 aircraft, derived from TAXIG. These tests support the hypothesis that the lateral landing gear load is transmitted directly to the underlying concrete when the aircraft is on the undamaged pavement.

b. Static Simulations

The second static moving load simulation series was conducted, on the assumption that the mat horizontal loads are generated only when the aircraft traverses the crushed stone subgrade. In addition, actual material properties were used in this phase of the finite-element analysis (Table 11) (Reference 7). The average ambient temperature of the mat during the test was assumed to be approximately 100 degrees Fahrenheit. The Modulus of Elasticity

and Poisson's ratio for the mat material were determined by static load tests using specimens instrumented with strain gages. Since strain gages could not be bonded to the hinge material, the Modulus of Elasticity for the hinge material was estimated from the slope of the load-deflection curve. The Poisson's ratio for the hinge material was not determined from the material characterization test series and is assumed to be 0.45. As before, static load influence tables were generated for each aircraft type. Table 12 shows the results from the F-15 simulations. The influence functions demonstrate anchor bolt behavior which more closely replicates the mat system behavior observed at North Field '87.

During field installation of the instrumented mat, the instrumented anchor bolts were installed with little or no tolerance between the bushing and the mat, but the noninstrumented bolt tolerance was greater than 0.25 inch in most cases. Horizontal deformation of the mat under maximum loading are generally small (less than 0.25 inch). Another refinement in the finite-element model was to assume that the mat horizontal loads were carried principally by the instrumented anchor bolts. Using the same procedure as before, Table 13 shows the influence table for the F-15. This version of the finite-element model of the mat system (i.e., anchorage provided by instrumented bolts only) provided the best replication of the observed mat system behavior.

c. Dynamic Simulations

Two dynamic simulations are conducted for this study. The first simulation assumes uniform braking across the mat, horizontal loads are transferred to the mat when the aircraft main gear traverse the crushed stone subgrade, the instrumented anchor bolts principally resist the induced lateral loads, and the horizontal force from the landing gear is transferred directly to the mat. The 20-knot braking taxi simulation was conducted for both the F-15 and F-16 aircraft. Figures 11 and 12 show the dynamic response for Bolts East-10 and East-11 for the F-16 simulation. The dynamic response closely matches the moving static load simulations, indicating that the horizontal natural frequency of the mat is much higher than the dynamic characteristics of the load application for the 20-knot simulation.

The second dynamic simulation is conducted to compare directly to Event 187 documented in the North Field Test. Event 187 was an east, 10-to 20-knot F-15 taxi with braking. Measured bolt load responses are included in Appendix B. The observed bolt responses had peak east-west load amplitudes ranging from 2250 pounds for Instrumented Bolt 6 to 870 pounds for Instrumented Bolt 2. The duration of the dynamic component of the response was approximately 0.2 second. Since the exact aircraft position on the mat, with reference to the measured bolt response, is unknown, the aircraft position is approximated. Also, the short duration of the observed event indicates that hard braking was applied only over a short segment of the mat. Using these extrapolations from the test data, a dynamic simulation was conducted to approximate this event. Figures 13 through 18 show the predicted bolt load response compared to the measured response. As shown, the predicted bolt loads are less than the observed response. One reason for the underprediction is the braking loads used in the analysis are average braking

loads and do not consider dynamic braking loads or dynamic loads induced by the antiskid braking system on the aircraft. Also, the mat-sliding phenomenon is complicated by the bolt anchorage system, which may lead to load amplification.

D. SUMMARY

The finite-element analysis of the mat system focused on the horizontal anchor bolt load response. Static moving load influence functions for the F-15 and F-16 were established. Dynamic analysis of the mat response showed that the in-plane mat stiffness is relatively large, with a corresponding high fundamental natural frequency. This response indicates that the horizontal dynamic loads imposed on the mat, that are not restricted by subgrade frictional forces, will be transmitted directly to the anchor bolts with limited dynamic load magnification. In other words, static moving load simulations closely replicate the peak loads determined from dynamic simulations.

Comparing the finite-element model and the measured mat response leads to the following observations. For aircraft main gear locations toward the mat center, the anchor bolts in the outer panels are subjected to significant horizontal loads. This response indicates that the mat hinges do transmit in-plane forces and should be considered load-carrying components. This response also was demonstrated in the mat static pull tests. Second, the anchor bolts experienced lateral loads only when the aircraft lateral loads are transmitted directly to the underlying layer when the aircraft is on undamaged pavement covered by the mat. This observation was further substantiated b static friction tests involving a mat section on crushed stone, similarly, on rough concrete. Next, the instrumented anchor bolts were installed with a close tolerance, but the remaining noninstrumented anchor bolts were placed with tolerances exceeding 0.25 inch in most cases.

The finite-element analysis showed that, even under large horizontal loads (6000 pounds per main gear) the mat does not deform enough to engage the offset bolts. Finally, the finite-element simulations reasonably correlated with the observed anchor bolt behavior but underpredicted (up to 50 percent) the maximum anchor bolt loads which were documented in the field. Underprediction can be attributed to the use of an average braking force in the analysis and dynamic load amplification which may occur from the restrained skidding of the mat (similar to aircraft landing gear shock strut stiction problem).

SECTION IV

MAT REPAIR ANCHOR SYSTEM RELIABILITY ANALYSIS

A. OVERVIEW

Reliability analysis involves studying systems subjected to events which can cause failures during the life of the system. This analysis is an extension of the finite-element analysis discussed in the previous section, which focused on the deterministic modeling of aircraft-induced loads on the mat repair anchoring system. The reliability analysis includes the results of the finite-element modeling, as well as aircraft operational considerations, random distribution of events, anchor bolt load history, and bolt failure relationships. The purpose of this preliminary analysis is to examine the mat-anchoring system and operating environment, to identify important parameters dominating anchoring system failure, and to provide preliminary results of an idealized anchoring system using assumed operational (environmental) and failure probability distributions.

B. RELIABILITY ANALYSIS METHODOLOGY

1. Reliability Analysis

System reliability is the probability that the system will operate under the defined environment without failure. Reliability is the converse of the probability of failure. To estimate system reliability, the operational environment and failure criteria must be explicitly defined. The general analysis approach is to relate the imposed environment to the resulting system response. The system component failure envelope is then compared to the system response to determine the probability of failure and the system reliability. In mechanical systems, the resulting system response is in the form of an imposed component load or stress. The comparison between the imposed component stress and the component failure envelope usually involves comparing two probability distributions, as shown in Figure 19. The distribution on the left represents the probability density function of a particular component stress, given the imposed environment; the right-side distribution represents the component's failure envelope. The overlay between the two distributions is the interference area and is the region of interest in determining the failure probability and, conversely, the system reliability. If the imposed component stress and failure envelope are described by the distributions shown in Figure 19, then the component reliability is defined as the probability that the failure stress envelope exceeds all possible values of the imposed component stress and is given by (Reference 11):

$$R = \int_{-\infty}^{\infty} f_S(s) \left[\int_{s}^{\infty} f_F(F)\, dF \right] ds \qquad (2)$$

where:

$f_S(s)$ = probability density function for imposed component stress
$f_F(F)$ = failure envelope probability density function

Equation 2 assumes independence between the imposed stress and the failure stress envelope.

2. Mat-Anchoring System Reliability Analysis

a. Approach

The mat-anchoring system reliability analysis follows an approach similar to that discussed previously. The problem is divided into three general segments. The first segment, the definition of the mat operational environment, considers the folded fiberglass mat located at a MOS position subjected to multiple landings from F-15 aircraft. The second segment is the determination of the peak load for each anchor bolt, given the landing event, using relationships derived from the finite-element modeling of the mat system. The final segment is the comparison between the imposed load on the bolt and the bolt failure criteria. The bolt failure criteria include cyclic degradation. Individual bolt reliability is evaluated, and the anchoring system reliability is found by assuming independence of individual bolts. Figure 20 shows the general approach, including the three segments.

The analysis flowchart (Figure 20) illustrates the analysis logic, input information, random draw of specific information, aircraft landing simulation, mat response simulation, anchor bolt reliability, anchor bolt load history, and system reliability. The analysis input information includes the following:

(1) Location of the mat along a MOS length;

(2) Weather conditions (dry, wet, icy);

(3) Distance between the finished edge of the crater and the mat anchor bolt line;

(4) Number of aircraft sorties;

(5) Probability distribution for aircraft landing weight;

(6) Distance from the aircraft centerline to the main landing gear (wheel track);

(7) Probability distribution for aircraft offset from the MOS centerline;

(8) Aircraft touchdown location probability distribution;

(9) Length of wheel spinup zone;

(10) Distance to nose gear touchdown;

(11) Horizontal load coefficients as a function of weather conditions for wheel spinup, rolling resistance, and braking force;

(12) Mean bolt failure load for one cycle;

(13) Mean bolt failure load for infinite load cycles;

(14) Bolt failure variance; and

(15) Minimum bolt load for cyclic bolt load count.

The input information is discussed in more detail in a later subsection. After the input phase, the sortie sequence begins by conducting random draws of the aircraft landing weight, the aircraft offset from the MOS centerline, and the aircraft touchdown location. The next step in the analysis process is the aircraft simulation. The aircraft motion, including the main gear wheel spinup, aerodynamic braking (if any), nose gear touchdown, and main gear braking, are simulated using aircraft performance specifications and time integration of the nonlinear equations of motion. The vertical and horizontal landing gear reaction forces are tracked until the aircraft reaches the mat location. The aircraft horizontal load is then used to determine the anchor bolt loads using load relationships derived from the mat finite-element analysis. The individual anchor bolt loads are compared to the bolt reliability criteria, considering the bolt load history. The individual bolt reliabilities are used to determine the overall anchoring system reliability. Tracking the minimum system reliability, the simulation is repeated for the number of sorties desired.

b. Assumptions

The mat-anchoring system reliability analysis presented here is based on a series of assumptions which simplify the reliability analysis. The assumptions also identify limitations of the approach and results. The following assumptions are used:

(1) Anchoring system failure is defined as the failure of any anchor bolt;

(2) Anchor bolt failures are independent events;

(3) Bolt loading and bolt failure criteria are independent (anchor bolts are rigid supports);

(4) Assumptions used for North Field finite-element simulations are valid;

(5) All anchor bolts actively engaged with the mat (small installation tolerance);

(6) Assumed aircraft operations probability distributions and bolt failure criteria;

(7) Aircraft average braking force is used in reliability study;

(8) Horizontal bolt loads only - no bow wave effects, vertical bolt loads;

(9) The mat is centered on the MOS; and

(10) The aircraft travels parallel to the MOS centerline.

The first assumption is used to quantify the anchoring system failure criteria and is based on the assertion that a failed anchor bolt would become a foreign object damage (FOD) hazard. Also, loosing an anchor bolt at a key location would substantially increase the failure probability of adjacent anchor bolts. Independence Assumptions (2) and (3) greatly simplify the reliability analysis and are justified by the modeling approach which separates the applied bolt loading from the bolt failure criteria. In other words, the anchor bolts are considered rigid restraints for the mat system (deflection of anchor bolts under loading is negligible) and, therefore, do not directly influence how the load is transferred from the aircraft to the mat, then to the anchoring system. This assumption may not be valid for reliability studies of mat anchoring systems in asphalt. Assumption 4 relates to the validity of the North Field finite-element simulations. Another major assumption (Assumption 5) is that anchors are properly installed with little or no tolerance (all anchors are actively engaged with the mat). The transfer of the aircraft-induced loads to the anchoring system depends greatly on the number and location of actively engaged anchors, as shown in the previous section.

c. Problem Formulation

This subsection discusses the implementation of the mat anchoring reliability analysis approach, including aircraft simulation and assumed distributions, anchor bolt load relationships, and bolt failure criteria. An F-15 landing operation, as related to induced horizontal loads on the mat repair system, can be divided into two elements. The first element is termed the initial touchdown and consists of the landing operation, beginning with main gear touchdown, continuing through to nose gear touchdown. As the main landing gear tires contact the runway, the tires undergo spinup, which is characterized by tire sliding. The tire-spinup zone varies, depending on several factors. For this analysis, the tire-spinup zone length is assumed to be 100 feet. The horizontal coefficient for the tire spinup is assumed to be one-half the average braking coefficent for the operating surface. Following the tire spinup zone, wheel brakes are not applied until nose gear touchdown. For operations in wet or icy conditions, the pilot holds the aircraft nose up (two-point attitude aerodynamic braking) until the forward velocity drops to 70 knots. Aerodynamic braking uses aerodynamic drag to decelerate the aircraft. For this study, the length of aerodynamic braking is assumed to be approximately 2500 feet. Without aerodynamic braking, the

touchdown zone is assumed to be approximately 250 feet. The horizontal coefficient during this stage equals the rolling resistance of the main landing gear, which was approximated from aircraft performance specifications as 0.025. The second stage of the landing operation is wheel braking. The average braking coefficient varies, depending on surface conditions. As before, the average braking coefficients are estimated from F-15 performance specifications to be 0.075 for icy, 0.15 for wet, and 0.34 for dry conditions.

The aircraft simulation sequence begins with the random draw of aircraft operational parameters: aircraft touchdown location with respect to the MOS centerline, aircraft touchdown longitudinal location on the MOS, and aircraft landing weight. Both aircraft touchdown location probability density functions are assumed to be normally distributed, as shown in Figures 21 and 22. The aircraft landing weight is assumed to follow a lognormal distribution, as shown in Figure 23. For the F-15 A/B models, the landing weight varies from the empty weight of 30,000 pounds to the maximum gross weight of 56,000 pounds. The aircraft motion is simulated by numerical integration of the nonlinear equations of motion. The simulation model is based on TAXIG/F15 runs discussed previously. The time-integration sequence is repeated until the aircraft location coincides with the mat location. The horizontal landing gear forces at the mat location are then passed to the next stage of the reliability analysis: anchor bolt load determination.

The anchor bolt load determination depends on relationships derived from the finite-element modeling of the mat system. The anchor bolt load relationships used in this analysis are based on a limited number of finite-element simulations and are subject to the same assumptions and approximations used in the finite-element analysis. These relationships should, therefore, be considered preliminary. The general equation for the anchor bolt load relationship is:

$$BL_i = BF*\alpha*\left\{ \frac{.02}{\alpha} + e^{/2\left[\frac{Y_{Bi} - (Y_p - W_T)}{\beta} \right]^2} + e^{-1/2\left[\frac{Y_{Bi} - (Y_p + W_T)}{\beta} \right]^2} \right\} \quad (3)$$

where:

BL_i = peak load on Bolt i

Y_{Bi} = location of Bolt i with respect to MOS width (ft)

Y_p = location of aircraft with respect to MOS width (ft)

BF = peak horizontal force on mat induced by aircraft per landing gear (lb)

W_T = distance between aircraft centerline and main landing gear (ft)

CL = distance between the finished edge of the crater and the anchor bolt line (ft) (0 < CL < 30 feet)

α = amplitude factor (function of CL)

$= 0.93 - 0.0757*CL + 0.00156*CL^2$

β = shape factor (function of CL)

$= 1.5 + 0.24*CL - 0.00356*CL^2$

In general, as the distance between the finished crater and anchor bolt line approaches zero, the load distribution among the individual bolts becomes focused on the few bolts close to the main gear wheel tracks. As the distance between the finished crater and anchor bolt line increases, the load distribution among the individual bolts becomes more uniform. Figure 24 demonstrates this trend for distances between the finished crater and anchor bolt lines of 0 and 15 feet, respectively.

Each bolt load is compared to a minimum bolt load used for the cyclic load count. In other words, if a bolt load is above the specified minimum bolt load, then the number of load cycles is updated. If the bolt load is below the specified minimum bolt load, then the number of load cycles remains the same.

The last segment of the analysis determines the individual bolt and anchoring system reliability by comparing the individual bolt loads and load history to the bolt failure criteria. For this analysis, the anchor bolt reliability function is assumed to be of the form:

$$R_i = e^{-\left(\frac{0.964 \times BL_i}{\mu_i}\right)^{10}} \qquad (4)$$

where:

R_i = reliability of Bolt i

μ_i = mean load to failure - Bolt i (function of load cycles)

The average load to failure for Bolt i is estimated from the following:

$$\mu_i = \mu_{min} + (\mu_{max} - \mu_{min}) * \left(\frac{1}{1 + (\log (cycle_i))}\right)^2 \qquad (5)$$

where:

μ_{max} = mean load to failure (1 cycle)

μ_{min} = mean load to failure (∞ cycle)

$cycle_i$ = number of load cycles - Bolt i

Figure 25 shows the one-cycle and infinite-cycle reliability function for average load to failure of 15,000 and 5,000 pounds, respectively. The corresponding average load-to-failure versus number-of-load-cycle relationship is illustrated in Figure 26. Following the individual bolt reliability calculation, the overall anchoring system reliability is determined from:

$$R_S = \prod_i R_i \qquad (6)$$

Tracking the minimum system reliability, the simulation is repeated for the number of sorties required.

C. PRELIMINARY RESULTS

Using the method described, a preliminary reliability analysis was conducted using assumed input values and probability density functions. The preliminary analysis involved two types of simulations. The first is single-event simulations used in a parametric sensitivity analysis. The second type is multiple-event simulations which predict the anchoring system reliability during aircraft sorties.

1. Single-Event Simulations - Parametric Analysis

The first step in the evaluation of an analysis approach is usually to identify input parameters having the greatest influence on the results. The sensitivity analysis described in this section is not intended to demonstrate the relative importance of each parameter for all possible parametric values and combinations thereof. It is intended to provide qualitative information on the interaction and sensitivity of parameters over a narrow spectrum. The parameter sensitivity analysis in this study involved establishing a base set of fixed input parameters, changing one parameter at a time, and conducting single-event (one aircraft pass) simulations. Changes in the reliability from the base case indicates the relative importance of each parameter.

The parametric investigation included aircraft landing weight, aircraft touchdown location on MOS, aircraft braking coefficient, mat location on MOS, distance from the finished crater to the anchor bolt line, and the bolt failure criteria. Table 14 shows the base simulation variables and parameter variations. With the exception of the aircraft braking coefficient, the parameter sensitivity study is conducted by changing only one variable while keeping the other base parameters constant. The aircraft braking coefficient substantially changes the aircraft velocity at the mat location and, consequently, the induced horizontal load on the mat. To provide a true

measure of the braking coefficient variation, the mat location was adjusted so the aircraft velocity at the mat location was constant for the three braking coefficient simulations, as denoted by the mat location values in parenthesis.

Table 15 shows the results from the sensitivity analysis. As illustrated, the parameters having the greatest influence on the anchoring system reliability are the aircraft landing weight, the failure criteria for the anchor bolts, the aircraft braking coefficient, and the distance between the finished edge of the crater and the anchor bolt line. The parameter with little to no influence for single-event simulations is the aircraft location with respect to the MOS centerline.

Another single-event simulation series focused on the influence of weather on the anchoring system reliability. The results of the simulation series showed that "hard" braking on dry pavement, with little to no clearance between the crater edge and the anchor bolt line, is the worst-case scenerio.

2. Multiple-Event Simulations

The next step in the preliminary reliability analysis is multiple-event simulations. In this series, the simulations involve 100 landing events. Random draws determine the aircraft landing weight and MOS touchdown location for each landing event. Next, the aircraft-induced horizontal force on the mat and the resulting loads on the anchoring system are estimated. Comparing the load on each anchor bolt and the bolt load history (number of load cycles) to the failure criteria determines the individual bolt reliability for each event. Assuming independence, the individual bolt reliabilities are used to determine the overall anchoring system reliability. The minimum system reliability represents the minimum system reliability observed for any landing event in the simulated sortie series.

Table 16 shows the results from the simulation series relating the variation of minimum anchoring system reliability with respect to the mat location on the MOS. Three runs are made for each mat location because of the variability of the random-draw process. The three runs are averaged to provide an estimate of the average minimum anchoring system reliability at the specified mat location. As shown, the minimum anchoring system reliability for 100 landing events varies substantially, depending on the mat location on the MOS. The reliability ranges from one in or near the touchdown zone to 0.768 at the end of the wheel-braking zone. Table 17 shows the increase in the anchoring system minimum reliability caused by an increase in the distance between the finished edge of the crater and the bolt line. Table 18 shows the substantial reduction in the minimum reliability of the anchoring system caused by reductions in the bolt failure criteria.

These preliminary simulations suggest that several different types of anchoring system reliability should be considered. The first is the average system reliability, which can be defined as the mean system reliability with respect to aircraft landing events, the mat location on the MOS, and any other combination of parameters. The second type, which is presented in this section, is the minimum system reliability concept. In

realistic terms, evaluation criteria should be established for both types of system reliability, with the mean system reliability criteria set at a higher value than the minimum system reliability. The mean system reliability would take into account the probability distributions of the mat location on the MOS, distributions for the distance between the crater edge and anchor bolt line, variations in aircraft braking, and weather conditions. Determining the mean system reliability would require thousands of simulations similar to those presented. The minimum system reliability would focus on worst-case situations involving the mat location on the MOS, distance between the crater edge and anchor bolt line, aircraft braking, and weather conditions. The minimum system reliability would be determined in a similar manner, as demonstrated in this preliminary analysis.

3. Summary

This section has presented a reliability methodology overview and preliminary analysis of the anchoring system reliability. Determining the mean system reliability requires minor alterations to the methodology presented and thousands of simulation runs. Important parameters in evaluating the system reliability include the aircraft landing weight, the number of sorties, aircraft braking characteristics, mat location on the MOS, the distance between the finished edge of the crater and the anchor bolt line, and the anchor bolt failure criteria. Hard braking on dry pavement with little or no clearance between the crater edge and the anchor bolt line is the worst-case scenerio. Given the anchor bolt failure criteria, the anchoring system reliability can be approximated using the methodology presented. Conversely, the minimum anchor bolt performance criteria can be defined to provide a specified mean and minimum anchoring system reliability.

SECTION V

CONCLUSIONS AND RECOMMENDATIONS

A. CONCLUSIONS

This study has produced the following observations:

1. Maximum measured horizontal anchor bolt loads for various F-15 aircraft ground operations from 30 selected events are:

a. Taxi with Hard Braking	4300 pounds
b. Takeoff with Afterburner	3870 pounds
c. Touch and Go without Afterburner	1400 pounds
d. Airblast - 80-Percent Engine Runup (1- to 2-second duration)	2650 pounds

(Loads are specific to North Field only and should not be extrapolated to other situations.)

2. F-16 induced loads are significantly less than those shown for the F-15.

3. Residual bolt loads occur in aircraft braking events with a maximum measured residual load of approximately 1000 pounds.

4. Static moving load simulations closely replicated the response from dynamic simulations because of the large in-plane mat stiffness and corresponding high natural frequency.

5. Mat hinges transmit in-plane forces and should be considered load-carrying components.

6. Anchor bolts experienced lateral loads only when the aircraft traversed the crushed-stone subgrade.

7. The instrumented anchor bolts with close installation tolerance carried all the induced horizontal loads. The remaining standard anchor bolts, with relatively large installation tolerances, did not actively resist the imposed loads.

8. The finite-element simulations correlated well with the observed anchor bolt response but underpredicted the maximum anchor bolt loads.

9. Two system reliability requirements should be determined: mean and minimum system reliability.

10. Important parameter governing mat anchoring system reliability are number of aircraft operations, aircraft landing weight, aircraft braking

characteristics, mat location on MOS, distance between finished edge of the crater and anchor bolt line, and the anchor bolt failure criteria.

B. RECOMMENDATIONS

Based on the study,results the following recommendations are presented:

1. Consider mat installation restrictions, such as the following, to maximize mat system reliability:

   a. A specified minimum distance from finished crater to anchor bolt line, and

   b. Avoid mat placement in specified narrow zones on the MOS,

2. Continue analytical model development (finite-element analysis) and validation testing to verify mat system behavior characteristics identified in this study and other scenarios not included in this effort (e.g., mat repairs on asphalt).

3. Conduct the second phase of the reliability analysis using actual input parameters and probability distributions.

4. Consider mat system improvements, such as analytical modeling, reliability analysis, and test data indicate.

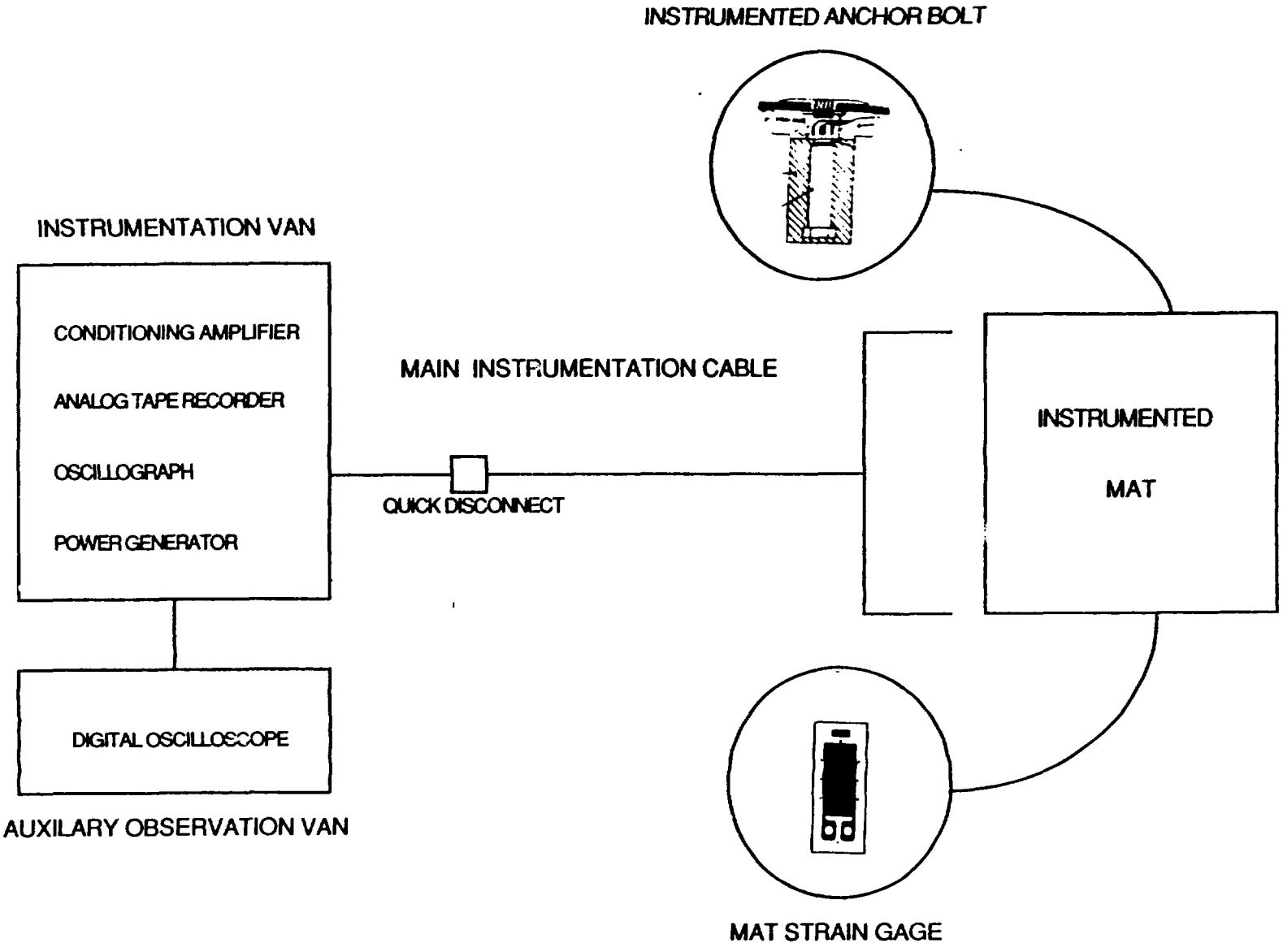

Figure 1. Mat Instrumentation System Configuration

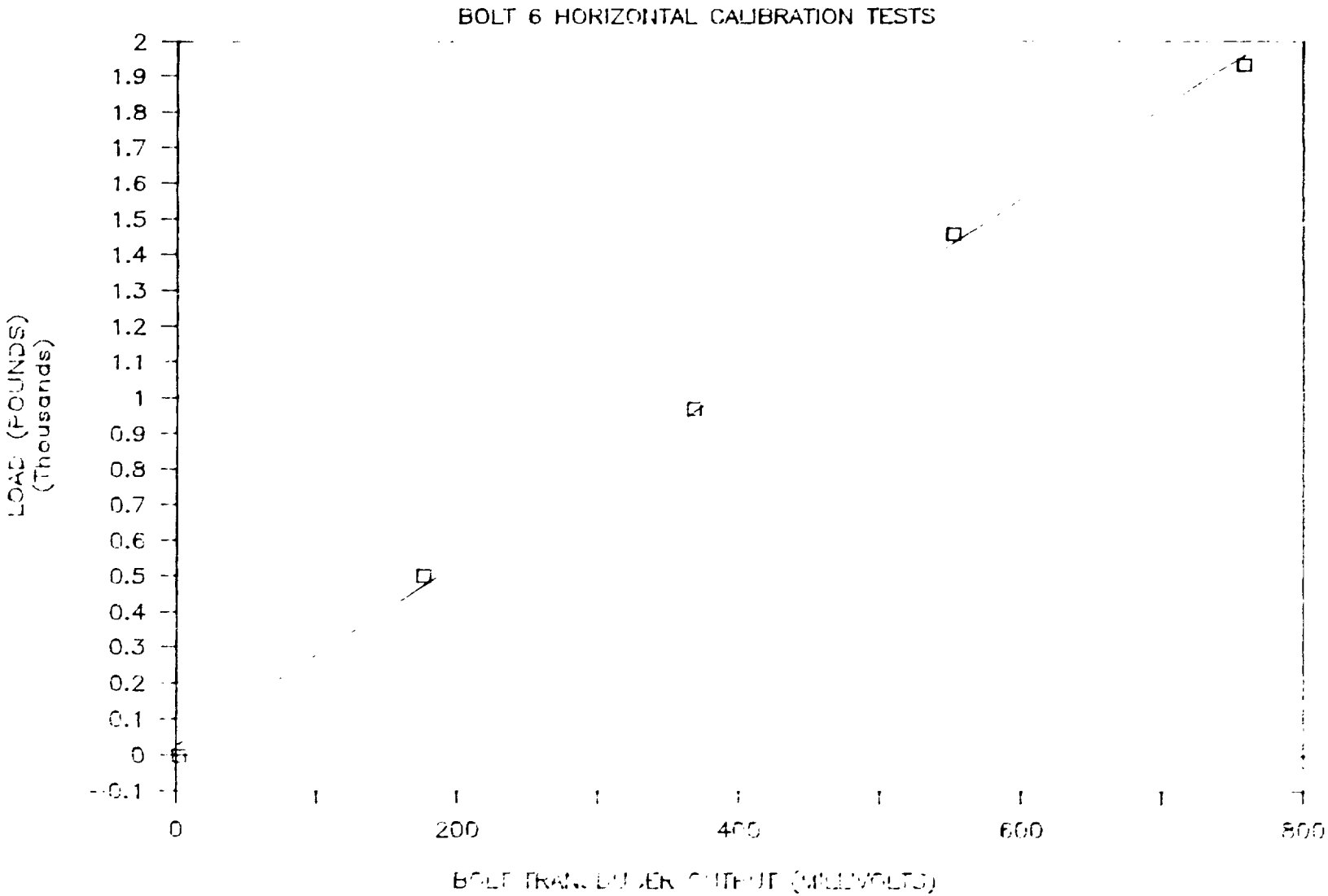

Figure 2. Typical Load-Signal Curve

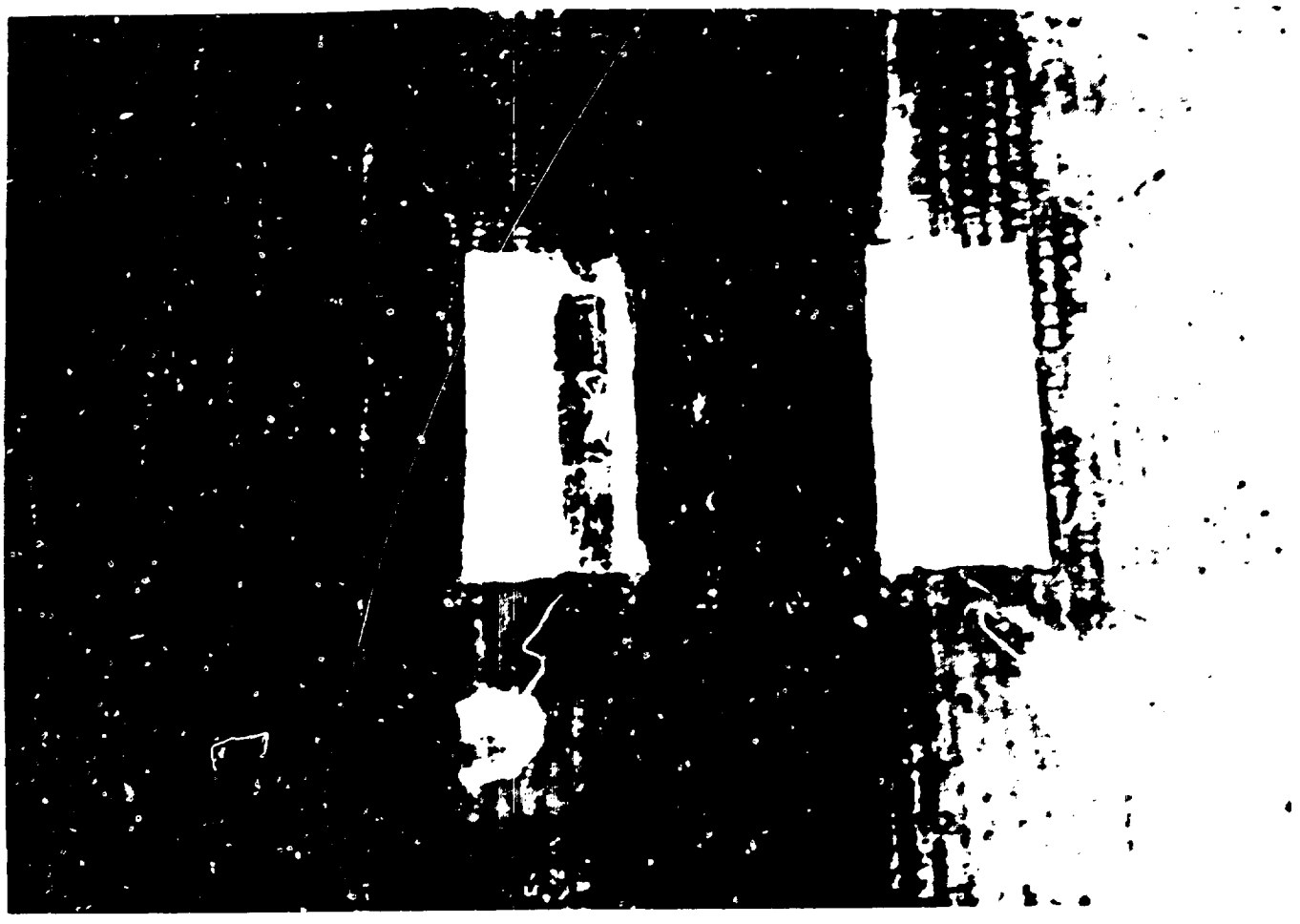

Figure 3. Mat Strain Gage Directly Under Aircraft Tire Print

TABLE 1. DATA EVENTS SELECTED FOR ANALYSIS

EVENT NUMBER	DATE	TIME	DESCRIPTION*
52	9-1	1049	West Taxi, F-15, light braking, nose gear on Panel 5, right main gear on Panel 4, left main gear appears to be on Hinge 5-6
53	9-1	1051	West Taxi, F-16, light braking, nose gear on Panel 5, right main gear on Panel Panel 4 or Hinge 4-5, left main gear on Panel 6
56	9-1	1059	West Taxi, F-15, light braking
57	9-1	1100	West Taxi, F-16, light braking
72	9-1	1420	Takeoff, F-15
73	9-1	1422	Takeoff, F-16
86	9-2	1004	T&G, F-15, right main gear on Panel 3, left main gear appears to be on Panel 4 or Hing 4-5
87	9-2	1005	T&G, F-16, right main gear on Panel 7, left main gear on Panel 8
91	9-2	1011	T&G, F-16, right main gear on Panel 6
93	9-2	1013	T&G, F-16, right main gear on Panel 5, left main appears to be on Panel 6
97	9-2	1020	T&G, F-15, right main gear on Hinge 3-4 or left center of Panel 4, left main gear on Panel 5
102	9-2	1026	T&G, F-16, right main gear on Panel 5, left main gear on Panel 6.
104	9-2	1028	T&G, F-15, right main gear near center of Panel 4, left main gear near center of Panel 5.
108	9-2	1119	Takeoff, F-16, nose gear on Panel 5, right main gear appears to be on Panel 5 or on Hinge 5-4, left main gear appears to be on Panel 6.
110	9-2	1124	Takeoff, F-15, right main gear appears to be just on Panel 4 or on Hinge 4-5, left main gear appears to be on Panel 6.

* Panels are counted from the left to right, facing the west direction

TABLE 1. DATA EVENTS SELECTED FOR ANALYSIS (CONCLUDED)

EVENT NUMBER	DATE	TIME	DESCRIPTION*
125	9-2	1144	T&G, F-16, right main gear on Panel 5, left main gear on panel 6.
153	9-3	1152	T&G, F-15, wheel spin up, right main gear on Panel 4, left main gear on Panel 5.
154	9-3	1154	T&G, F-15, wheel spin up, right main gear appears to be on Panel 4.
156	9-3	1202	T&G, F-15, wheel spin up, right main gear appears to be near to center of Panel 4.
159	9-3	1206	T&G, F-15, right main gear on Panel 4, left main gear on Panel 5.
163	9-3	1212	T&G, F-15, wheel spin up, right main gear appears to be on Panel 4.
171	9-3	1222	T&G, F-15, right main gear appears to be just on Panel 3 or on Hinge 3-4.
176	9-3	1228	T&G, F-16, right main gear appears to be on Panel 4.
181	9-3	1233	T&G, F-15, wheel spin up, right main gear is near Hinge 4-5.
183	9-3	1237	T&G, F-16, right main gear appears to be on Hinge 4-5, left main gear is on Panel 6.
186	9-3	1243	T&G, F-16, right main gear appears to be on Panel 5, left main gear appears to be on Panel 6.
187	9-3	1250	East Taxi, F-15, braking, nose gear on Panel 5, right main gear appears to be on Panel 6, left main gear is on Panel 4.
189	9-3	1252	East Taxi, F-15, possible braking, nose gear on Panel 5, left main gear appears to be on Panel 4, right main gear is on Panel 6.
190	9-3	1254	East Taxi, F-16, nose gear on Panel 5, left main gear appears to be on
216	9-3	1543	East Taxi, F-16, engine run up

TABLE 2. QUALITATIVE WAVEFORM MATRIX OF SELECTED EVENTS

	Bolts																						Mat Gauges																					
	1		2		3		4		5		6		7		8		9		10		11		12		13		14		1	2	3	4	5	6	7	8	9	10	11	12	13	14	15	16	17	18	19	20
Event	V	H	V	H	V	H	V	H	V	H	V	H	V	H	V	H	V	H	V	H	V	H	V	H	V	H	V	H																				
52	1	2	2	2	2	2	1	3	3	3		2							3				2		1	3		2																		1		
53	1	2	1	1	2	1	1	2	3	1		2							1		1						2	1																	1		
56	2	3	2	3	3	2	3	3	1	2													1		2	3		2																			
57	1	1	1	1	2	3	1		1	3									1							1																					
72	2	1	2	1	2	1	2			1		1															1																				
73	1	1	1	2	1	2	1	1	1	1		1							1						1	2		1,2																		1		
86	1	1	1			1						1		1			2	1			2			2	1		1																				
87	1	1	1			1						2	1	1				1			1			1	1		1																				
91	1	1	1		1	1	2					1		1	2		2	1						2	1		1																				
93	1	1	1		1	1	3					1		1	1		1	1						1	1																						
97	1	1	1		2	1	1					1		1	2		1	1						2	1																					1	
102	2	1	2		1	1	1					1		1	1			1						1	2																						
104	1	1	1		2	1	2							1	1			1						2	1																						
108	1	1	1		2	1	1					1		1	1			1						1	1																						
110		3			3	3	1					3		3	2			1																												
125		1			1	1						1		1				1																												
153	1	1	1	1		1		1		1	1												1		1		1																		1		
154	1	1	1	1		1	1	1	1	1	1	1					1						1		1		1																		1		
156	1	1	1	1			1	2	1	1	1						2						1		1		1																2		1		
159	1	1	1	1			1	1	2	1	1	1			1	2							1		1		1																2		1		
163	1	1	1	1			1	1	1	1	1	1			1	1							1		1		1																2		1		
171	1	1	1	1			1	1	1	1	1	1			1	1							2		2		2																1		1		
176	1	1	1	1			1	1		1	1	1			1	1							1		1		1																		1		
181	1	1	1	1			1	2	2	1	1	1			1	1							1		1		1																2		1		
183	1	1	1	1			1	1	2	1	1	1			1	1							1		1		1																2		1		
186		1		1			1	1	1	1		1			1	1																															
187	1	3	1	3			2	3	2	3	2	3			3	3							3		2		1																2		2		
189	1	1	1	2			1	2	1	3	1	3	2		1	2							3		2		1																1		1		
190	1	1	1	1			1	1	2	1	1	1			1	1							3		1		1																1		1		
216	1	2	1	3			2	3		3	1	3	2			2							3		1		1																2		2		

1 = no load signal evident

2 = fair load signal

3 = good load signal

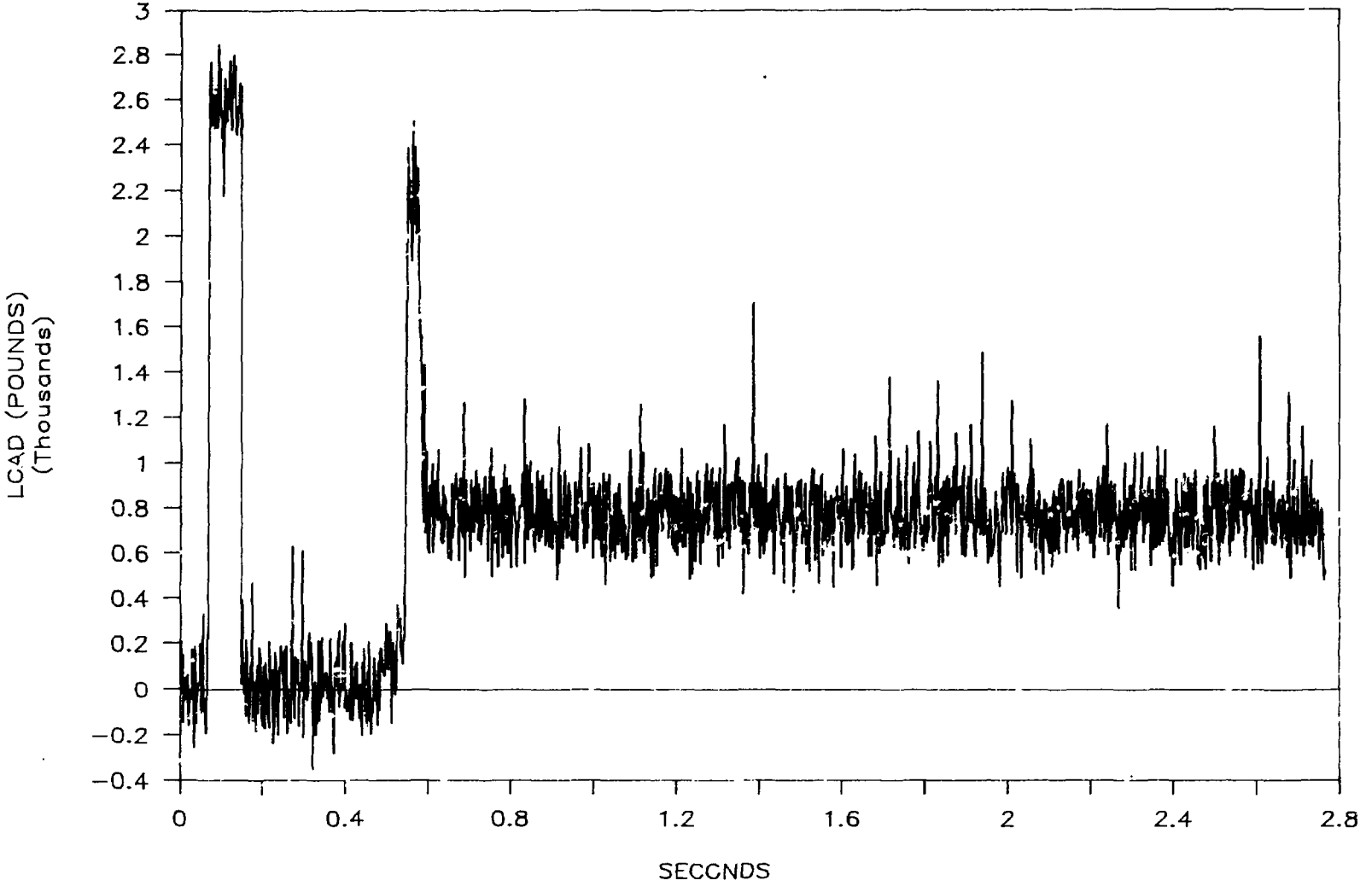

Figure 4. Bolt 6, In-Plane Horizontal Anchor Bolt Load, Event 187, F-15 East Taxi (Hard Braking)

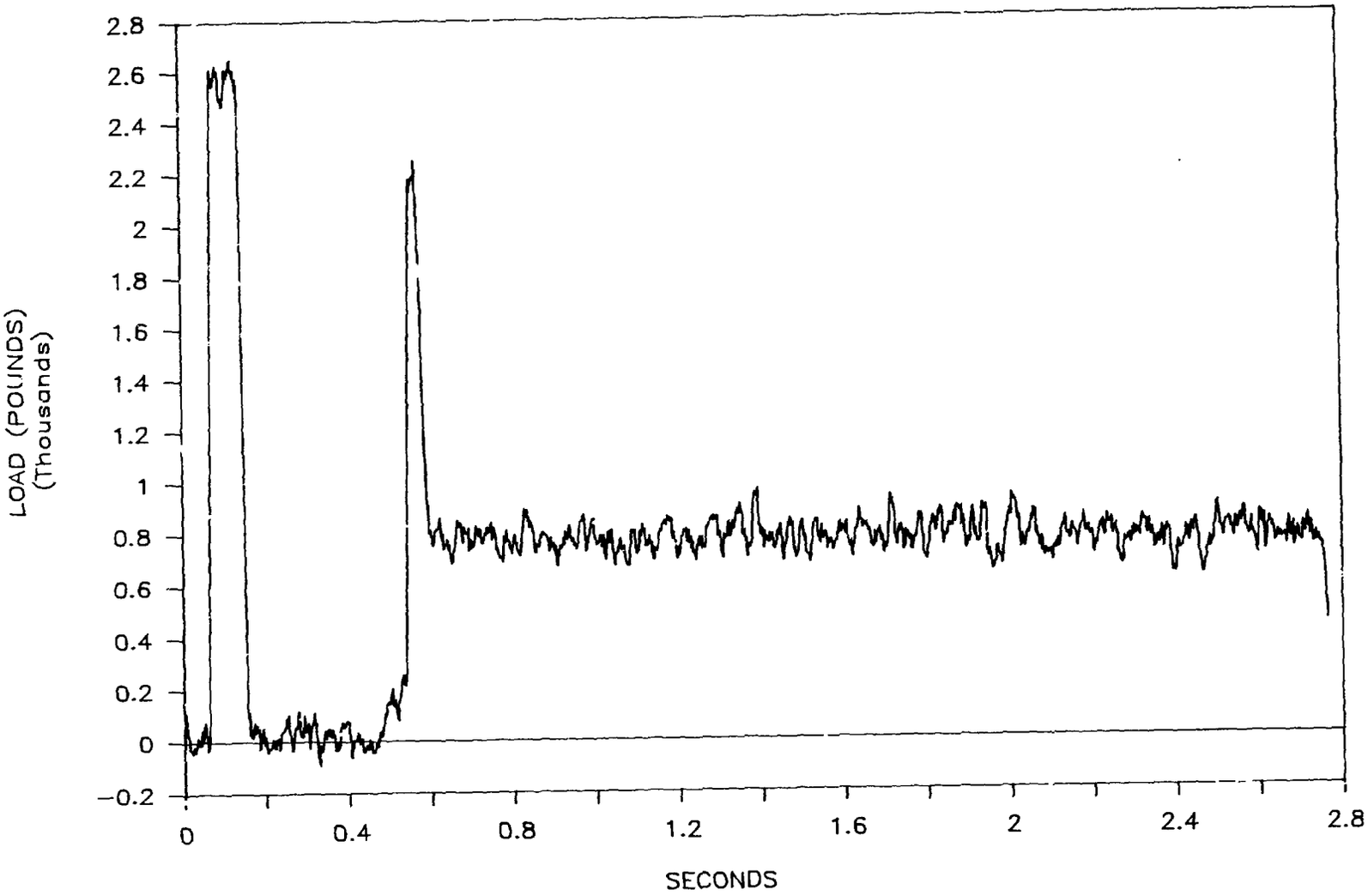

Figure 5. Bolt 6, Filtered In-Plane Horizontal Anchor Bolt Load, Event 187, F-15 East Taxi (Hard Braking)

TABLE 3. MAXIMUM HORIZONTAL ANCHOR BOLT LOADS (POUNDS) FOR 30 SELECTED EVENTS

EVENT	1	2	3	4	5	6	7	8	9	10	11	12	13	14
52	1697*	2303*	2134*	2455*	4274*	2973*								2209*
			1049	441	1299	2876								1042
53	351			3280*		734								
55	736	879	2311*	2215*									968	
57			540		957									
72														
73	317*	315	528*										477	
86										(110)		290		
87						2452								
91												187*		
93														
97												172*		
102														
104												392		
108														
110	547	564*				3875*	1297			(267)				

* = High degree of uncertainty in these values due to excessive noise

( ) = Loads Recorded by oscillioscope; other loads recorded by recorders in the instrumentation van.

TABLE 3. MAXIMUM HORIZONTAL ANCHOR BOLT LOADS (POUNDS) FOR 30 SELECTED EVENTS (CONCLUDED)

EVENT	1	2	3	4	5	6	7	8	9	10	11	12	13	14
125														
153										(1336)				
154										(958)				
156				141						(566)				
159														
163										(205)				
171														
176										(319)				
181				609						(227)				
183														
186														
187	969	867		1814	2190	2254		1409		(367)				
189		164		109*	716	2692				(170)				
190														
216	324*	328		761	1529	2646								

* = High degree of uncertainty in these values due to excessive noise

( ) = Loads Recorded by oscillioscope; other loads recorded by recorders in the instrumentation van.

TABLE 4. AIRCRAFT CONFIGURATIONS

	F-15	F-16
Gross Weight	42,500	24,700
Center of Gravity Location - Percent Mean Aerodynamic Channel	26.65	33.6
Rolling Resistance Coefficient	0.025	0.012
Braking Coefficient		
Light	0.15	0.10
Medium	0.25	0.20
Heavy	0.34	0.30

TABLE 5. F-15 VERTICAL AND HORIZONTAL LANDING GEAR REACTION FORCES

	Nose Gear								Main Gear							
	Vertical Reaction (lb)				Horizontal Reaction (lb)				Vertical Reaction (lb)				Horizontal Reaction (lb)			
Braking	None	Light	Med	Heavy	None	Light	Med	Heavy	None	Light	Med	Heavy	None	Light	Med	Heavy
Speed (knots)																
20	4740	6890	8210	9300	119	172	205	233	18810	18070	17420	16880	470	3160	4790	6160
40	4720	6820	8120	9210	118	171	203	230	18810	17560	17260	16740	470	3070	4750	6110
60	4680	6700	7970	9050	117	168	199	226	18010	17520	16980	16510	450	3070	4670	6030
80	4620	6530	7770	8810	116	163	194	220	17630	17050	16600	16190	441	2980	4560	5910
100	4530	6320	7500	8520	113	158	188	213	16770	16440	16100	15770	419	2880	4430	5760

TABLE 6. F-16 VERTICAL AND HORIZONTAL LANDING GEAR REACTION FORCES

	Nose Gear								Main Gear							
	Vertical Reaction (lb)				Horizontal Reaction (lb)				Vertical Reaction (lb)				Horizontal Reaction (lb)			
Braking	None	Light	Med	Heavy	None	Light	Med	Heavy	None	Light	Med	Heavy	None	Light	Med	Heavy
Speed (knots)																
20	3250	3310	3370	3430	39	40	40	41	10630	10600	10570	10540	128	1190	2240	3290
40	3180	6510	8800	10560	38	78	106	127	10370	8790	7670	6810	125	990	1630	2130
60	3060	6320	8560	10290	37	76	103	123	9940	8500	7440	6620	119	980	1580	2060
80	2880	6050	8230	9900	35	73	99	119	9290	8080	7110	6340	111	910	1510	1980
100	2640	5700	7790	9380	32	68	94	113	8420	7540	6680	5980	101	840	1420	1870

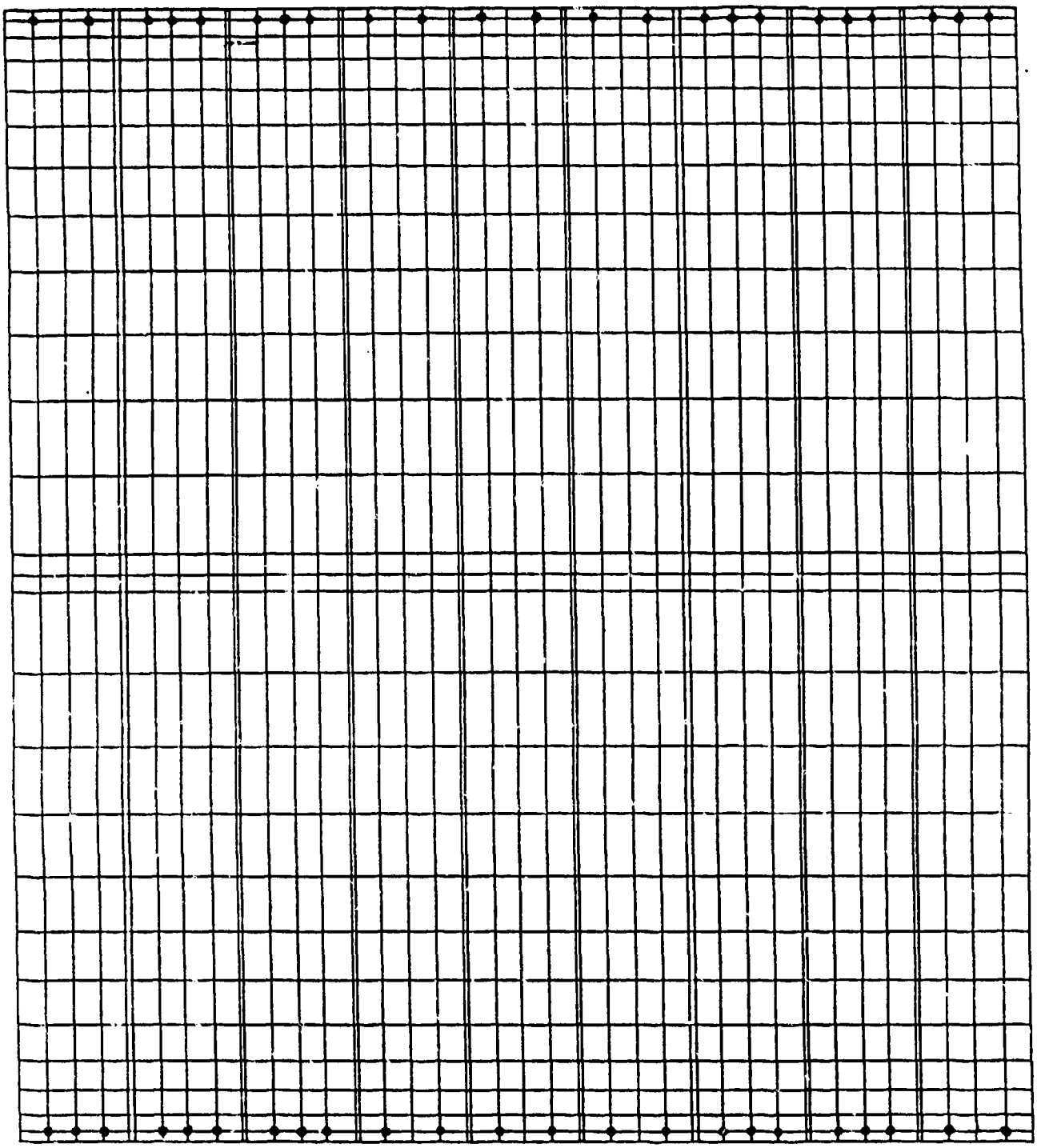

● = Anchor Bolt Location -
Fixed Boundary Condition

Figure 6. Mat Model Finite-Element Grid

TABLE 7. ASSUMED MAT AND HINGE MATERIAL PROPERTIES FINITE-ELEMENT ANALYSIS, SEGMENT 1

	Modulus of Elasticity (psi)	Poisson's Ratio
Mat	3,000,000	0.30
Hinge	300,000	0.45

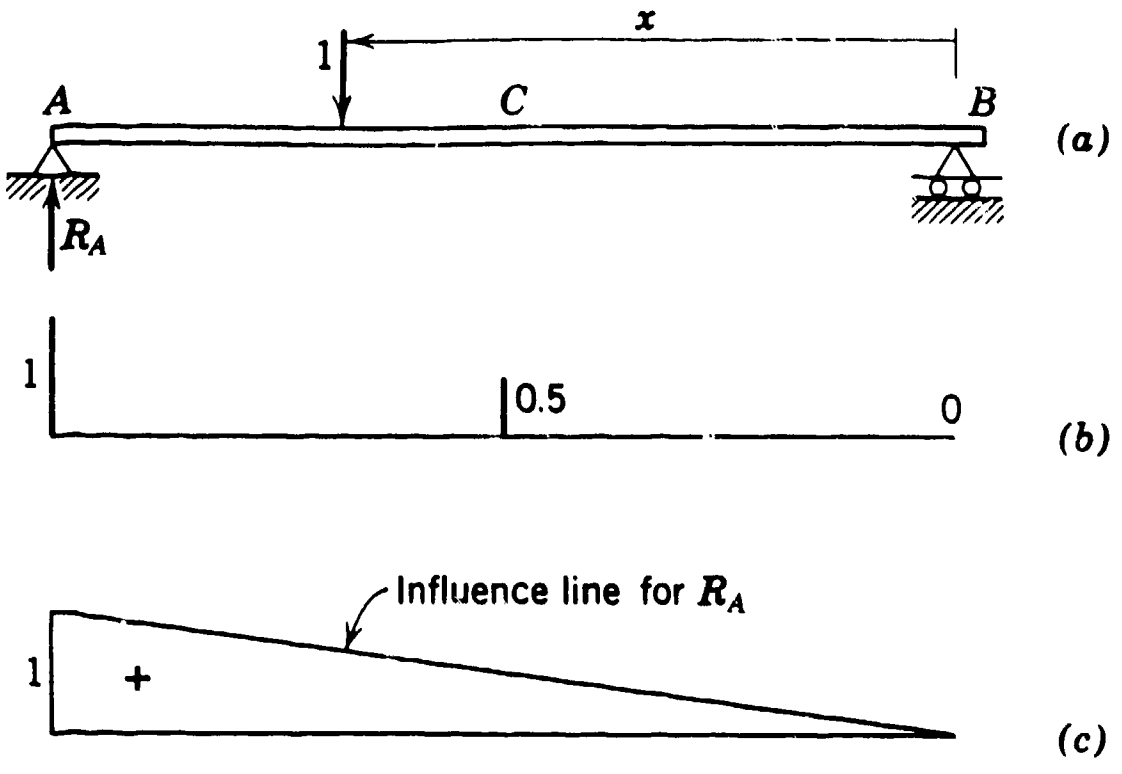

Figure 7. Influence Function Example

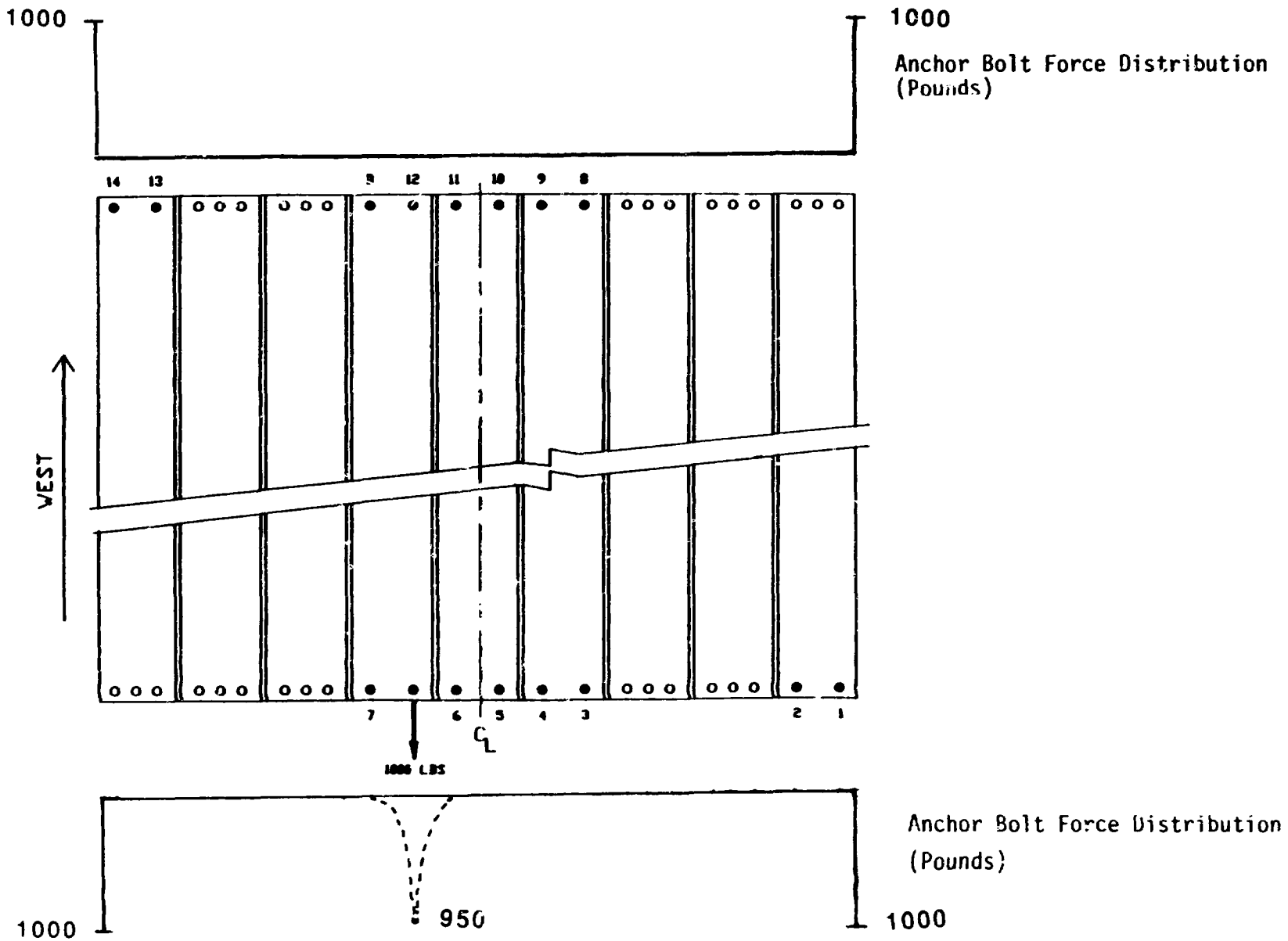

Figure 8. Concentrated Load Location, West Edge, F-15 Track

TABLE 8. PREDICTED ANCHOR 'L' LOADS FROM CONCENTRATED 1000-POUND LOAD AT WEST EDGE OF MAT - F-15 TRACK (REFER TO FIGURE 9)

MAT BOLT NUMBER	INST BOLT NUMBER	FE NODE NUMBER	HORIZONTAL BOLT LOAD
W- 1		1139	-0.07978
W- 2		1150	-0.04682
W- 3		1161	-0.05375
W- 4		1012	-0.07700
W- 5		1023	-0.05896
W- 6		1034	-0.07634
W- 7		885	-0.10547
W- 8		896	-0.08494
W- 9		907	-0.11526
W-10	8	758	-0.18397
W-11	9	780	-0.20278
W-12	10	631	-0.2289
W-13	11	653	-0.25339
W-14	12	504	-0.25661
W-15	B-2	526	-0.28589
W-16		377	-0.20279
W-17		388	-0.17514
W-18		399	-0.24579
W-19		250	-0.21051
W-20		261	-0.18938
W-21		272	-0.28446
W-22	13	111	0.35186
W-23	14	133	-0.51945
E- 1	1	1183	-0.22748
E- 2	2	1205	-0.11501
E- 3		1056	-0.16250
E- 4		1067	-0.10977
E- 5		1078	-0.13044
E- 6		929	-0.22777
E- 7		940	-0.33013
E- 8		951	-0.89681
E- 9	3	802	-1.35803
E-10	4	824	-4.08056
E-11	5	675	-12.4139
E-12	6	697	-950.031
E-13	B-1	548	-15.8037
E-14	7	570	-4.71913
E-15		421	-1.68939
E-16		432	-1.07316
E-17		443	-0.93196
E-18		294	-0.44684
E-19		305	-0.29018
E-20		316	-0.41146
E-21		167	-0.14139
E-22		178	0.164197
E - 2 3			

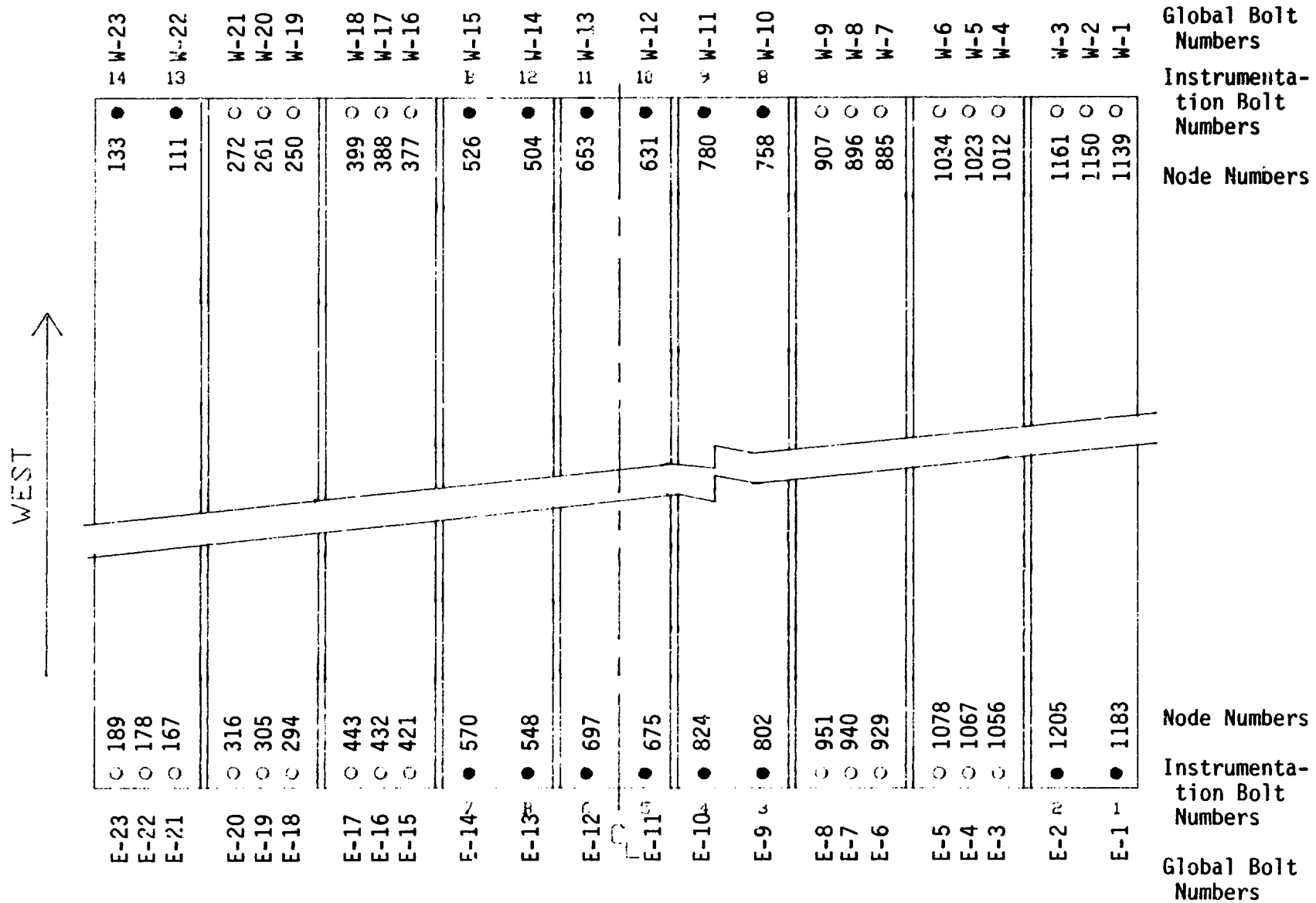

Figure 9. Global, Instrumentation, and Node Bolt Numbers

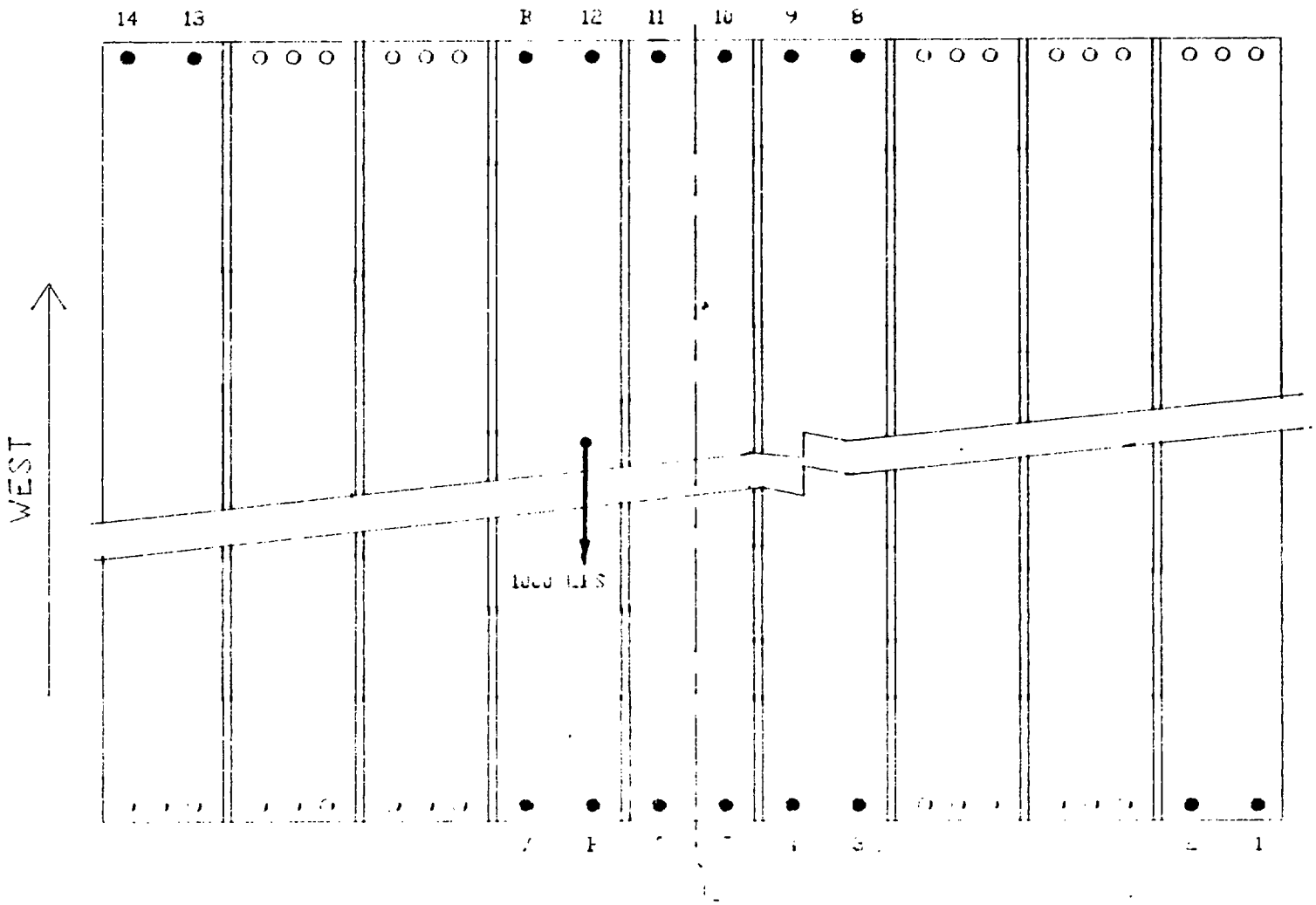

Figure 10. Concentrated Load Location, Mat Center, F-15 Track

TABLE 9. PREDICTED ANCHOR BOLT LOADS FROM CONCENTRATED 1000-POUND LOAD AT MAT CENTER - F-15 TRACK (REFER TO FIGURE 10)

MAT BOLT NUMBER	INST BOLT NUMBER	FE NODE NUMBER	HORIZONTAL BOLT LOAD
E- 1		1139	-13.7183
E- 2		1150	-6.0674
E- 3		1161	-5.00188
E- 4		1012	-10.312
E- 5		1023	-6.72392
E- 6		1034	-7.36601
E- 7		885	-15.258
E- 8		896	-11.1566
E- 9		907	-13.8821
E-10	8	758	-29.11
E-11	9	780	-29.2914
E-12	10	631	-38.9734
E-13	11	653	-39.5711
E-14	12	504	-42.0908
E-15	16	526	-42.205
E-16		377	-27.248
E-17		388	-21.4625
E-18		399	-28.1877
E-19		250	-18.8211
E-20		261	-15.8786
E-21		272	-22.7297
E-22	13	111	-20.7194
E-23	14	133	-33.882
W- 1	1	1183	-16.35
W- 2	2	1205	-7.65546
W- 3		1056	-10.6121
W- 4		1067	-6.8284
W- 5		1078	-7.4239
W- 6		929	-15.3276
W- 7		940	-11.1788
W- 8		951	-13.8771
W- 9	3	802	-29.1516
W-10	4	824	-29.2785
W-11	5	675	-39.0076
W-12	6	697	-39.5509
W-13	15	548	-42.1153
W-14	7	570	-42.1653
W-15		421	-27.2463
W-16		432	-21.4218
W-17		443	-28.0754
W-18		294	-18.6725
W-19		305	-15.6539
W-20		316	-22.1087
W-21		167	-14.5068
W-22		178	-14.4544
W-23		189	-27.6808

TABLE 10. F-15 INFLUENCE TABLE - ASSUMED MATERIAL PROPERTIES - ANCHORAGE BY ALL BOLTS

MAT BOLT NUMBER	INST BOLT NUMBER	FACTOR	HORIZONTAL ANCHOR BOLT LOAD (POUNDS) 0	25	50	75	100
W- 1		1	0.025816	25.54864	41.3978	24.15881	0.495351
W- 2		1	0.228127	12.36054	20.5228	13.06181	0.285804
W- 3		1	0.487957	12.84858	19.50838	13.16417	0.303477
W- 4		1	0.447974	28.94264	32.4203	17.29358	0.351535
W- 5		1	0.554616	21.79464	22.37832	11.85092	0.244522
W- 6		1	1.060555	28.94628	26.03771	13.5723	0.283915
W- 7		1	1.357438	59.7079	43.3328	19.10401	0.349309
W- 8		1	1.915396	48.7447	32.579	14.08784	0.257217
W- 9		1	5.045229	69.1608	41.1276	17.39991	0.317567
W-10	8	1	16.68432	147.7011	71.2737	27.7209	0.469008
W-11	9	1	951.4317	154.0458	71.4053	27.2696	0.459309
W-12	10	1	16.47882	162.8829	78.5232	29.2709	0.481793
W-13	11	1	16.47926	162.9193	78.5776	29.3039	0.482403
W-14	12	1	951.4308	154.0191	71.3686	27.249	0.459027
W-15	16	1	16.68508	147.754	71.3558	27.7719	0.470066
W-16		1	5.045371	69.1515	41.1247	17.40236	0.317818
W-17		1	1.916005	48.7818	32.6418	14.12866	0.258158
W-18		1	1.359041	59.8236	43.5152	19.21787	0.351726
W-19		1	1.06326	29.05855	26.2447	13.71143	0.287153
W-20		1	0.557818	21.99809	22.70733	12.05843	0.249049
W-21		1	0.455829	29.53853	33.3418	17.86005	0.363606
W-22	13	1	0.582508	18.25699	28.37503	18.77366	0.425771
W-23	14	1	0.130531	30.74797	50.2313	29.84722	0.620067
E- 1	1	1	0.619577	29.84718	50.2332	30.75071	0.130662
E- 2	2	1	0.425424	18.77308	28.37476	18.25731	0.582976
E- 3		1	0.363309	17.85947	33.342	29.53911	0.456217
E- 4		1	0.248833	12.05743	22.7063	21.99724	0.558234
E- 5		1	0.286923	13.71128	26.2457	29.05992	1.064094
E- 6		1	0.351437	19.21723	43.5159	59.8236	1.36014
E- 7		1	0.257932	14.12742	32.6406	48.7789	1.91733
E- 8		1	0.317557	17.40193	41.126	69.1518	5.049259
E- 9	3	1	0.46968	27.7712	71.3581	147.7516	16.70061
E-10	4	1	0.458647	27.2481	71.3706	154.0154	951.3880

TABLE 10. F-15 INFLUENCE TABLE - ASSUMED MATERIAL PROPERTIES - ANCHORAGE BY ALL BOLTS (CONCLUDED)

MAT BOLT NUMBER	INST BOLT NUMBER	FACTOR	HORIZONTAL ANCHOR BOLT LOAD (POUNDS) 0	25	50	75	100
E-11	5	1	0.482003	29.3029	78.5799	162.9166	16.49446
E-12	6	1	0.481393	29.2699	78.5254	162.8803	16.49392
E-13	15	1	0.458929	27.2688	71.4074	154.0431	951.3889
E-14	7	1	0.468623	27.7201	71.2761	147.6988	16.69985
E-15		1	0.317307	17.39937	41.1288	69.1611	5.049116
E-16		1	0.256991	14.08662	32.5779	48.7419	1.916731
E-17		1	0.349024	19.10348	43.3336	59.7079	1.358538
E-18		1	0.283689	13.57222	26.03883	28.94776	1.061389
E-19		1	0.244310	11.85001	22.37753	21.79401	0.555031
E-20		1	0.351252	17.29326	32.4208	28.94335	0.448358
E-21		1	0.303236	13.164	19.50874	12.84931	0.488340
E-22		1	0.285552	13.06054	20.52129	12.35999	0.228305
E-23		1	0.494964	24.15902	41.3998	25.55122	0.025865

TABLE 11. ACTUAL MAT AND HINGE MATERIAL PROPERTIES FINITE-ELEMENT ANALYSIS, SEGMENT 2

	Modulus of Elasticity (psi)	Poisson's Ratio
Polyester Mat	2,010,000	0.374
Re Pneu Hinge	92,000	0.45*

* Poisson's Ratio for the hinge was not measured in the material test series. Poisson's ratio shown is assumed.

TABLE 12. F-15 INFLUENCE TABLE - ANCHORAGE BY ALL BOLTS

GLOBAL BOLT NUMBER	INST BOLT NUMBER	FE NODE NUMBER	FACTOR	HORIZONTAL ANCHOR BOLT LOAD (POUNDS) 25	50	75
W- 1		1139	1	24.32968	40.4637	23.93517
W- 2		1150	1	10.61521	18.45392	12.14177
W- 3		1161	1	9.47198	15.38819	11.27907
W- 4		1012	1	28.38762	32.3709	17.20351
W- 5		1023	1	20.09586	21.10195	11.24345
W- 6		1034	1	25.31901	23.21188	12.26534
W- 7		885	1	60.7365	44.9161	19.61573
W- 8		896	1	47.82269	32.665	14.03596
W- 9		907	1	66.7715	40.3014	16.96419
W-10	8	758	1	156.7996	75.2369	28.914
W-11	9	780	1	159.3501	73.8683	27.9067
W-12	10	631	1	164.9188	82.6147	30.4982
W-13	11	653	1	164.9566	82.6714	30.5324
W-14	12	504	1	159.3164	73.823	27.882
W-15	B-2	526	1	156.8469	75.3133	28.9628
W-16		377	1	66.7502	40.2831	16.95942
W-17		388	1	47.84883	32.7137	14.06989
W-18		399	1	60.8342	45.075	19.71784
W-19		250	1	25.3941	23.27049	12.38048
W-20		261	1	20.2565	21.37533	11.42292
W-21		272	1	28.88162	33.1621	17.70502
W-22	13	111	1	14.08051	23.33865	16.49409
W-23	14	133	1	28.8434	48.4718	29.25636
E- 1	1	1183	1	29.25641	48.4738	28.8462
E- 2	2	1205	1	16.49354	23.33822	14.08053
E- 3		1056	1	17.70457	33.1624	28.88246
E- 4		1067	1	11.42197	21.37432	20.25586
E- 5		1078	1	12.38034	23.2713	25.39525
E- 6		929	1	19.71732	45.0759	60.8347
E- 7		940	1	14.06864	32.7124	47.84594
E- 8		951	1	16.95899	40.2842	66.7505
E- 9	3	802	1	28.9619	75.3157	156.8446
E-10	4	824	1	27.8811	73.825	159.3127
E-11	5	675	1	30.5314	82.6737	164.9542
E-12	6	697	1	30.4972	82.6171	164.9164

TABLE 12. F-15 INFLUENCE TABLE - ANCHORAGE BY ALL BOLTS (CONCLUDED)

GLOBAL BOLT NUMBER	INST BOLT NUMBER	FE NODE NUMBER	FACTOR	HORIZONTAL ANCHOR BOLT LOAD (POUNDS) 25	50	75
E-13	B-1	548	1	27.9058	73.8705	159.3463
E-14	7	570	1	28.9132	75.2393	156.7964
E-15		421	1	16.96376	40.3026	66.7718
E-16		432	1	14.03473	32.6639	47.81991
E-17		443	1	19.61512	44.9171	60.7369
E-18		294	1	12.26526	23.11268	25.32017
E-19		305	1	11.24258	21.10108	20.09524
E-20		316	1	17.20321	32.37153	28.38859
E-21		167	1	11.27891	15.38837	9.47237
E-22		178	1	12.1406	18.45257	10.61474
E-23		189	1	23.93548	40.4657	24.33234

TABLE 13. F-15 INFLUENCE TABLE - ANCHORAGE BY INSTRUMENTED BOLTS ONLY

MAT BOLT NUMBER	INST BOLT NUMBER	FE NODE NUMBER	FACTOR	25	50	75
W-10	3	758	1	273.3862	183.7977	96.8094
W-11	9	780	1	204.029	120.6632	60.7843
W-12	10	631	1	202.9195	123.8546	60.1765
W-13	11	653	1	193.9913	114.0877	53.8889
W-14	12	504	1	200.4521	122.1305	61.2472
W-15	16	526	1	246.9085	154.284	77.7304
W-22	13	111	1	76.1615	94.6084	65.4666
W-23	14	133	1	63.1219	86.5606	56.9308
E- 1	1	1183	1	56.9294	86.5607	63.123
E- 2	2	1205	1	65.4673	94.6121	76.1666
E- 9	3	802	1	77.7311	154.2909	246.9096
E-10	4	824	1	61.245	122.1312	206.447
E-11	5	675	1	53.8875	114.0896	193.9883
E-12	6	697	1	60.1752	123.857	202.9167
E-13	15	548	1	60.7821	120.6639	204.0239
E-14	7	570	1	96.8114	183.8076	273.39

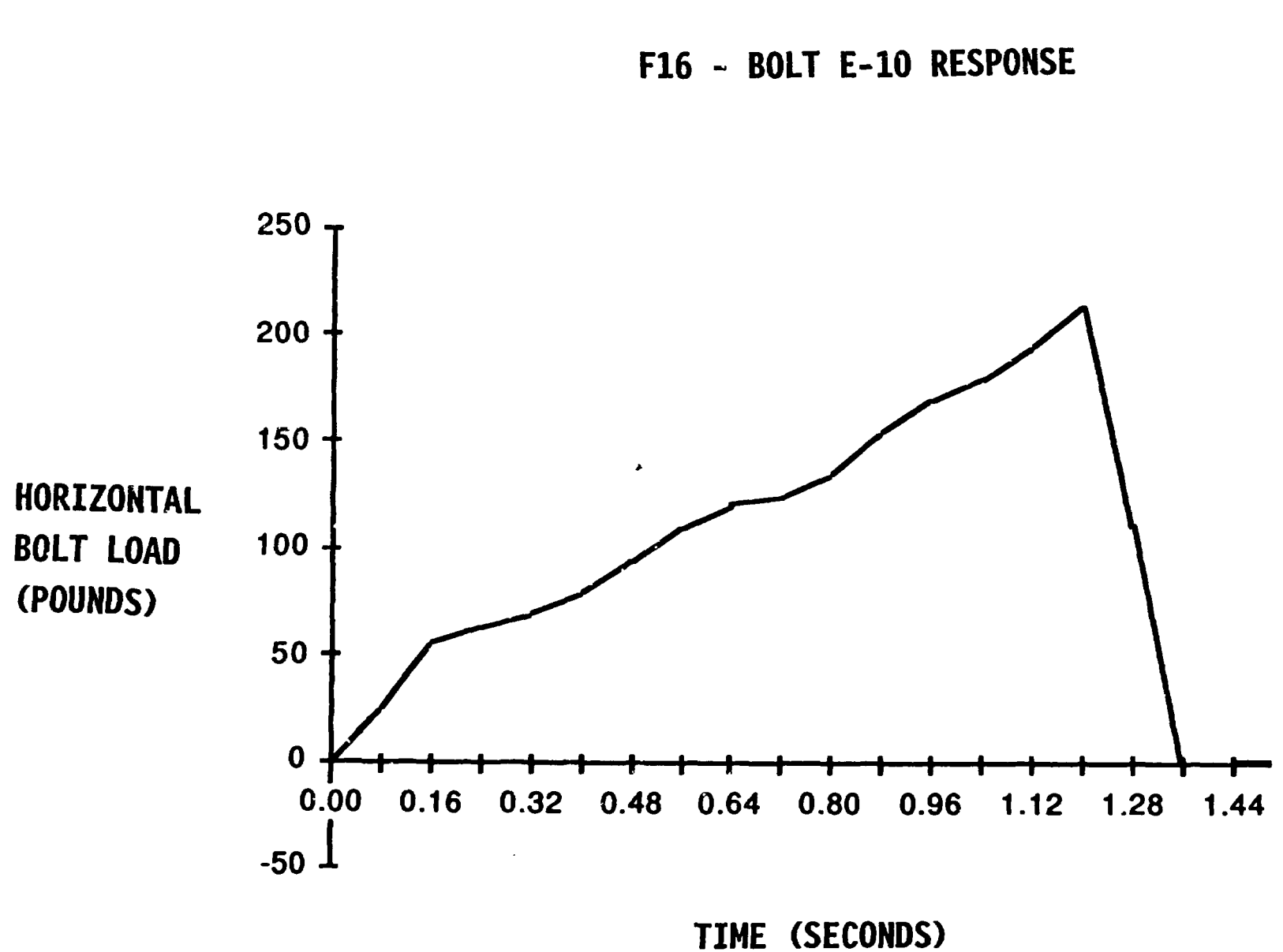

Figure 11. Dynamic Response of Bolt East-10, F-16 Loading

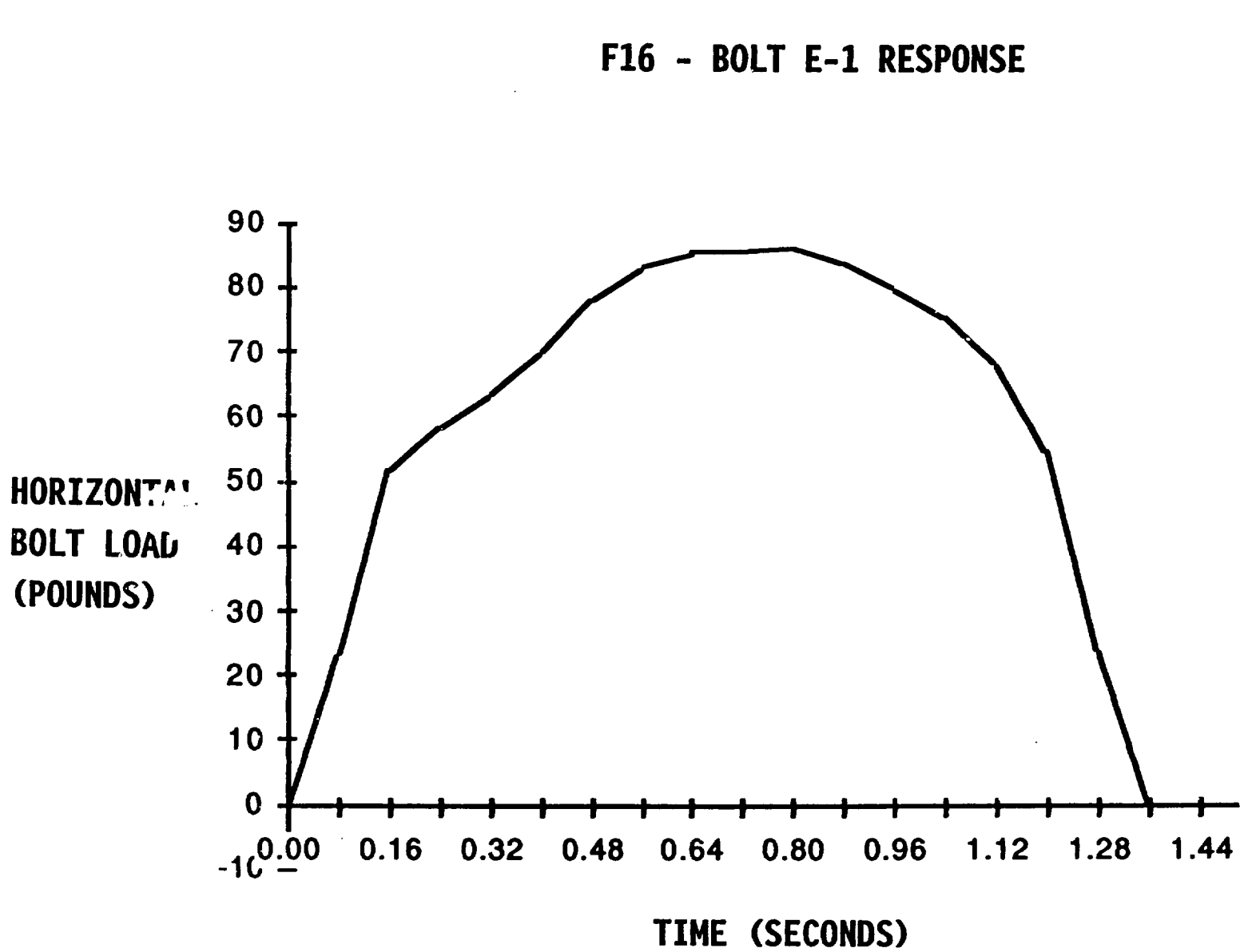

Figure 12. Dynamic Response of Bolt East-1, F-16 Loading

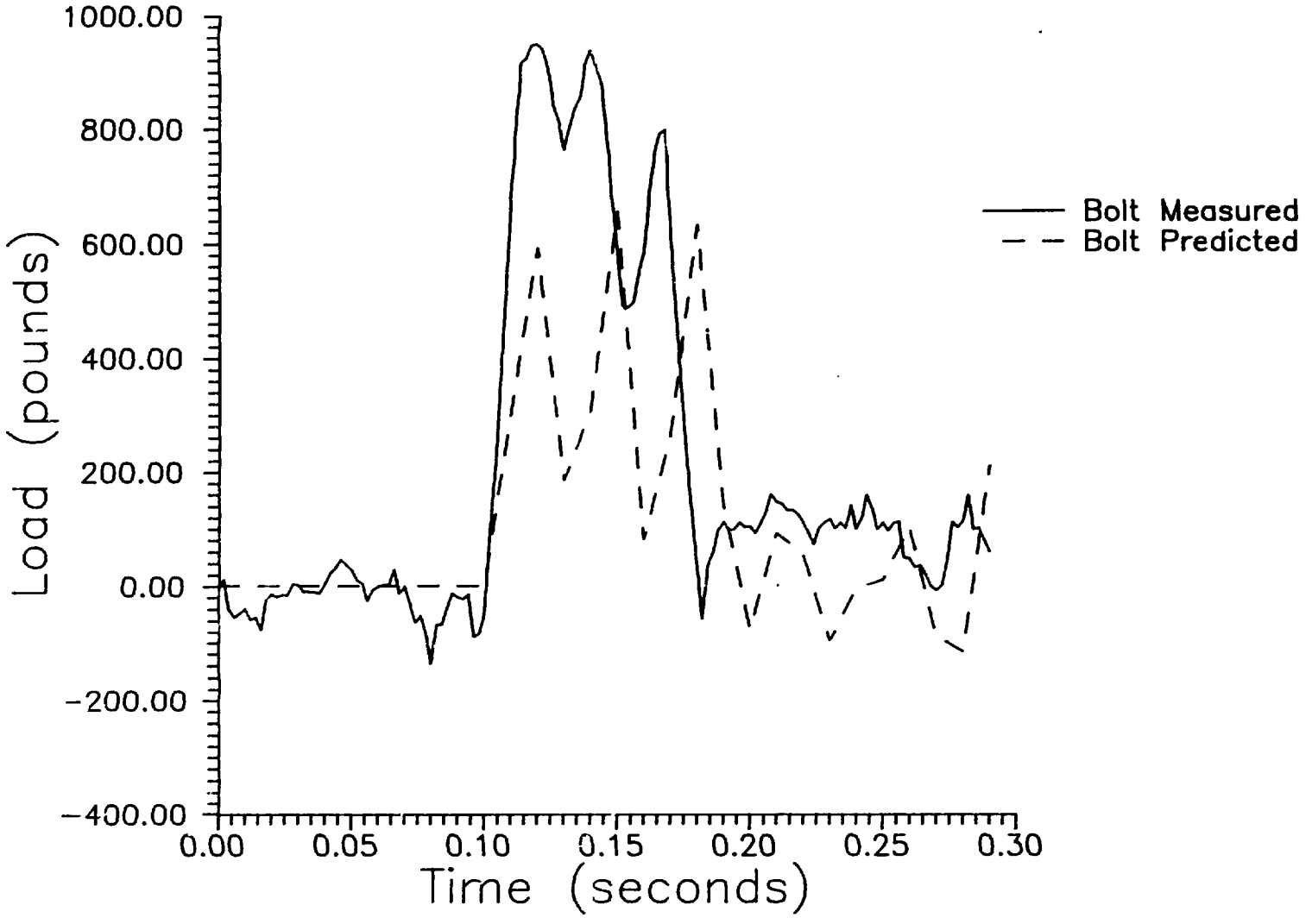

Figure 13. Predicted and Measured Horizontal Anchor Bolt Loads for Bolt 1, Event 187

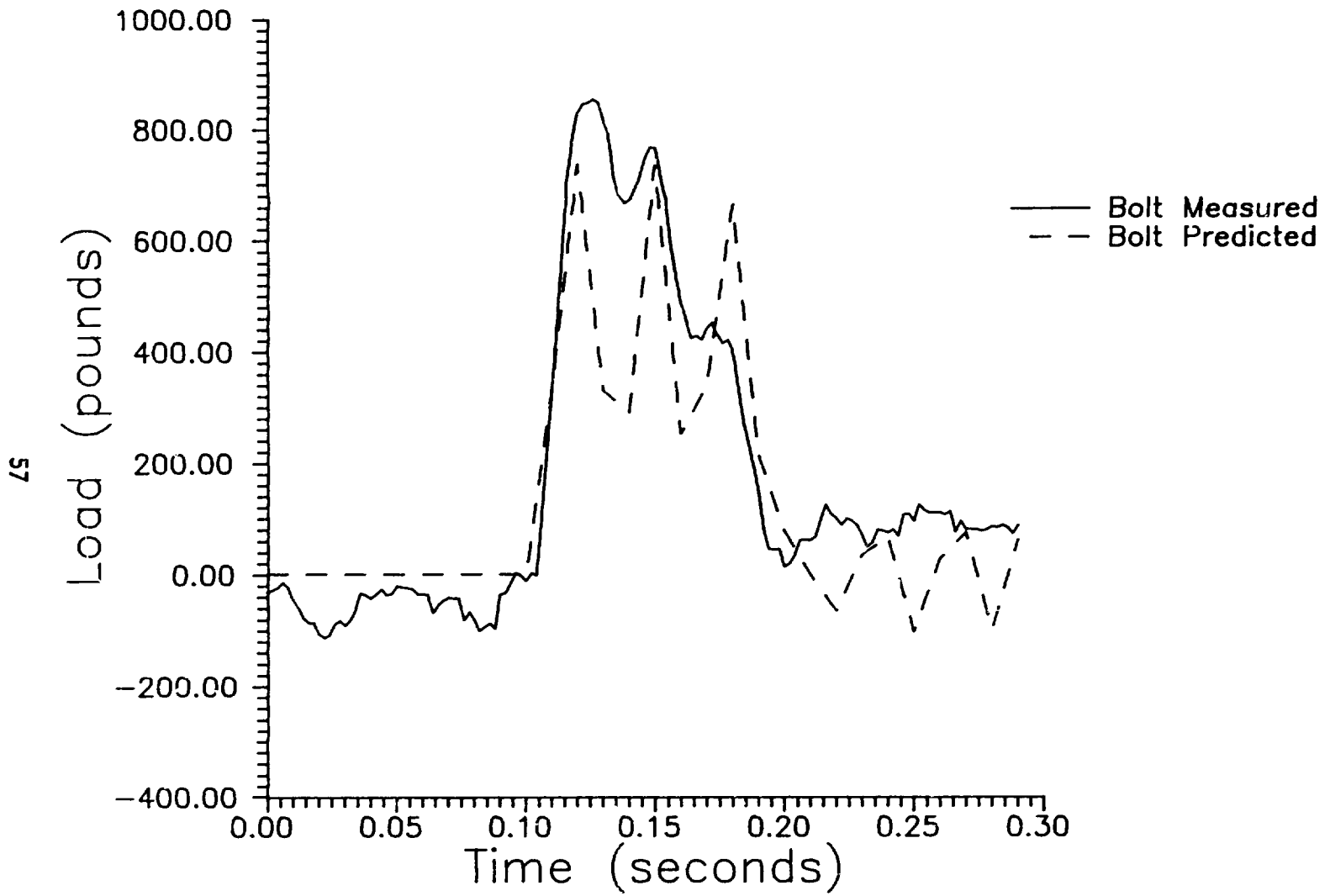

Figure 14. Predicted and Measured Horizontal Anchor Bolt Loads for Bolt 2, Event 187

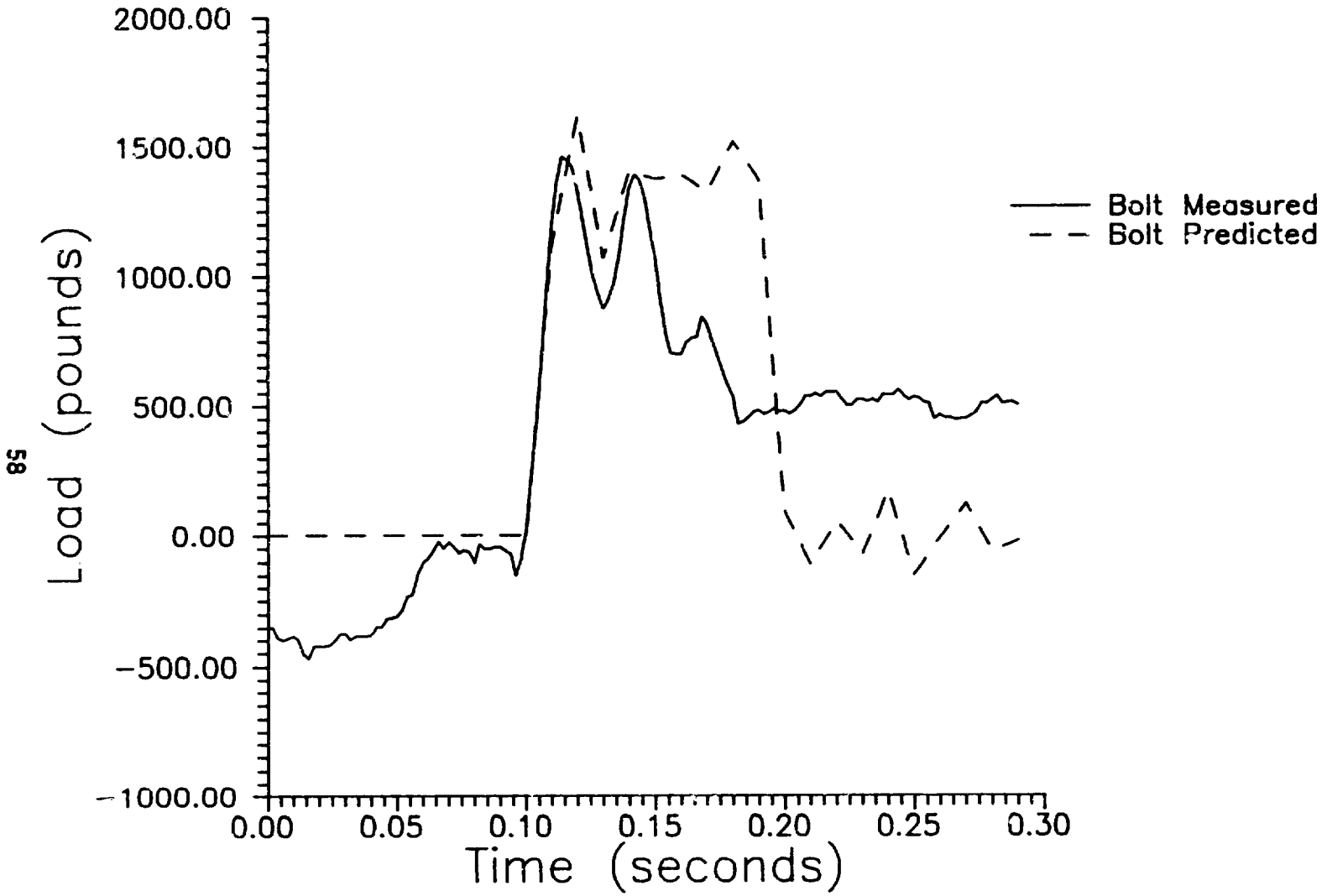

Figure 15. Predicted and Measured Horizontal Anchor Bolt Loads for Bolt 4, Event 187

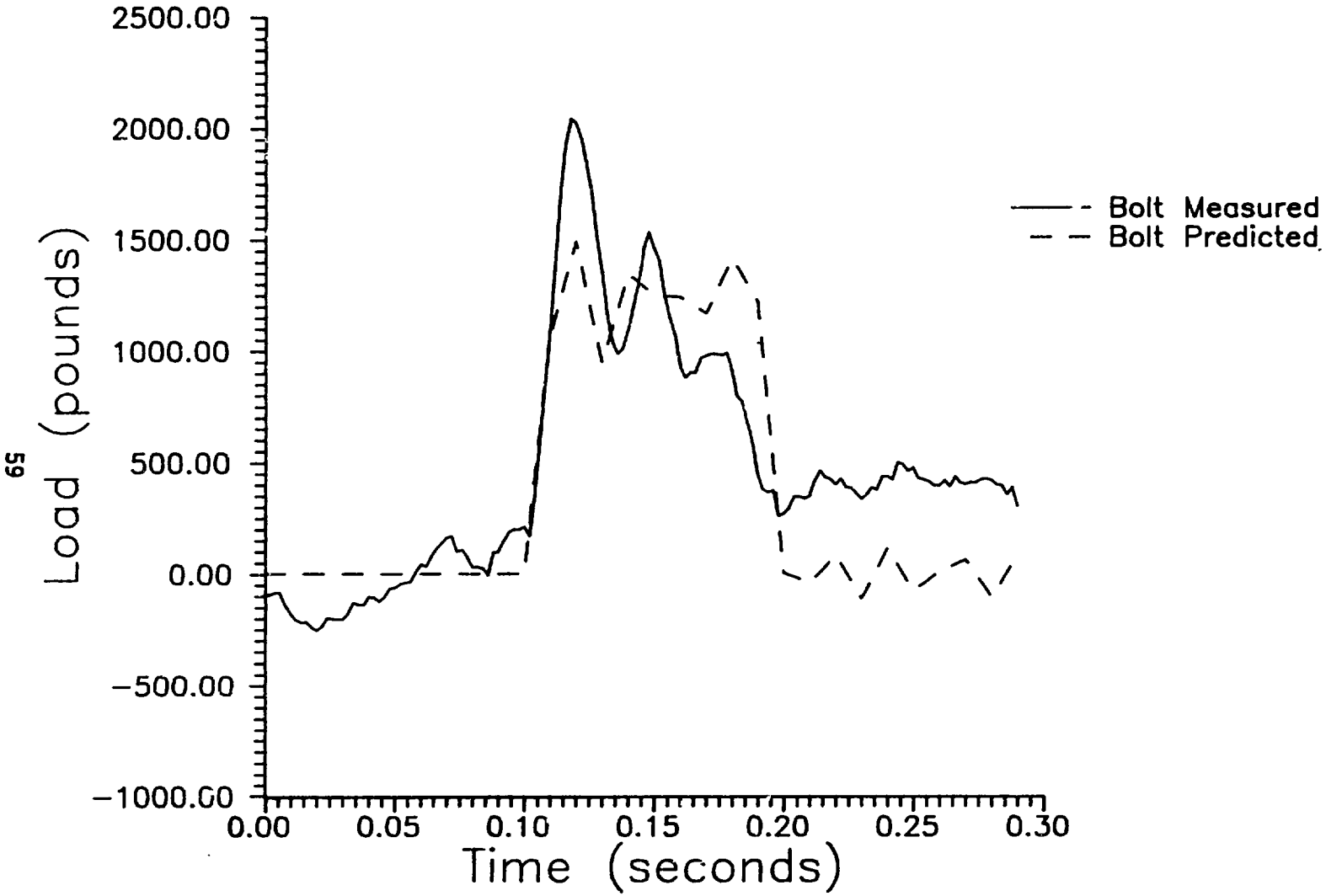

Figure 16. Predicted and Measured Horizontal Anchor Bolt Loads for Bolt 5, Event 187

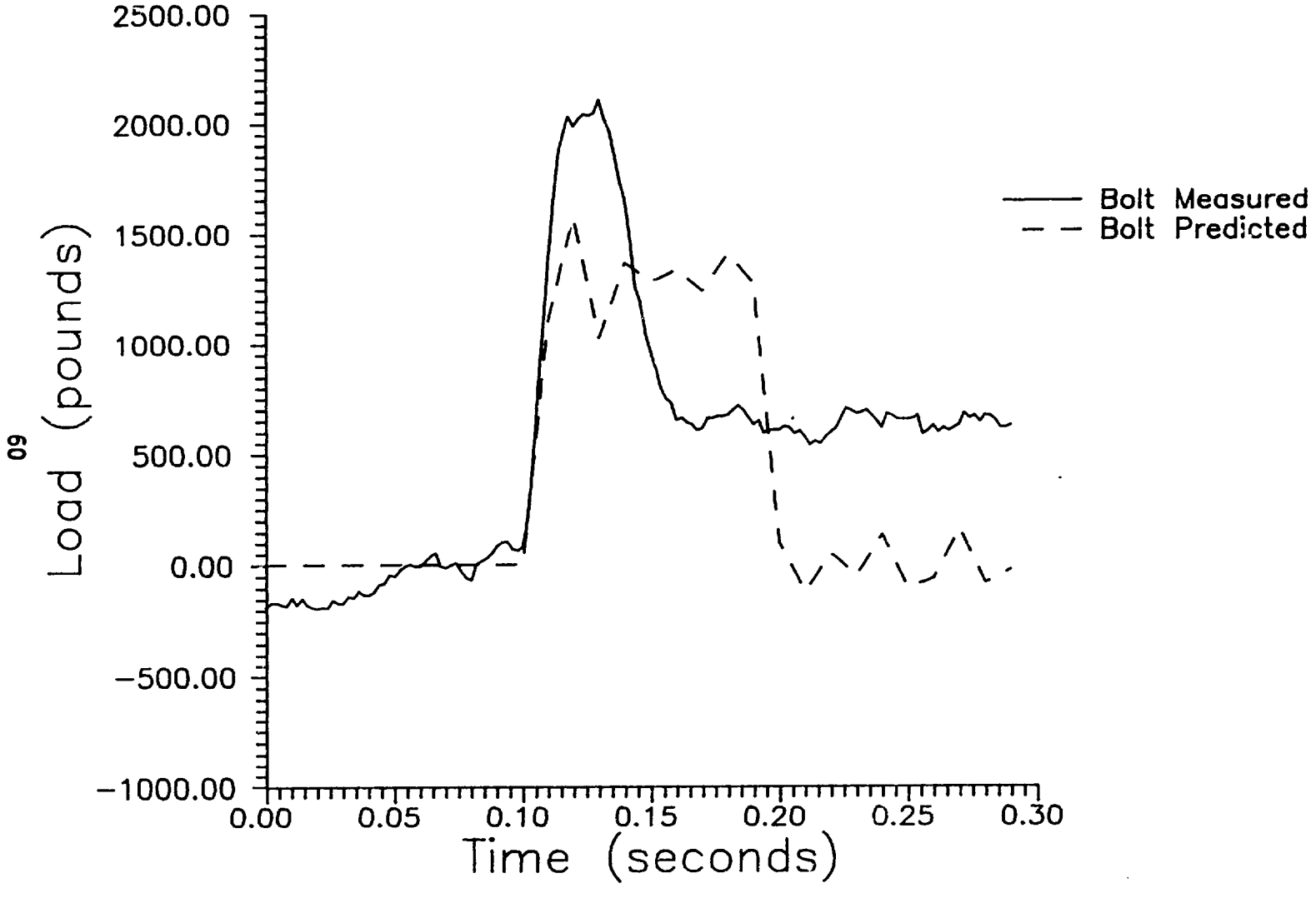

Figure 17. Predicted and Measured Horizontal Anchor Bolt Loads for Bolt 6, Event 187

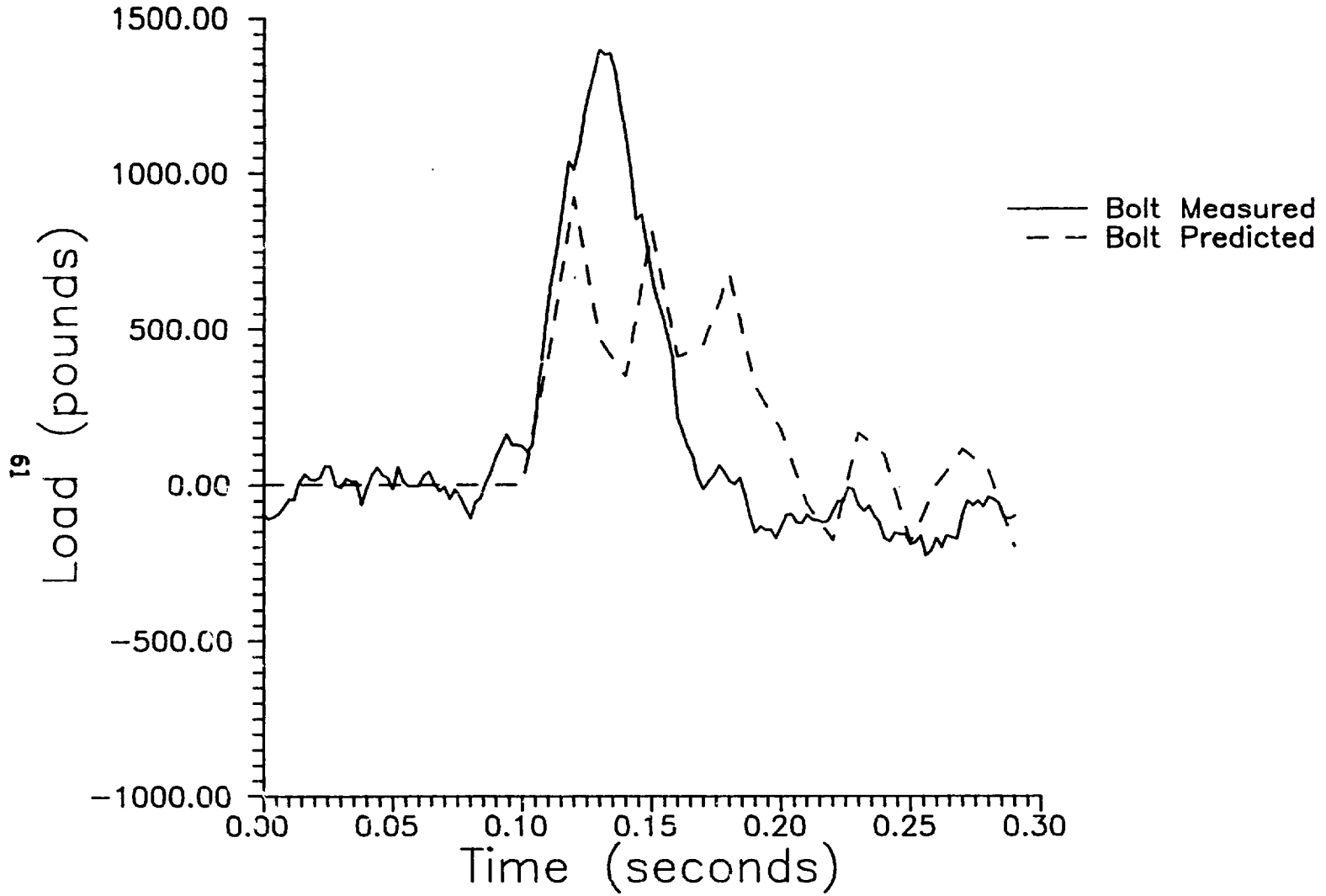

Figure 18. Predicted and Measured Horizontal Anchor Bolt Loads for Bolt 8, Event 187

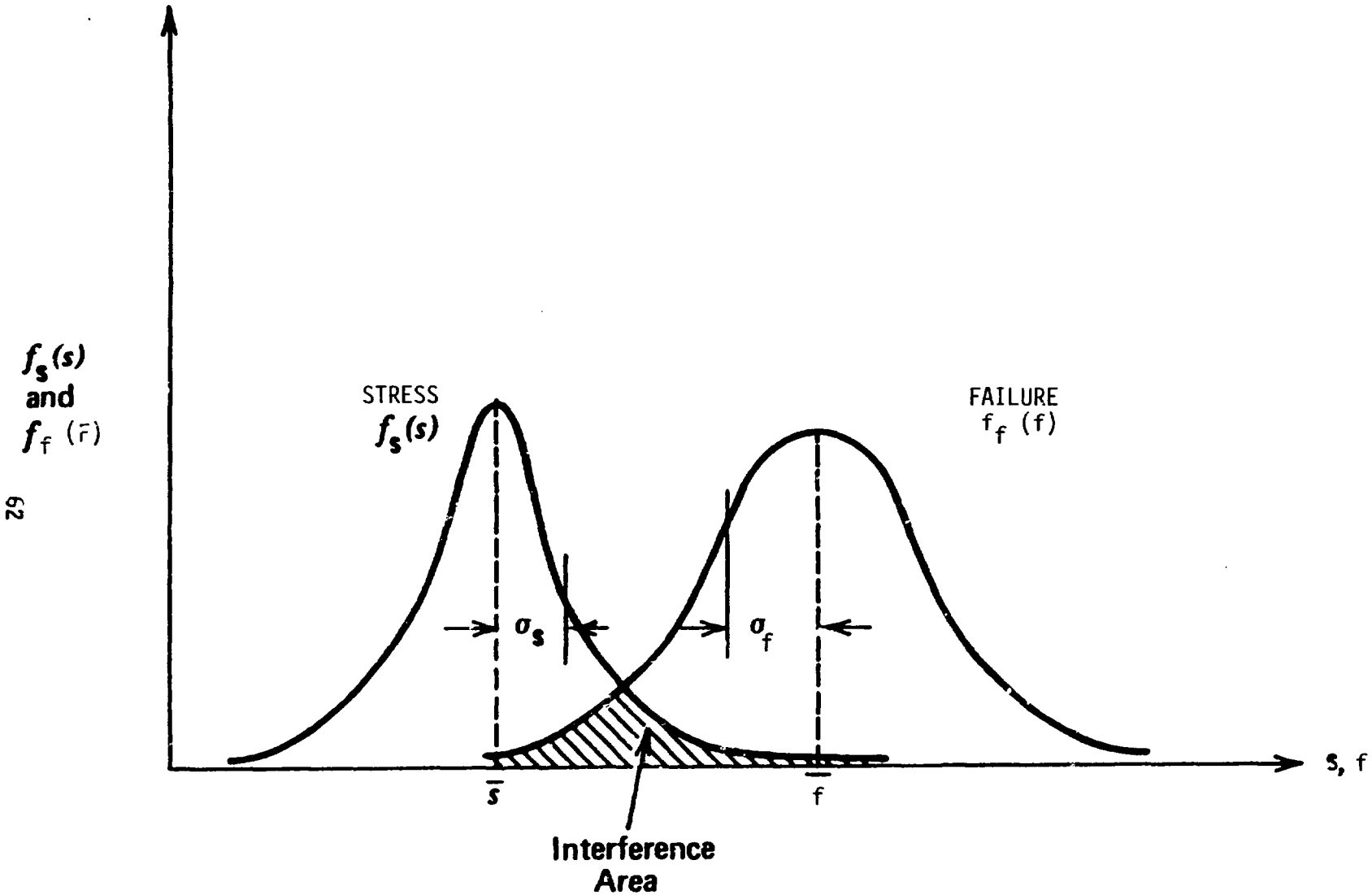

Figure 19. Stress-Failure Interference (Reference 11)

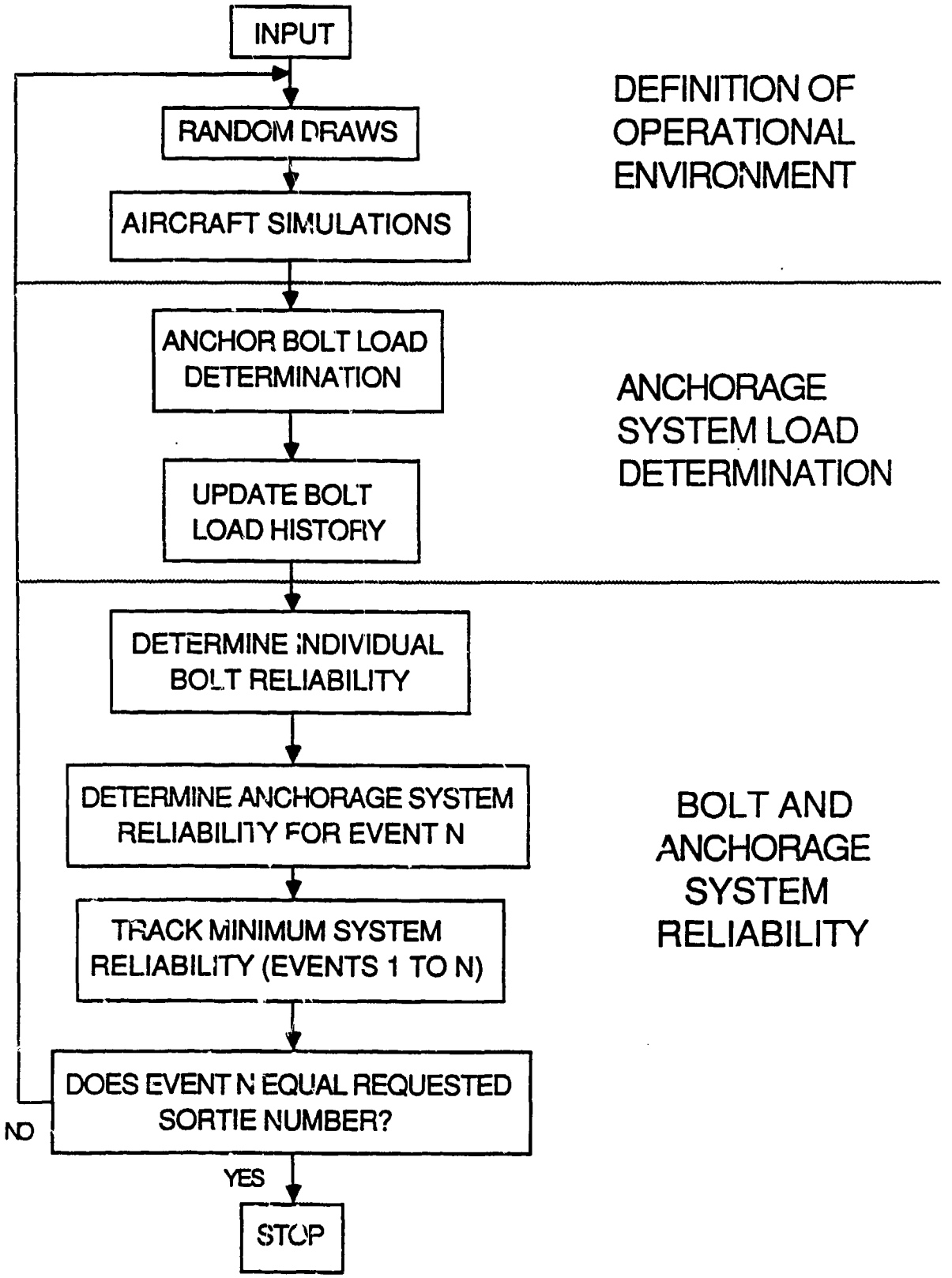

Figure 20. Anchoring System Reliability Methodology

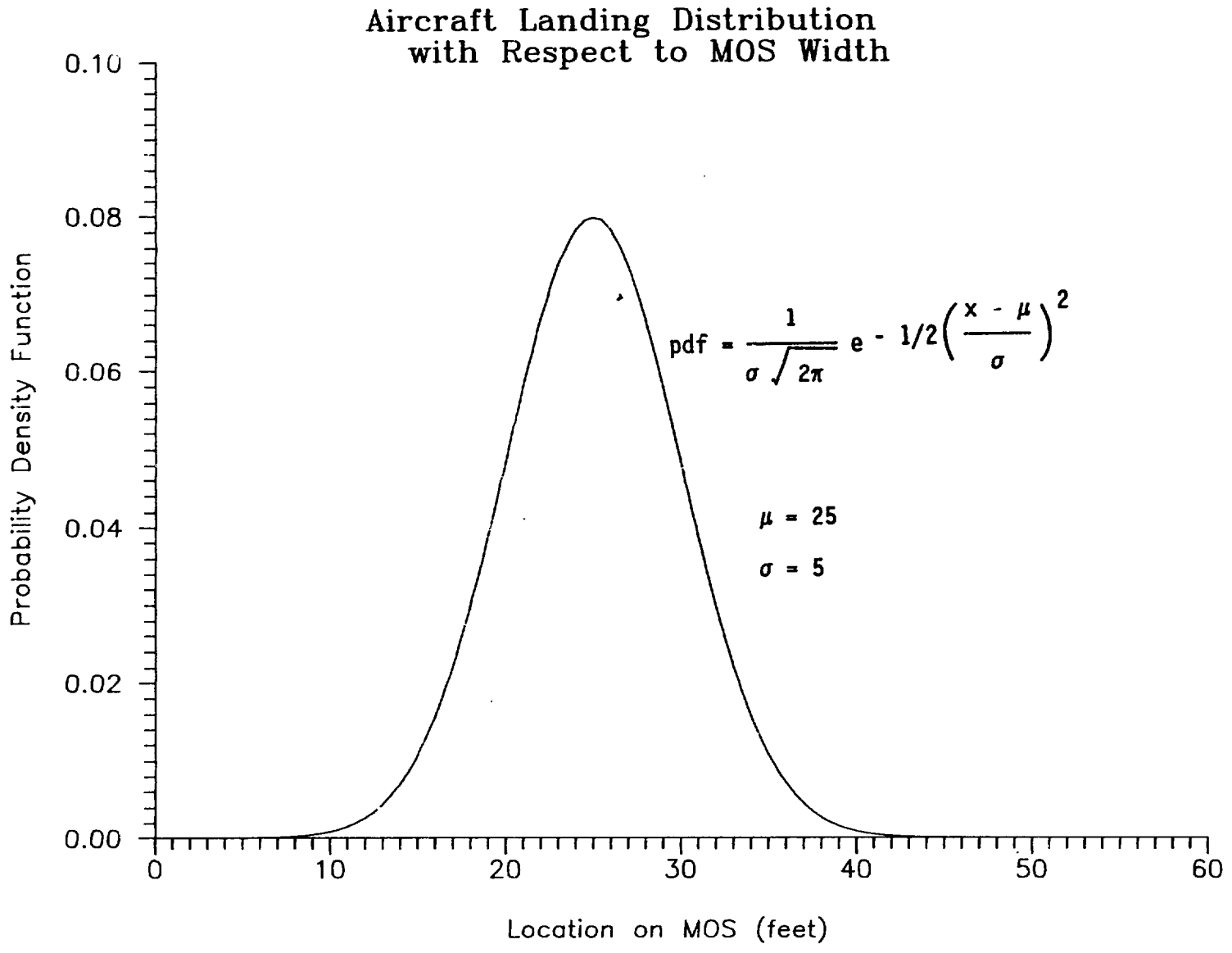

Figure 21. Aircraft Landing Distribution with Respect to MOS Width

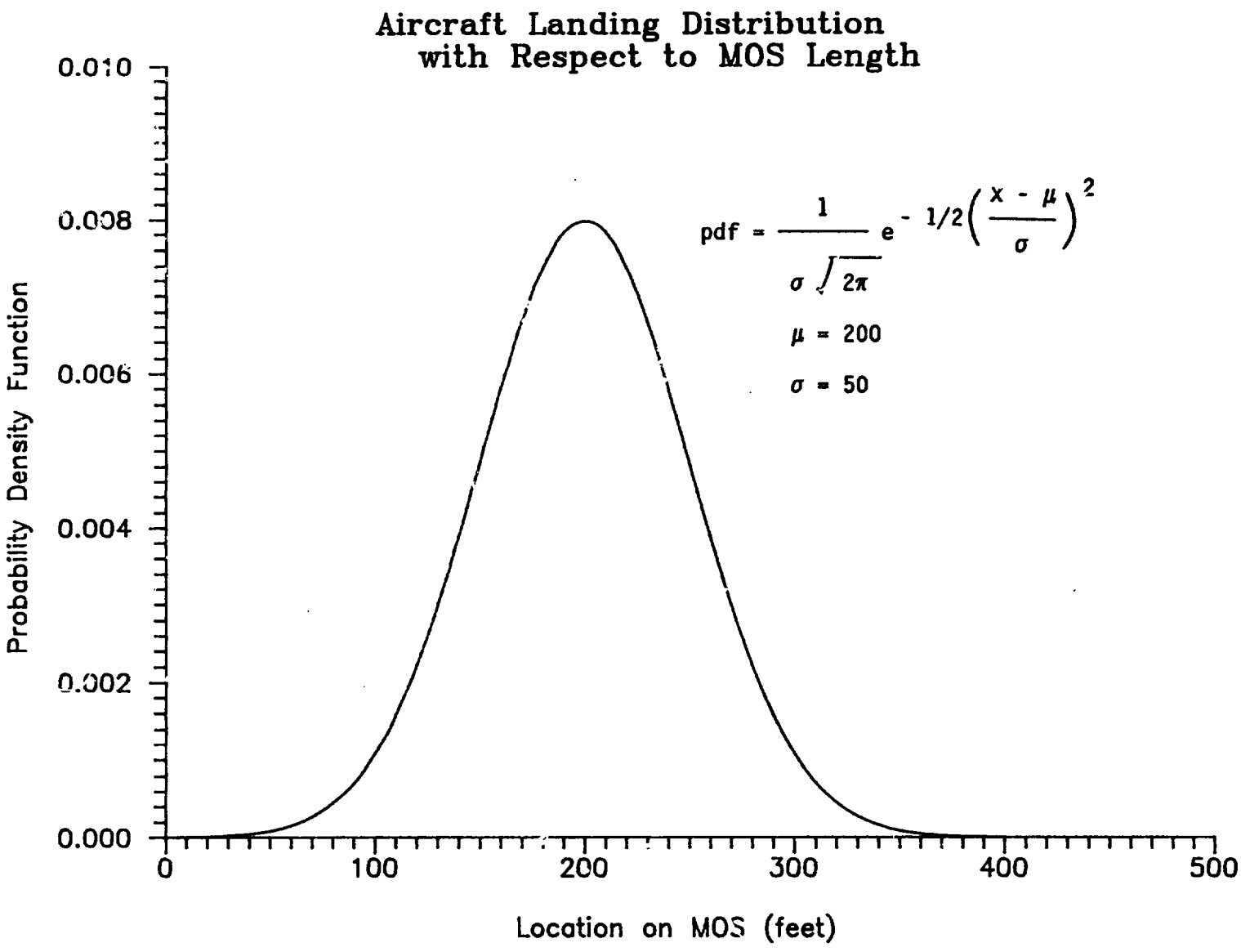

Figure 22. Aircraft Landing Distribution with Respect to MOS Length

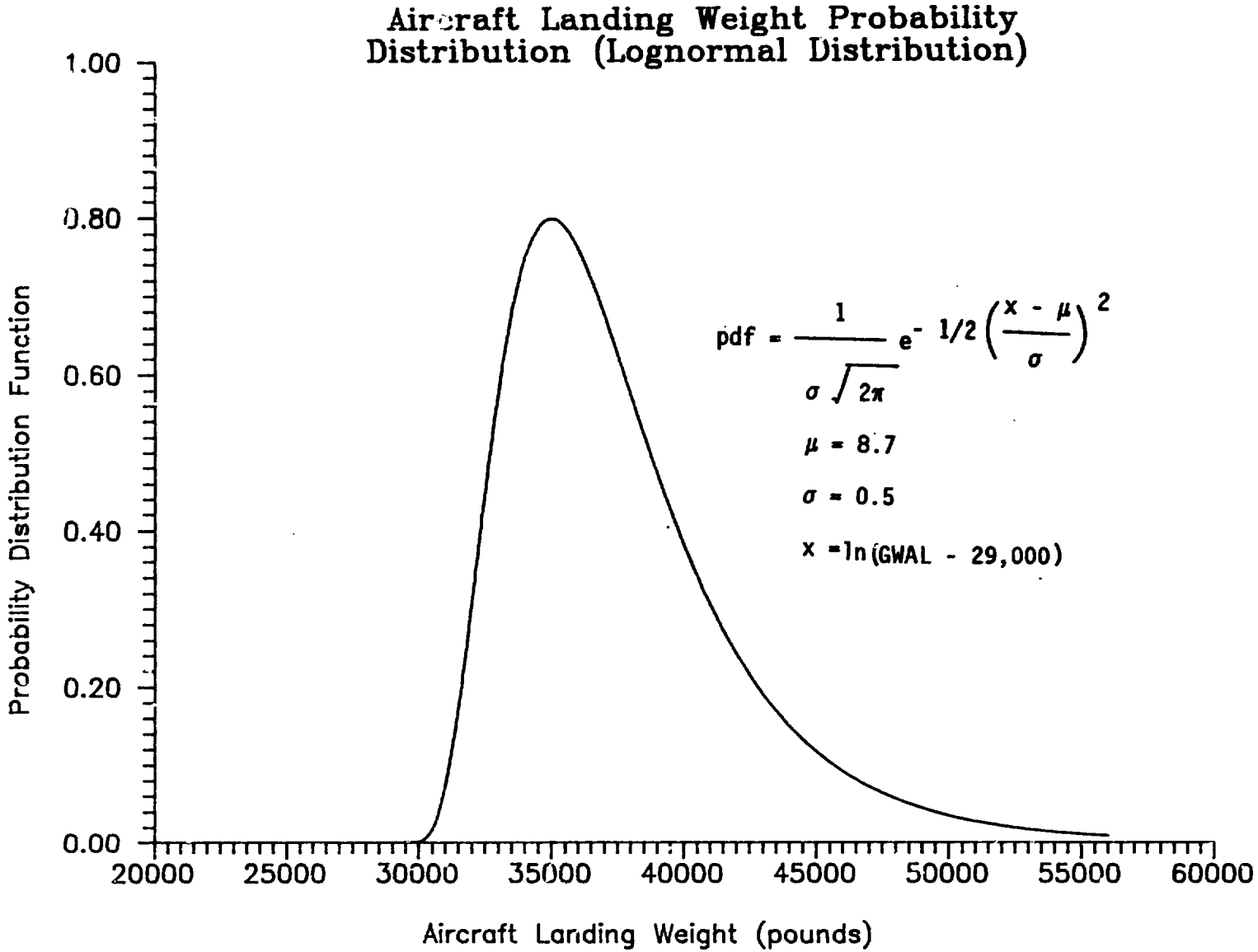

Figure 23. Aircraft Landing Weight Probability Distribution

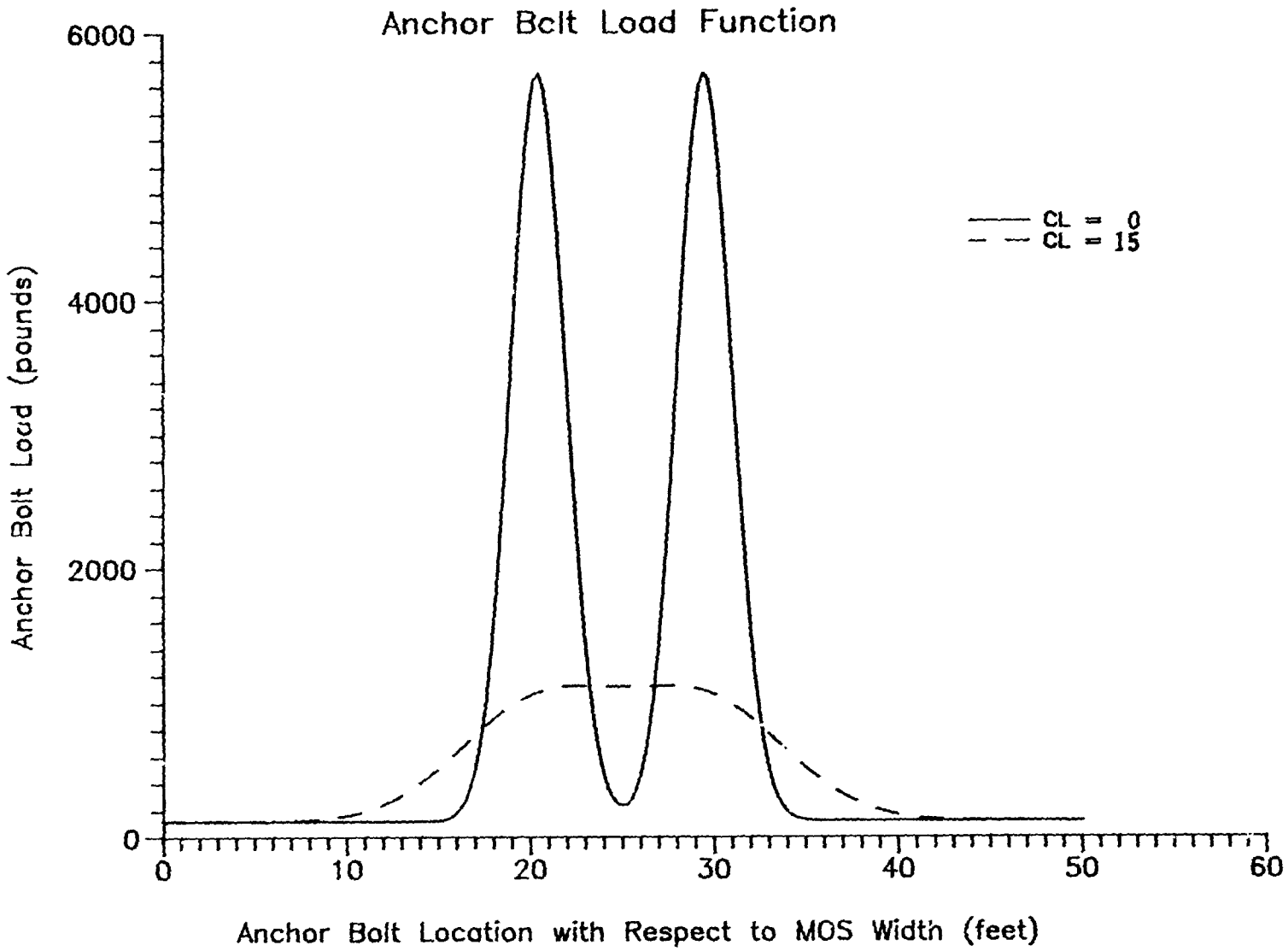

Figure 24. Anchor Bolt Load Function

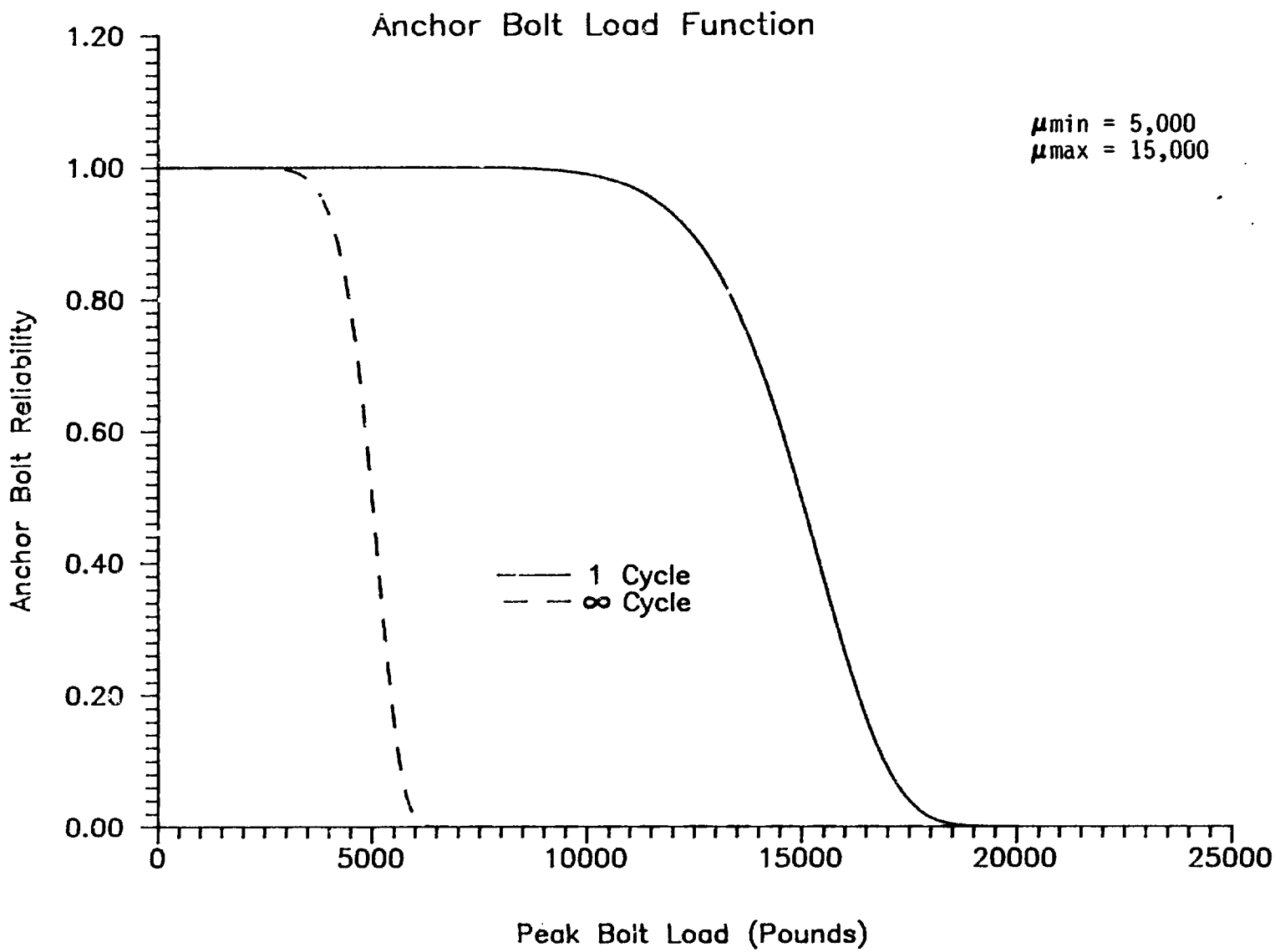

Figure 25. One-Cycle and Infinite-Cycle Anchor Bolt Reliability Functions

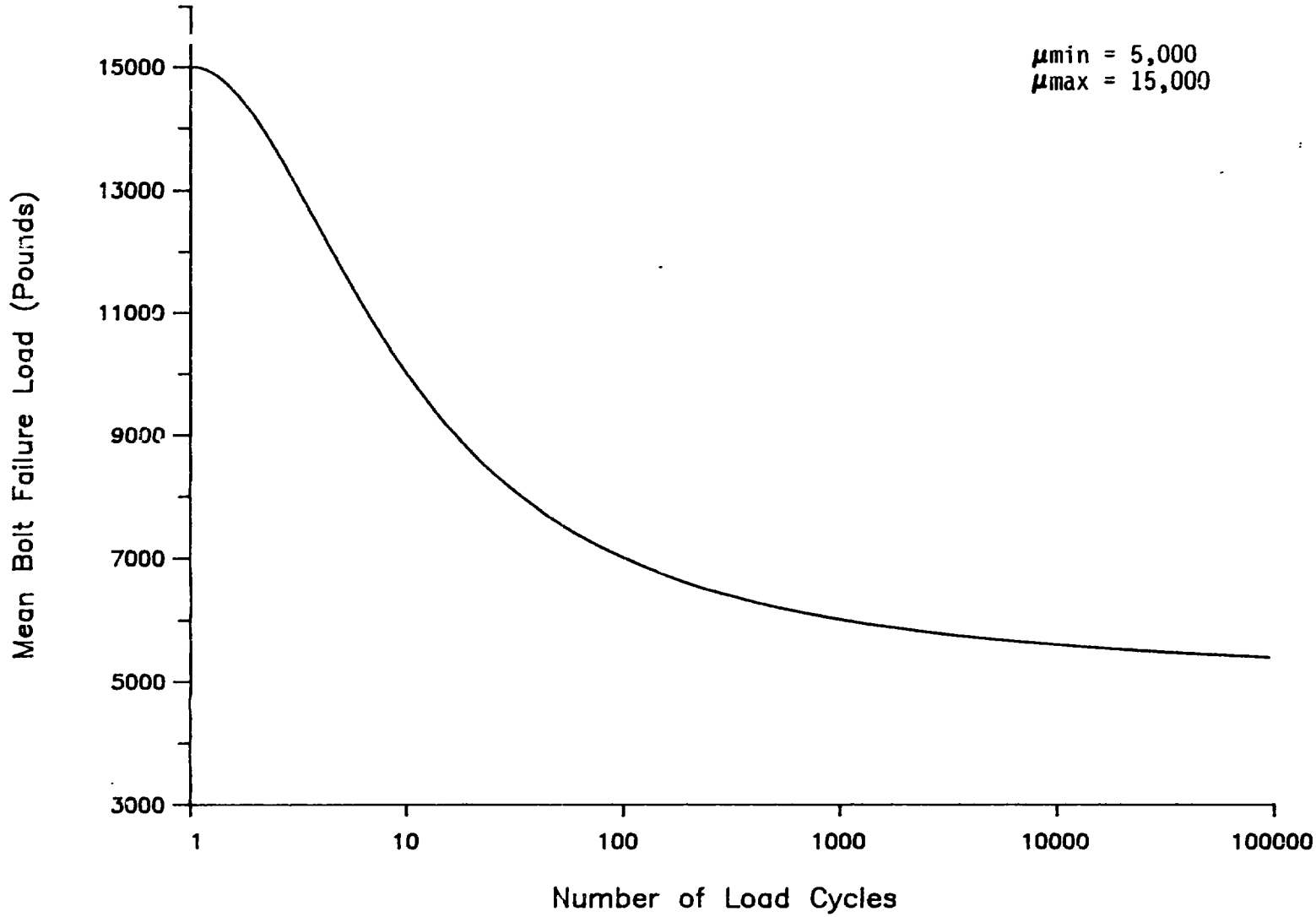

Figure 26. Anchor Bolt Cyclic Degradation Function

TABLE 14. SINGLE-EVENT SIMULATIONS INPUT VARIABLES

Simulation Number	Aircraft Landing Weight (lb)	Aircraft Touchdown Location (ft) Width	Aircraft Touchdown Location (ft) Longitudinal	Aircraft Breaking Coefficient	Location of Mat on MOS (ft)	Distance Between Crater and Anchor Bolt Line (ft)	Anchor Bolt Mean Failure Load (lb)
1	40,000	25	200	0.37	3000	5	7500
2	35,000	25	200	0.37	3000	5	7500
3	45,000	25	200	0.37	3000	5	7500
4	40,000	25	100	0.37	3000	5	7500
5	40,000	25	300	0.37	3000	5	7500
6	40,000	20	200	0.37	3000	5	7500
7	40,000	30	200	0.37	3000	5	7500
8	40,000	25	200	0.37	3000	5	5000
9	40,000	25	200	0.37	3000	5	10000
10	40,000	25	200	0.25	(4000)	5	7500
11	40,000	25	200	0.50	(2500)	5	7500
12	40,000	25	200	0.37	2500	5	7500
13	40,000	25	200	0.37	3500	5	7500
14	40,000	25	200	0.37	3000	0	7500
15	40,000	25	200	0.37	3000	10	7500

TABLE 15. SINGLE-EVENT SIMULATIONS - RESULTS

AIRCRAFT LANDING WEIGHT (LB)	ANCHORING SYSTEM RELIABILITY
35,000	0.999
40,000	0.997
45,000	0.991

AIRCRAFT LOCATION ON MOS (WIDTH)	ANCHORING SYSTEM RELIABILITY
20	0.997
25	0.997
30	0.997

AIRCRAFT LOCATION ON MOS (LONGITUDINAL)	ANCHORING SYSTEM RELIABILITY
100	0.997
200	0.997
300	0.998

AIRCRAFT BRAKING COEFFICIENT	ANCHORING SYSTEM RELIABILITY
0.25	1.000
0.37	0.997
0.50	0.967

LOCATION OF MAT ON MOS (FT)	ANCHORING SYSTEM RELIABILITY
2500	0.998
3000	0.997
3500	0.996

DISTANCE BETWEEN CRATER AND ANCHOR BOLT LINE (FT)	ANCHORING SYSTEM RELIABILITY
0	0.896
5	0.997
10	1.000

ANCHOR BOLT MEAN FAILURE LOAD (LB)	ANCHORING SYSTEM RELIABILITY
5000	0.856
7500	0.997
10000	1.000

TABLE 16. 100-EVENT SIMULATIONS ANCHORING SYSTEM RELIABILITY VARIATION WITH MAT LOCATION ON MOS

MAT LOCATION ON MOS (FT)	ANCHORING SYSTEM MINIMUM RELIABILITY SIMULATION NUMBER 1	2	3	AVERAGE
500	1.000	1.000	1.000	1.000
1000	1.000	1.000	1.000	1.000
1500	0.999	1.000	1.000	1.000
2000	0.985	0.931	0.981	0.966
3000	0.887	0.823	0.717	0.809
3500	0.775	0.782	0.748	0.768

OTHER INPUT VARIABLES:

ANCHOR BOLT MEAN LOAD TO FAILURE (1 CYCLE)$^{(LB)}$ = 15000

ANCHOR BOLT MEAN LOAD TO FAILURE (∞ CYCLES)$^{(LB)}$ = 5000

MINIMUM BOLT LOAD FOR CYCLE COUNT (LB) = 1000

AIRCRAFT BRAKING COEFFICIENT = 0.34

DISTANCE FROM CRATER TO ANCHOR BOLT LINE (FT) = 0

TABLE 17. 100-EVENT SIMULATIONS - ANCHORING SYSTEM RELIABILITY VARIATION WITH DISTANCE BETWEEN CRATER AND ANCHOR BOLT LINE

DISTANCE BETWEEN CRATER AND ANCHOR BOLT LINE	ANCHORING SYSTEM MINIMUM RELIABILITY SIMULATION NUMBER 1	2	3	AVERAGE
0	0.775	0.782	0.748	0.768
5	0.996	0.989	0.987	0.991
10	1.000	1.000	1.000	1.000

OTHER INPUT VARIABLES:

ANCHOR BOLT MEAN LOAD TO FAILURE (1 CYCLE)$^{(LB)}$ = 15000

ANCHOR BOLT MEAN LOAD TO FAILURE (∞ CYCLES)$^{(LB)}$ = 5000

MINIMUM BOLT LOAD FOR CYCLE COUNT (LB) = 1000

AIRCRAFT BRAKING COEFFICIENT = 0.34

MAT LOCATION ON MOS (FT) = 3500

TABLE 18. 100-EVENT SIMULATIONS - ANCHORING SYSTEM RELIABILITY VARIATION WITH ANCHORING SYSTEM FAILURE CRITERIA

ANCHOR BOLT MEAN LOAD TO FAILURE (1 CYCLE)	ANCHOR BOLT MEAN LOAD TO FAILURE (∞ CYCLES)	MINIMUM BOLT LOAD FOR CYCLE	ANCHORAGE SYSTEM MINIMUM RELIABILITY SIMULATION NUMBER 1	2	3	AVG
15000	5000	1000	0.990	0.997	0.998	0.995
12000	4000	800	0.916	0.964	0.943	0.941
9000	3000	600	0.576	0.567	0.485	0.543

OTHER INPUT VARIABLES:

AIRCRAFT BRAKING COEFFICIENT = 0.34

MAT LOCATION ON MOS (FT) = 3000

DISTANCE FROM CRATER TO ANCHOR BOLT LINE (FT) = 5

APPENDIX A

FIBERGLASS MAT INSTRUMENTATION SYSTEM

APPENDIX A

FIBERGLASS MAT INSTRUMENTATION SYSTEM

A. SYSTEM COMPONENTS

1. Transducer System

The transducers are the actual measurement devices used to measure mat and bolt strains and were designed to meet the stringent requirements discussed in the main body of this report. The transducers selected were foil-type strain gages (Figure A-1) because of their commercial availability, versatility, low cost, and direct measurement capability. For the reader's convenience, all figures are located at the end of this appendix. This type of strain gage consists of an electrical grid superimposed on a thin insulation backing. The gage is bonded to the test article and measures strain by physical distortion of the strain gage, which affects the grid resistance. In the completed instrumentation setup, the gage is wired as one resistor in a Wheatstone Bridge (Figure A-2). The other fixed resistors in the bridge usually are contained in the conditioning amplifier and are normally termed the bridge completion circuitry. The conditioning amplifier also provides the precision excitation voltage (Figure A-2).

a. Transducer Layout

From previous analysis and tests, it was decided that anchor bolt loads and mat strains were the two aspects of the mat response which would be monitored at the North Field test. The transducer locations were based on previous mat response understanding, preliminary finite-element analysis, and transducer system criteria. A preliminary finite-element analysis was conducted to aid in placing the transducer and is discussed in

Section III. Transducer system structural response measurement requirements included:

(1) Investigating aircraft wheel loadings on the mat system and how loads are transferred from the mat to the anchor bolts,

(2) Measuring the load transfer across panels,

(3) Documenting bow wave effects on the mat and anchor bolts,

(4) Determining the load transfer symmetry of the mat panels,

(5) Monitoring airblast loads on the mat system.

Figure A-3 shows the final instrumented anchor bolt and mat strain gage locations on the mat repair. Fourteen active instrumented bolts, two backup instrumented bolts, and twenty axial mat strain gages comprised the transducer system. The backup instrumented bolts would replace active bolts or strain gages that became unoperative during the test. Instrumented Bolts

3, 4, 8, and 9 were designated to monitor the loads transferred to the anchor bolts on Panel 4, the panel which the F-15 and F-16 main landing gear traverses and on which braking loads were imposed. Bolts 7 and 12 were placed to monitor loads on Panel 6 and load symmetries. Bolts 5, 6, 10, and 11 measured loads imposed on Panel 5 by the nose landing gear and the loads transferred from Panels 4 and 6. Likewise, Bolts 1, 2, 13, and 14 documented loads transferred to the panels on the free edge.

As with the instrumented anchor bolts, the mat gages were designated for specific functions. Gages 2, 3, 7, 11, 13, 15, and 17 measured mat strains in Panel 4. The longitudinal spacing of the gages, both on the leading and trailing edges, were set so bow wave phenomena could be monitored. Likewise, Gages 4, 5, 8, 12,14, 16, and 18 monitored mat strains in Panel 5. As with Bolts 7 and 12, Gages 6 and 19 documented loading symmetries. Gages 1 and 20 measured mat strains in the free-edge panels (Panels 1 and 9). The mat gages were situated close to the leading and trailing edges to correlate with the bolt loads, monitor bow wave response, and minimize the field installation effort.

b. Instrumented Anchor Bolt

The design requirements for the instrumented anchor bolts included stiffness characteristics similar to standard mat anchor bolts, equivalent or greater load capacity, linear load deflection characteristics, and reasonable load-signal ratios. The anchor bolt stiffness similitude and equivalent load capacity requirement ensured that the mat system response or capabilities would not be affected. The linear load relationship was a typical characteristic of transducers enabling the electrical signal to be converted to a physical measure (e.g., pounds). The sensitivity of the instrumented bolt ensured that the electrical signal produced was large enough to realistically amplify and record. As with the overall instrumentation system design requirements (see Section IV, Subsection B) the requirements for the instrumented bolt conflicted. For example, the stiffness requirements were inversely related to the instrumented bolt sensitivity ratio.

The instrumented bolt functioned both as an anchor bolt and as a load cell. As a load cell, the bolt measured horizontal and vertical loads. The horizontal loads were monitored in two orthogonal directions. The instrumented anchor bolt used in the test series is illustrated in Figure A-4. The 1.25-inch diameter bolt was instrumented with three strain gages and bonded to the concrete using a polymer plug. The region of the bolt on which the strain gages were attached was machined to a 1-inch diameter. The reduction in diameter was necessary to increase the sensitivity of the resulting load cell. The bolt was attached to the mat by a bottom-threaded washer and specially modified bushing engaging the mat. The clearance between the polymer plug and mat allowed the bolt to deflect slightly when loaded. This deflection was recorded by the strain gages. In short, the bolt acted as miniature cantilever beam load cell.

The two opposing gages were aligned with the long dimension of the mat in the final installation. These gages monitored horizontal loads in the traffic direction. The single gage measures horizontal loads perpendicular to the traffic direction and monitors vertical loads for events

involving airblast and bow wave phenomena. Ideally, the out-of-plane horizontal and vertical loads should be measure with dedicated gages having separate channels. The gages used are CEA-06-25QUN-350, manufactured by Measurements Group, Inc. The gages are 0.25 by 0.50 inch in size, with an undeformed precision resistance of 350 Ohms. Gage specifications are included in Appendix B. Tests were conducted to verify the performance of the short cantilever beam load cell.

c. Mat Strain Gage

The mat strain gage posed unique transducer design problems. These problems included field installation, protection in a severe environment, and gage stability. Even under laboratory conditions, strain gage installation is a challenge. Proper gage operation and lifespan is related directly to the quality of installation. The installation process involved surface preparation, gage bonding, and environment protection (to prevent moisture and mechanical damage). The surface preparation segment was the most labor-intensive and included polyester resin placement, extensive sanding, and special surface cleaning. The second phase, bonding, required extensive placement and curing time. During gage bonding, the absence of moisture was essential. Thus, the gage protection phase should be completed as soon as possible after the gage-bonding segment.

The final phase of mat gage installation was applying the protective coating to prevent moisture and mechanical damage. Since the gages would be exposed directly to weather and aircraft trafficking, including wheel spin-up, the protection system for the gages was essential. At North Field, the strain gages were installed using the manufacturer's recommended protection system for severe environments. A further description of the mat strain gage installation process is contained later in this appendix.

The last concern involving the mat strain gages was gage stability. Strain gages, while in operation, are subjected to a small dc current (excitation voltage). Also, the gages are extremely sensitive to temperature changes, particularly those associated with internal heat generation. Typically, the gage transfers excess heat to the test specimen, which usually is composed of metal. Because of its low specific heat ratio, the mat is an extremely poor heat sink for the gage. To overcome this problem, 1000 Ohm gages, manufactured by Measurements Group, Inc. (Model S2K-00-250BF-10C), were used in the test series (Reference 6); standard gages are 120 and 350 Ohm. The increased resistance of the gage substantially decreases the heat sink requirement for gage stability. The North Field Test was the first field application of the new 1000 Ohm gages

2. Instrumentation Cable

The instrumentation cable was an essential element of the instrumentation system. Typical signal outputs from a strain gage bridge before amplification are on the order of microvolts. The instrumentation cable at the test was approximately 300 feet long. Cable shielding, line-resistance compensation, protection from aircraft trafficking, and quick-disconnect capabilities were the primary design concerns. Cable

shielding was accomplished by proper cable selection and shield grounding at the instrumentation van. Because of the small signal voltages and long lead lines involved in this application, shielding was extremely important. Line-resistance compensation was provided by using an additional lead with each strain gage circuit. Protection was assured by locating the cable in a covered trench near aircraft ground operations. The quick-disconnect capability allowed the vulnerable instrumentation equipment to be isolated from the exposed strain gages and instrumentation cable during electrical storms.

3. Data Acquisition System

The data acquisition system was housed in the instrumentation van and auxiliary observation van. The system was composed of conditioning amplifiers, tape recorders, digital oscilloscope, oscillograph, and miscellaneous support equipment. The data acquisition system is shown in Figure A-5. The main instrumentation cable carried the strain gage signal to the instrumentation van. The conditioning amplifiers contained the bridge completion circuitry and signal amplifiers (up to 1000 gain). Forty-eight conditioning amplifiers (one for each channel) comprised the signal processing subsystem. Following the signal processing, the amplified signal was recorded on four 14-channel instrumentation analog tape recorders. A coded reference time signal, known as IRIG, was recorded on one channel of each recorder, leaving 13 channels for test data acquisition per recorder. Two amplified channels were paralleled to a dual-channel digital oscilloscope for real-time data acquisition and assessment. Additionally, the oscillograph was used to provide quick-look hard copy output of recorded events. An onboard electrical generator powered the instrumentation van.

B. DEMONSTRATION AND PREPARATORY TESTING

In developing the instrumentation system design, several aspects of the pretest design were considered unique and unproven. The purpose of the preparatory tests was to demonstrate the validity of the design concept, indicate appropriate changes in the system design or test procedure, and provide practical training for the instrumentation team. The tests involved demonstrating the instrumented anchor bolt design; bolt field placement procedures; bolt field calibration; mat field installation; and instrumentation cable design, including the quick-disconnect and the 300-foot lead tests.

1. Instrumented Anchor Bolt Field Placement Demonstration

As shown in Figure A-4, the anchor bolt was placed in a 3-inch diameter hole and bonded to the concrete by a polymer plug. The objective of this test was to evaluate the entire instrumented anchor bolt placement procedure, including concrete boring, hole preparation, polymer mix requirements, bolt placement, and polymer placement and curing.

The tests were conducted at the Small Crater Test Facility. To test the drilling operation time requirement and prepare the test holes for bolt installation, six holes were drilled in the concrete slab within a 20- by

10-foot area. Next, the holes were prepared for bolt placement. Bolt placement consisted of threading a plywood alignment block on the bolt and centering the bolt in the hole, while suspending the bolt from the plywood block. Polymer was added to the concrete bore holes to the proper depth, and the bolt was realigned before the polymer set.

The following problems were encountered during the test demonstration. First, drilling required approximately 30 to 40 minutes per hole. It was determined that drilling in the field would be a large time constraint (16 holes were required in the field installation). Also, moisture was present in several holes during polymer placement, and the moisture-sensitive polymer expanded above the design polymer line. Since the strain gages are located only 0.25 inch above the design polymer line, the polymer expansion was considered a major problem. The bolt placement procedure was modified to include drying the bore holes before polymer placement. In addition, the design polymer line was lowered 0.125 inch to allow for incidental polymer swelling.

2. Instrumented Anchor Bolt Design and Field Calibration Demonstration Tests

The goal of this test series was to evaluate various instrumented anchor bolt designs and field calibration procedures. The instrumented bolts had to function both as a mat anchor and as a load cell. Three different anchor bolt designs were considered. The first was the 1.25-inch diameter bolt, with an embedment length of approximately 6 inches. The second design candidate was the same bolt diameter, with an embedment depth of 4 inches. The last design was the 1.25-inch diameter bolt, turned down to 1-inch diameter in the strain gage attachment area, and a 6-inch embedment depth. Preliminary design calculations showed that the load cell sensitivity of the first design probably was not adequate for this test series. The embedment length on the second design was questionable, but did allow the bolt to be installed in 6-inch thick concrete without penetrating the subgrade. The last design candidate was determined to give an acceptable sensitivity ratio and to provide the requisite anchor strength.

Strain gages were installed on the three types of anchor bolt designs in preparation for this test series. The gages were located as shown in Figure A-4 and installed according to the manufacturer's recommendations. After strain gage installation, the bolts were installed during the field installation tests described previously.

Three types of tests were conducted on the test anchor bolt specimens. The first test was a horizontal calibration test. As stated previously, the calibration tests would provide the key link between the observed signal and the conversion to physical units. The test setup for the horizontal calibration test is shown in Figure A-6 and consisted of a jacking reaction mass (fork-lift); hand winch; 5000-pound capacity load cell; and various cables, chains, and special connectors. Figure A-7 shows the instrumentation system used in the calibration test series. The strain gage and load cell were connected to conditioning amplifiers. Signal output from the strain gages and load cell were monitored by digital voltmeters. The bolts were loaded at 250-pound increments, up to a maximum load of 2000

pounds. At each load increment, the voltage outputs of both the load cell and strain gage channels were recorded simultaneously.

The vertical calibration tests were conducted similar to the horizontal tests. Figure A-8 shows the vertical calibration test setup. The instrumentation setup was the same as that used for the horizontal calibration tests. Again, the bolts were loaded at 250-pound increments, up to a maximum load of 2000 pounds. The results from the calibration tests showed that the load-versus-signal-output curves were linear. Horizontal and vertical load-signal ratios for the two 1.25-inch diameter bolts were small. The horizontal sensitivity for the turned bolt was relatively large; however, the vertical sensitivity was only marginally acceptable.

The last instrumented bolt test series was a large vertical load test up to 5000 pounds. The purpose of the test was to observe the bolt behavior at the large loads and to test the ultimate load capacity of the anchors. The test setup was similar to that used in the vertical calibration tests, except the 5000-pound capacity load cell was replaced with a 50,000-pound capacity load cell. As before, the loading increment was approximately 250 pounds. Both bolts, with 6-inch embedment lengths, were loaded up to 5000 pounds. The load-versus-signal curves became slightly nonlinear beyond 3000 pounds. The bolt with a 4-inch embedment length failed at approximately 3500 pounds. Failure was identified by the reduction in the load cell output. Failure was abrupt and occurred in the polymer plug around the embedded bolt head.

Based on the tests results, the anchor bolt design with the reduced diameter at the strain gage location was chosen for use at North Field. Also, the embedment length used in the field installation would be 6 inches. The field calibration would be conducted up to 2000 pounds, including an unloading phase. Special attention would be given to the vertical load instrumentation channels because of the limited sensitivity of the instrumented anchor bolts in the vertical direction.

3. Mat Strain Gage Installation Tests

The mat strain gage installation was demonstrated in this test series. One-foot square segments of a polyester mat were used as the test specimens. The first part of the installation process tested was the surface preparation, which consisted of applying polyester resin to the mat section, sanding the attachment area, and conducting a special cleaning operation. The last part of the demonstration test was attaching the strain gage using the manufacturer's recommended procedures. The demonstration results showed that the polyester resin had to be contained in a small area to perform properly, the sanding operation required considerable time, and the gage bonding would be extremely difficult under field conditions.

4. Instrumentation Cable Tests

Two types of tests were conducted to evaluate potential problems with the instrumentation cable. The first test involved the quick disconnect and the corresponding increase in signal noise caused by the connector.

According to the connector manufacturer (Amphenol), if installed properly, the joined noise should be less than one microvolt. The test used one 5-pin connector joined to a segment of the instrumentation cable and the digital oscilloscope. A similar segment of instrumentation cable, without a connector, was used as a control specimen. In both cases the shield was properly grounded. There was no discernible increase in cable noise because of the connector, given a measurement accuracy on the order of 0.1 microvolt.

The second test evaluated the increase in cable noise because of 300-foot lead lengths. A strain gage circuit was connected to the conditioning amplifier using 10- and 300-foot leads. The digital oscilloscope monitored the output signal from the conditioning amplifier, set at 1000 gain. The signal noise test was conducted with and without shield grounding. Tests with the 300-foot leads and shield grounding did not show an appreciable increase in signal noise (less than 5 percent). This included tests with the 300-foot lead coiled and a large diameter circular arrangement. Tests involving the 300-foot lead and no shielding showed a substantial increase in cable noise compared to the 10-foot lead test. It was concluded from this test that using 300-foot leads with proper shielding should not appreciably increase the signal noise of the instrumentation system.

C. INSTRUMENTATION SYSTEM FIELD INSTALLATION

In tests involving instrumentation, the time required for field installation of the instrumentation system is usually the governing factor for the test schedule. A major constraint on the mat instrumentation study was that instrumentation installation and data acquisition could not affect the test schedule at the North Field Test. The system design, pretest planning, test preparation, and field installation had to reflected optimum installation time while maintaining accepted instrumentation installation standards. This section discusses the field installation procedures and instrumentation details.

1. Field Installation Schedule

Figure A-9 shows the test schedule for the crater repairs and aircraft events. As illustrated, the time interval between completing the crater repair subgrade and starting aircraft trafficking was only 5 days. The mat instrumentation installation, calibration, and processing/recording equipment setup had to be completed within these 5 days. Given the time constraints, it was imperative that all possible prerequisite tasks be completed before the final installation period. Figure A-10 shows the instrumentation installation schedule. As shown, installation began 3 weeks before the test series and was completed on the target date.

2. Crater Repair

At the test site, two runway craters, with apparent diameters of 25 and 26 feet, respectively, were formed with explosive charges. Crater 1 (25 feet in diameter) was chosen for the instrumented mat repair. The crater repair began with upheaval removal. Final crater diameter following upheaval removal was 48 feet at the crater centerline in the traffic direction. The

crater was filled with debris backfill to within 2 feet of the runway surface. The remaining depth was filled with compacted crushed stone, then leveled. The repair was covered with two 30- by 54-foot mat sections, joined to give one 60- by 54-foot mat. The mat was oriented with the hinges parallel to the runway centerline and anchored to the pavement on 18- or 36-inch centers (leading and trailing edges only). Anchoring was done with the standard 5/8-inch Wej-It® bolt and 16 specially designed instrumentation bolts, discussed previously.

3. Instrumented Anchor Bolt Installation

a. Bolt Preparation

Three axial gages were mounted to a 1.25-inch hardened-steel bolt turned down to a 1-inch outer diameter at the gage location, as shown in Figure A-11. Before attaching the gages, the mounting surface was sanded to create a suitable bonding surface. The mounting surface then was prepared using cleaners and degreasers, as described by the vendor (Measurements Group, Inc., Raleigh, North Carolina) (Reference 2). Next, three general-purpose 350 Ohm axial strain gages were bonded to the bolts with M-Bond 200 Adhesive (supplied by the gage manufacturer). Two gages were placed opposite each other, and the third gage was 90 degrees from the paired gages. The distance from the gage bottom to the top of the bolt bottom washer was 1.75 inches. Immediately after attachment, the gages were coated with polyurethane. Wire leads then were soldered to the two opposite gages as a half bridge (two active gages in the Wheatstone bridge), and the third gage was wired as a quarter bridge (See Figure A-2). Before coating the entire gage area with a 0.1875-inch thick butyl rubber coating, the gage installation was checked by loading the bolt as a cantilever beam and monitoring the strain gage output for linearity and accuracy.

b. Field Installation

The instrumented bolts were anchored to the pavement with polymer plugs. Using a core drill, a 3-inch diameter hole was bored 8 inches into the pavement/subgrade. A 4-inch diameter countersink hole was bored 1 to 2 inches deep to prevent the bolt from contacting the pavement and to provide clearance for wire leads. The bolt was placed in the hole with the threads facing up and held at the proper depth by a piece of plywood, as shown in Figure A-12. After the bolt was centered in the hole so the opposite gages lined up with the traffic direction and the single gage faced North, the pavement was marked to facilitate recentering. As shown in Figure A-13, the bolt then was moved to one side of the hole. Ashland polyurethane, catalyzed for a 3-minute set time (Ashland resins 65-088 and B65-032, and Ashland catalyst 65-018), was poured into the hole. Before the polymer set, the bolt was recentered in the hole to give the final installation shown in Figure A-14.

4. Mat Strain Gage Installation

To facilitate gage attachment, it was first necessary to create a smooth area on the mat surface. To do this, the polyester resin

(Owens-Corning CX-1854), which is used in mat construction, was catalyzed at a rate of 1 percent by weight with Freeman Thermacure Super Fast catalyst to give a 15-minute set time. The catalyzed resin was added to a circular area approximately 2 inches in diameter and was contained by a 0.25-inch high ring of DAP sealant. Just enough polyester was added to give a thin layer on the mat surface. After the polyester had cured sufficiently (approximately 1 hour), the area was sanded smooth. Two of these circular areas were created for each gage attachment, one for the strain gage and the other for a bondable terminal. The circular areas were approximately 5 inches apart, center to center. After surface preparation, the strain gages and terminals were installed. First, the surfaces were prepared using cleaners and degreasers, as described in (Reference 3). Next, a general-purpose 1000 Ohm axial strain gage was bonded to the innermost circular area, and a bondable terminal was attached to the outermost circular area (Figure A-15). Both the strain gage and terminal installation used M-Bond AE-10 (Reference 4). The axial gage was oriented in the longitudinal panel direction. Immediately after attachment, the gage was given a protective polyurethane coating. Wire leads were soldered from the gage to the terminal, as shown in Figure A-15. To provide strain relief, the wires were bonded to the mat using the M-Bond 200 adhesive.

To protect the gage from moisture and mechanical damage, the gage area was covered with a protective coating of M-Coat F (Reference 5). The coated area included the strain gage and the lead wires running from the gage to the terminal. Figure A-16 shows the completed mat gage installation. After the gage area was coated with the M-Coat F, a 0.25-inch hole was drilled in the mat 3.5 inches from the gage and terminal area. The instrumentation lines running under the mat were pulled through the access hole and soldered to the terminal. For additional protection, a piece of randomly oriented, chopped fiberglass, soaked in polyester resin, was placed over the entire gage area. To provide strain relief, the instrumentation wires were looped on the mat surface and covered with tape before adding the polyester-soaked fiberglass.

5. Instrumentation Cable Installation

The mat sensors were connected to an instrumentation van by the main instrumentation cable. The cable consisted of 52 separate lines, each consisting of two individually shielded, twisted pairs. The main cable terminated at the instrumentation van with six 37-pin Amphenol connectors (quick-disconnect).

At the instrumented mat, the main cable was divided into two groups of 26 lines each, with one group going to the East side of the mat and the other going to the West. Narrow trenches were cut in the concrete and underneath the mat to recess the instrumentation wire, protecting both the wires and the aircraft from potential damage (Figure A-17). At each side of the mat, the main trench ran parallel with the anchor bolts. Smaller side trenches ran from each main trench to the mat gages and the instrumented bolts (Figures A-18 and A-19). After the wires were in place, the portion of each main trench from the mat edge to the runway edge was filled with grout.

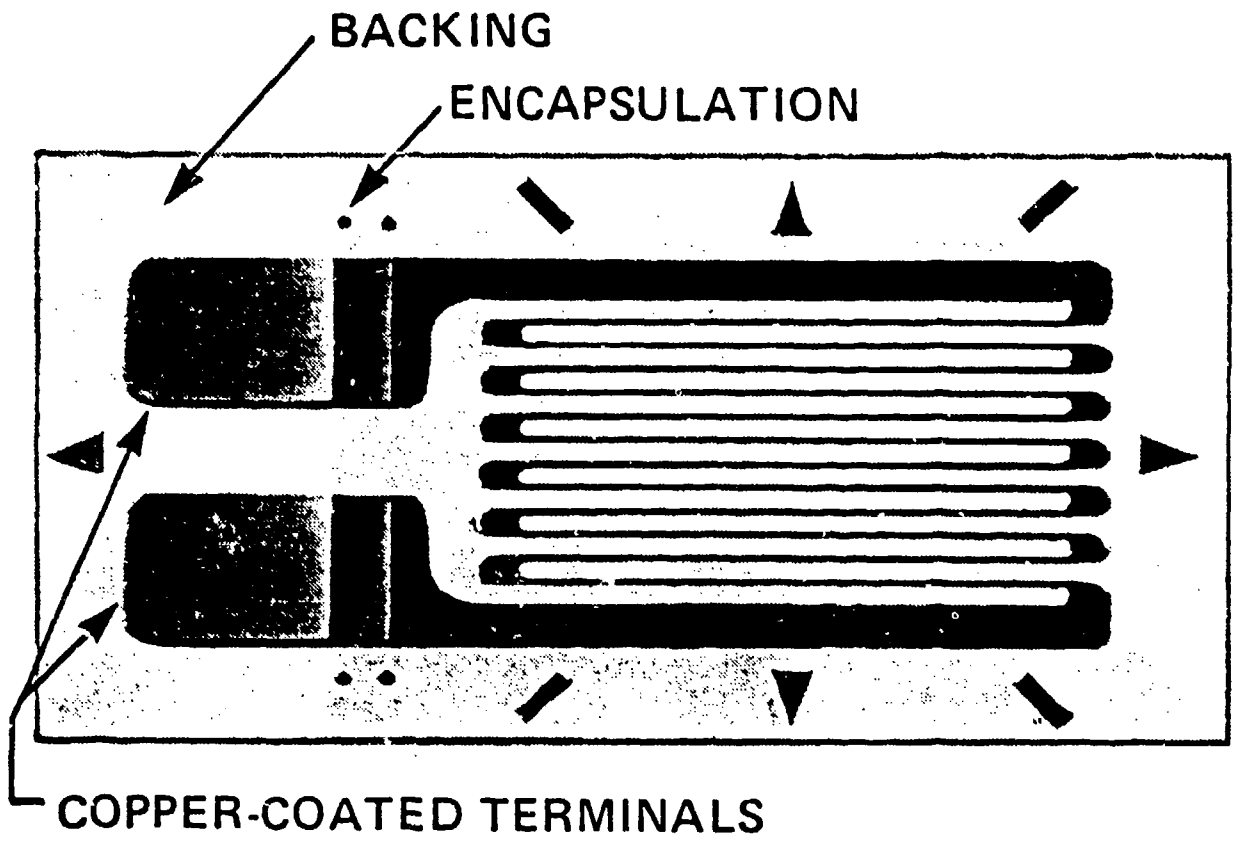

Figure A-1. Expanded View of Foil-Type Strain Gage

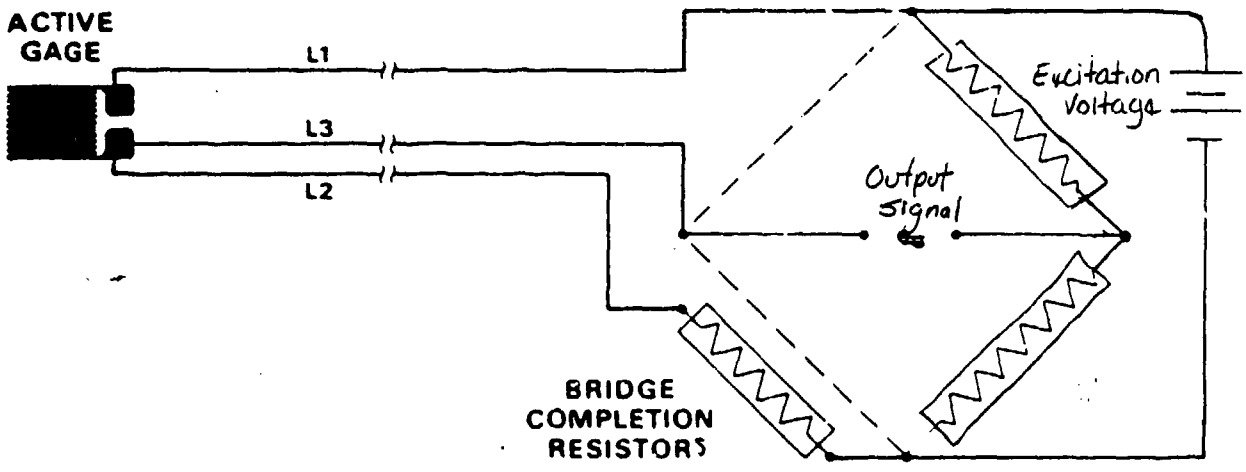

Figure A-2. Single Active Gage - Quarter Bridge Wheatstone Bridge

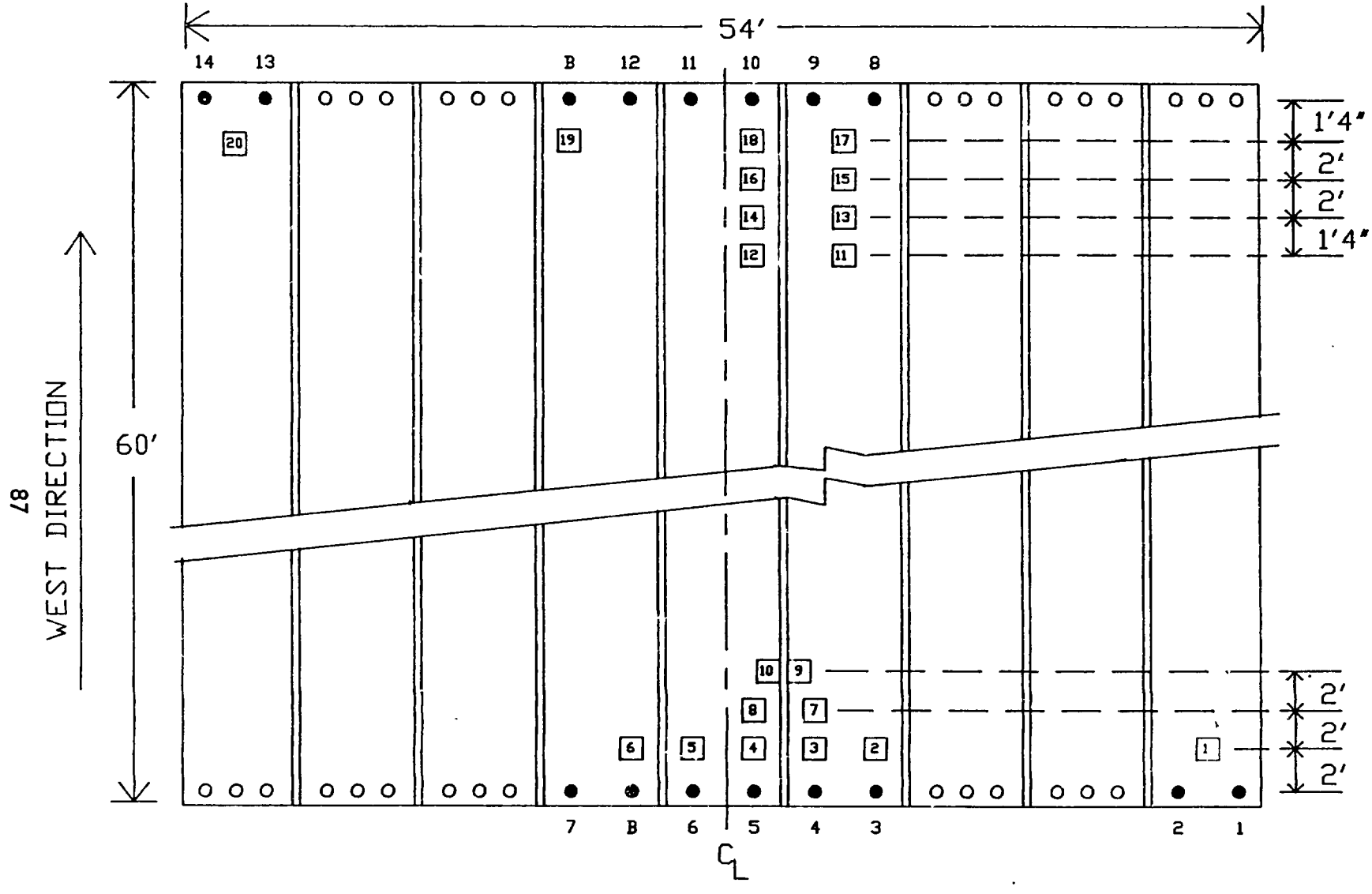

Figure A-3. Final Mat Instrumented Anchor Bolt and Strain Gage Locations

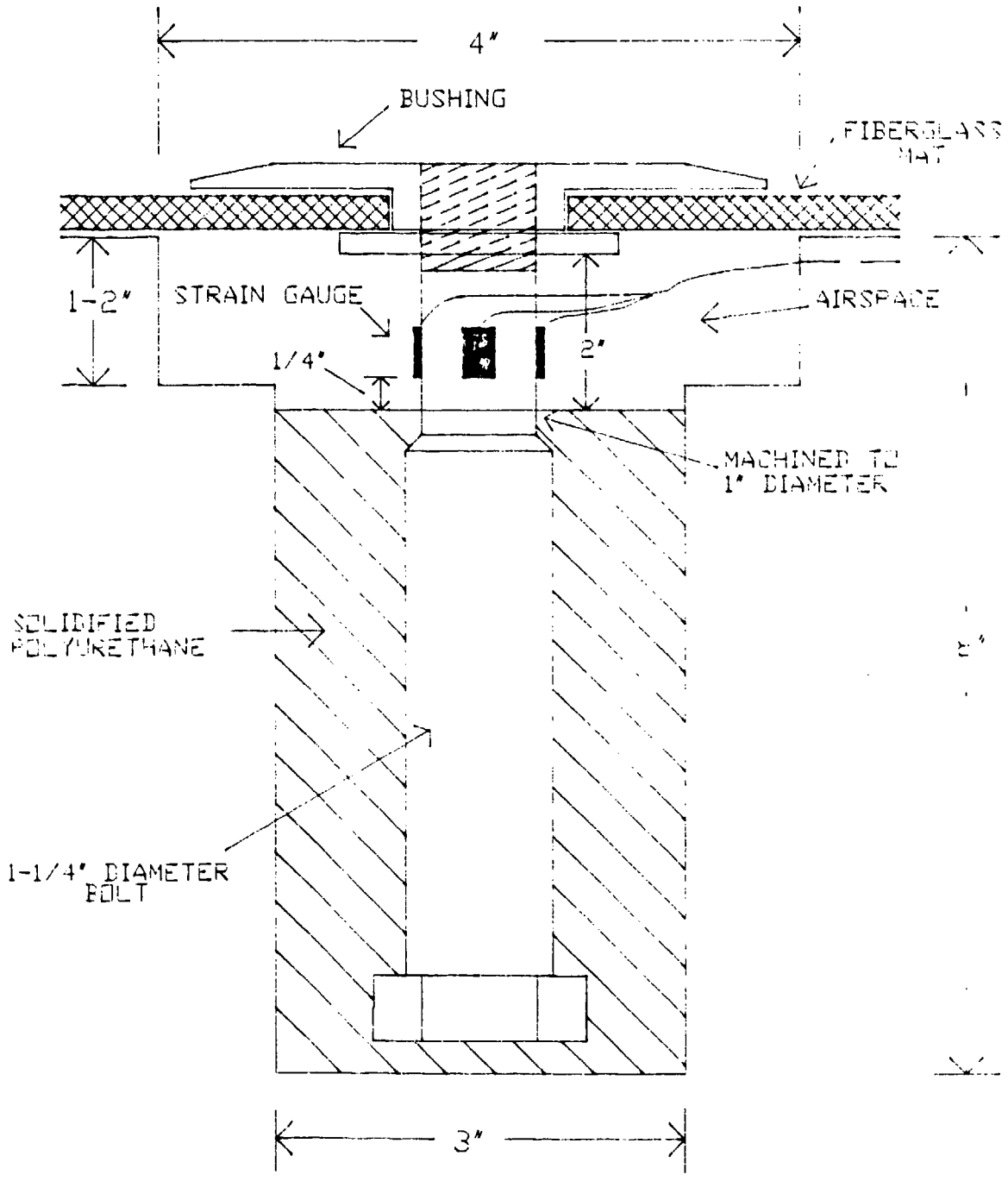

Figure A-4. Instrumented Anchor Bolt Design

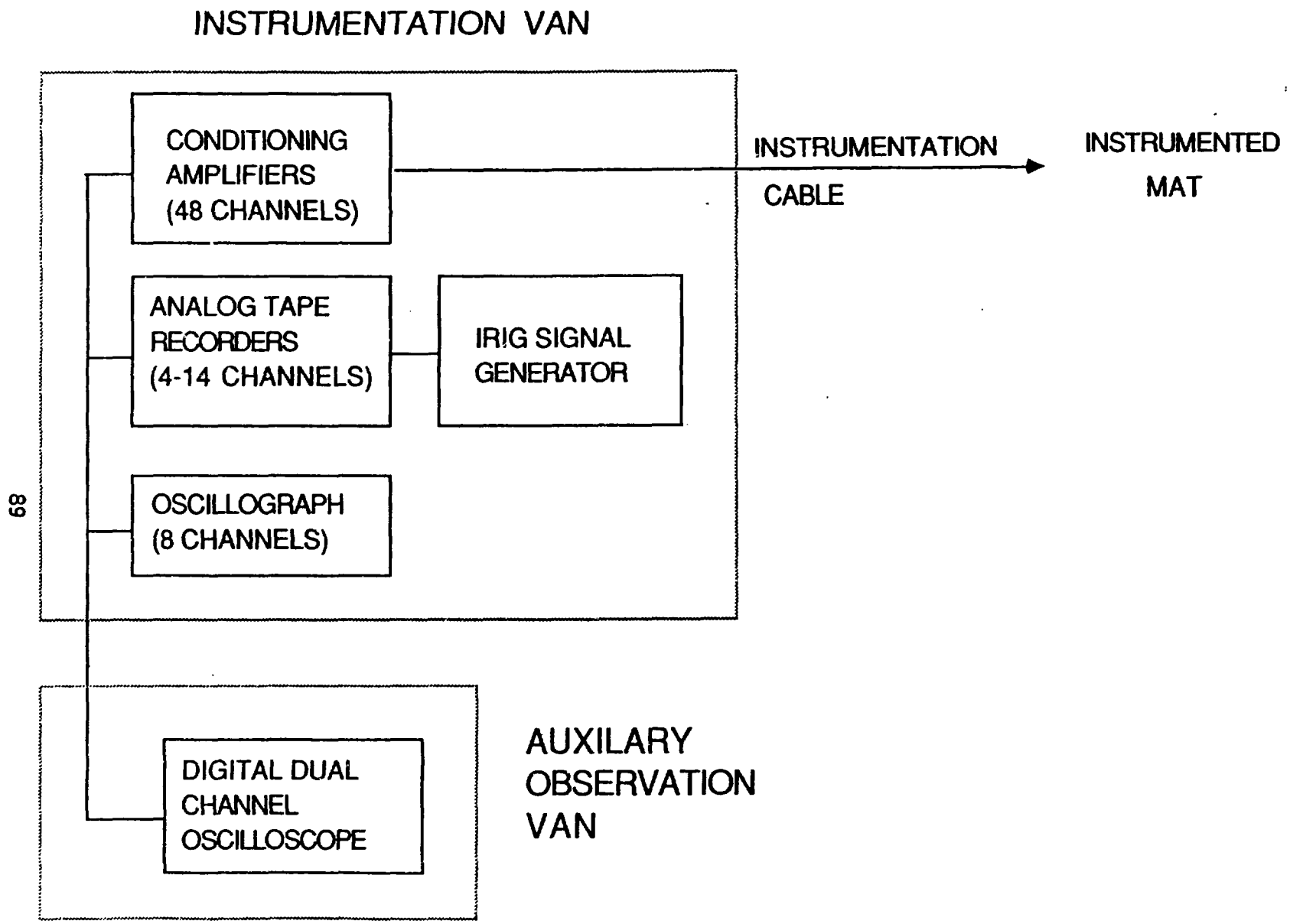

Figure A-5. Signal Conditioning and Data Acquisition System

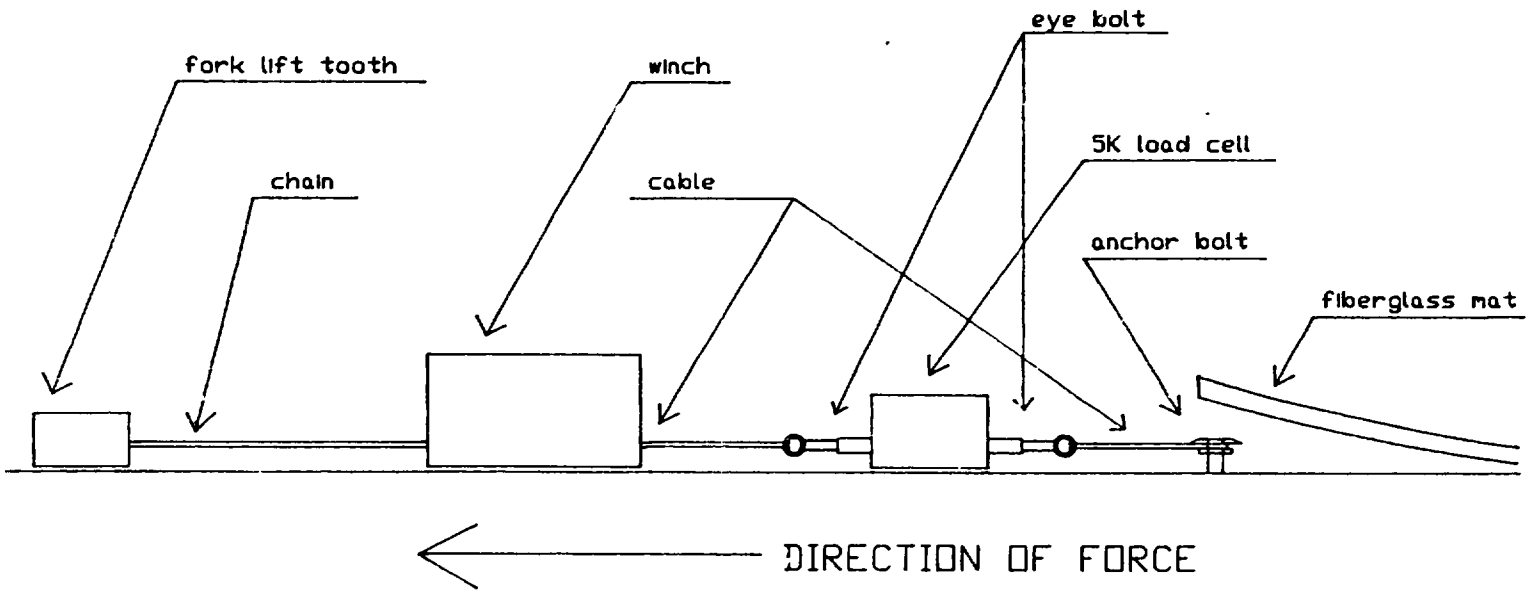

Figure A-6. Setup Used for Static Horizontal Load Anchor Bolt Calibration Tests

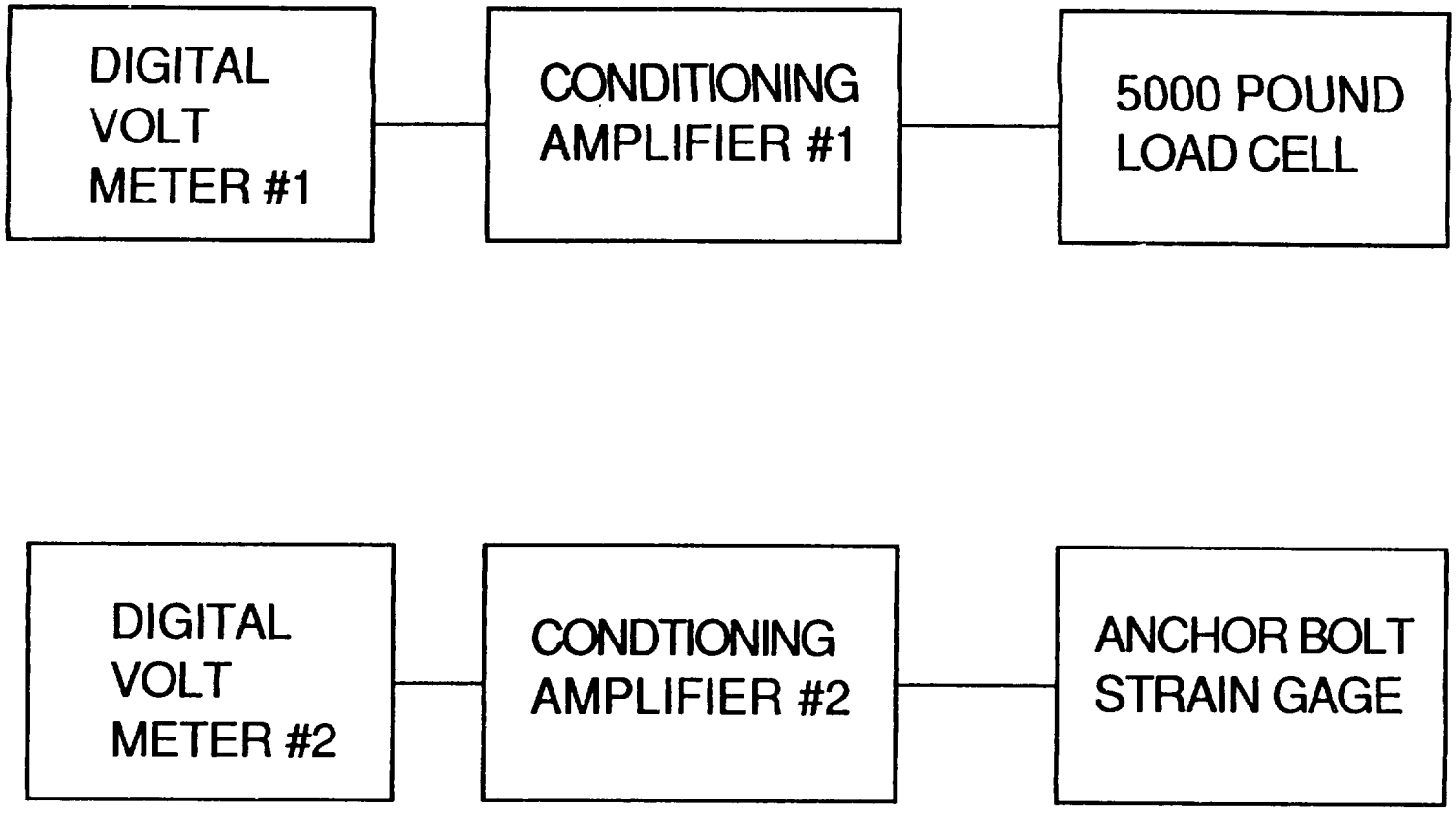

Figure A-7. Instrumentation Setup for Anchor Bolt Calibration Tests

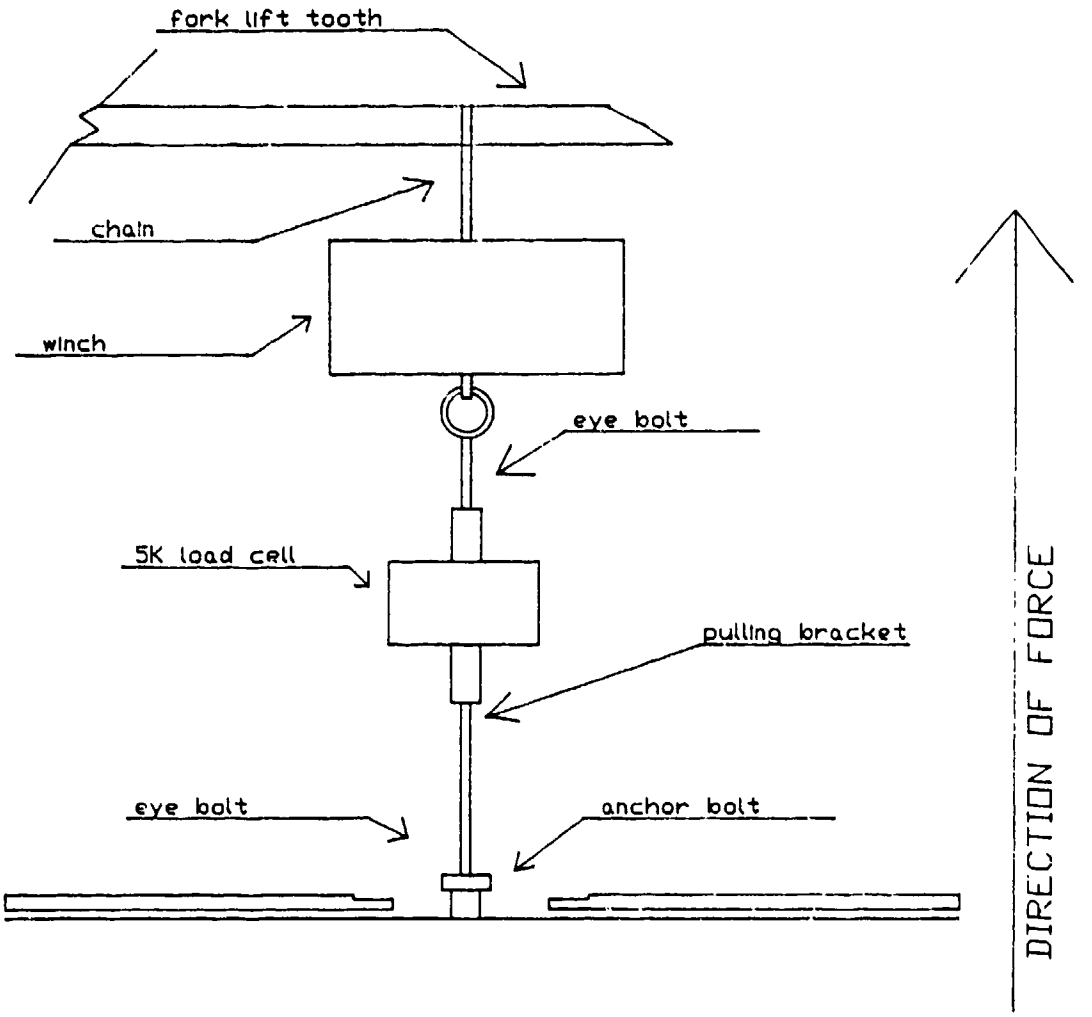

Figure A-8. Setup Used for Static Vertical Anchor Bolt Calibration Tests

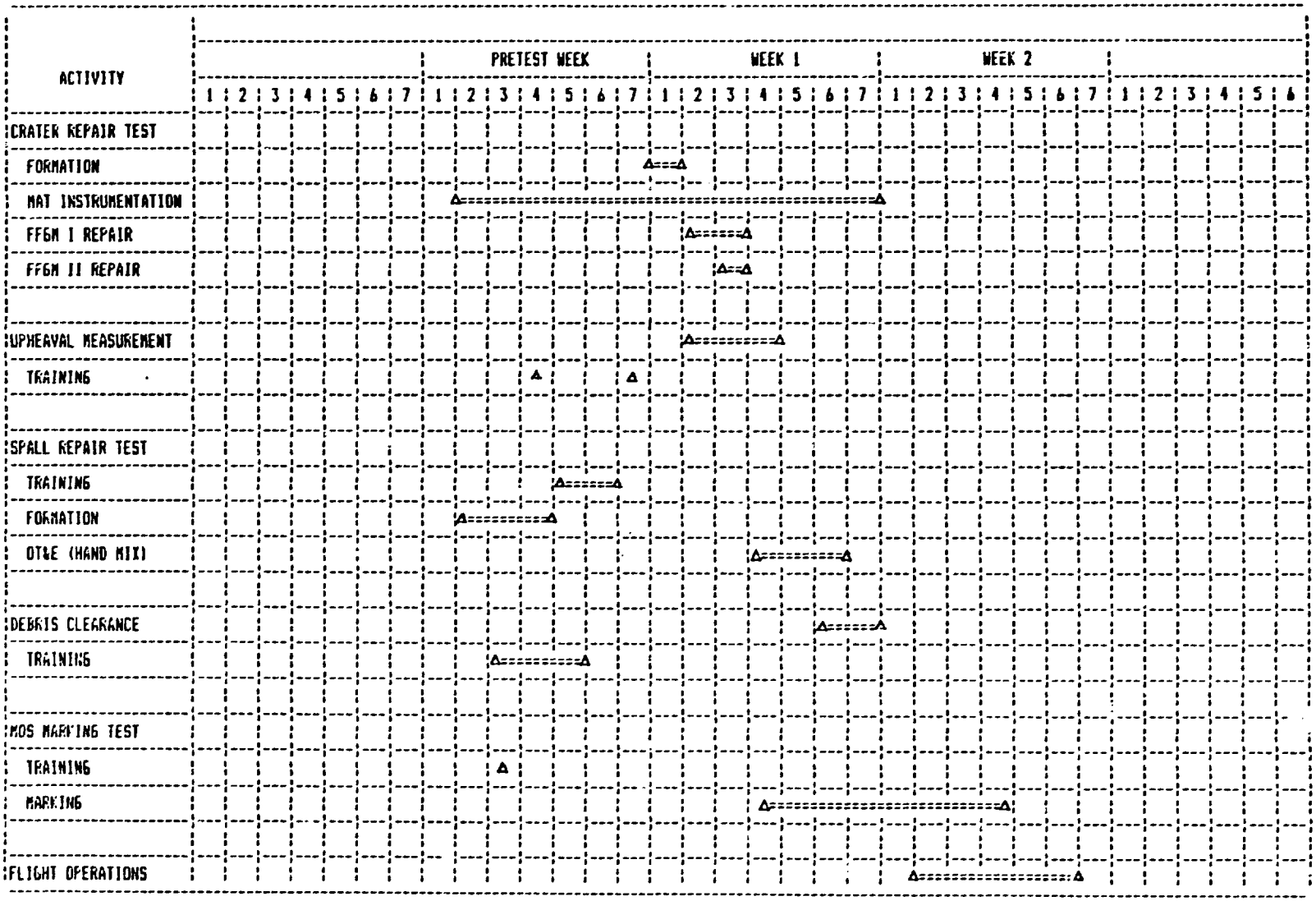

Figure A-9. North Field 87 RRR Test Schedule

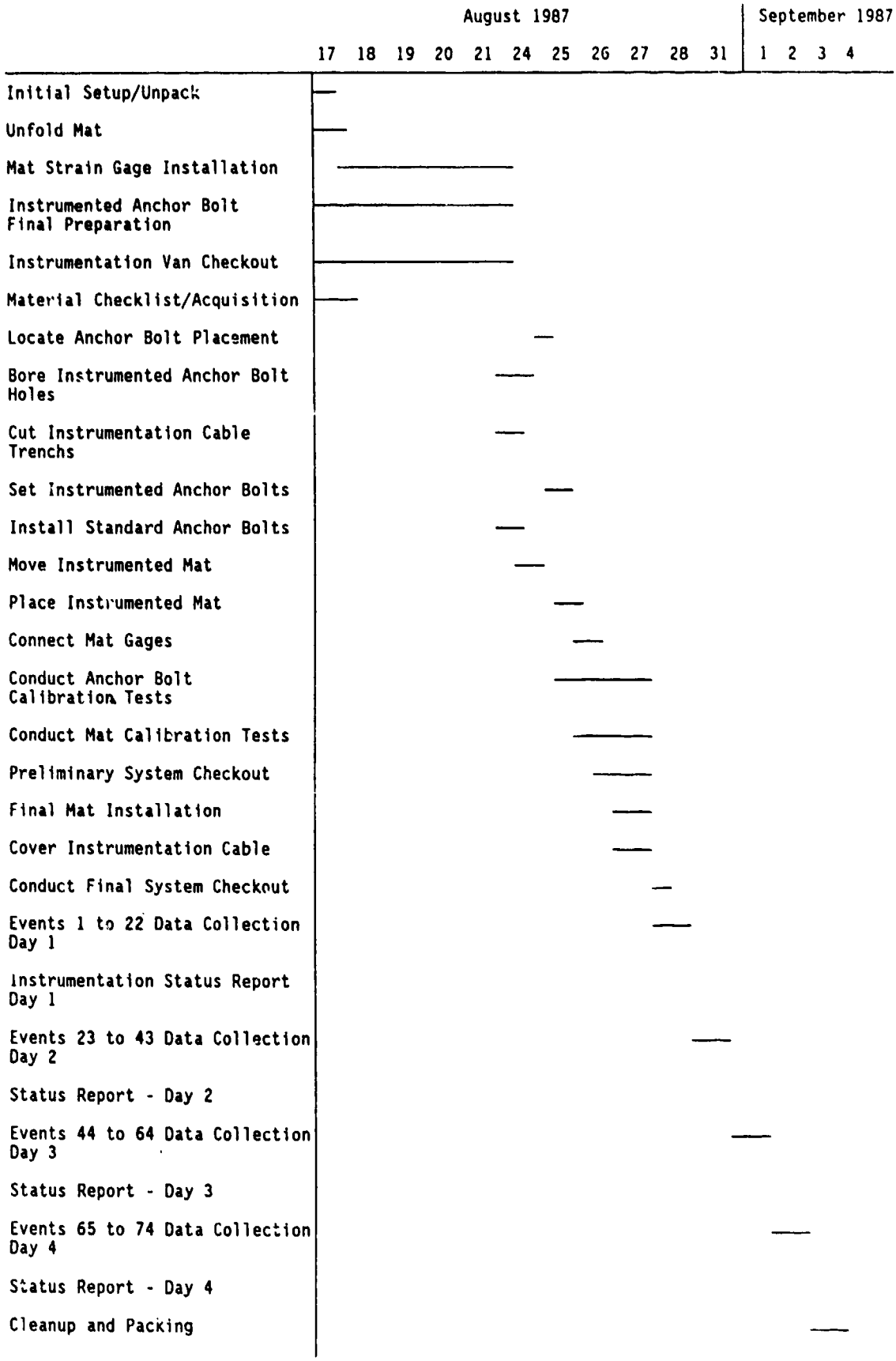

Figure A-10. Instrumentation Installation Schedule

Figure A-11. Axial Gages Mounted to 1.25-Inch Steel Anchor Bolts

Figure A-12. Mechanism Used to Place the Bolt to the Proper Depth in the Anchor Hole

Figure A-13. Polymer Being Added to Anchor Hole

Figure A-14. An Instrumented Anchor Bolt Set in a Polymer Plug

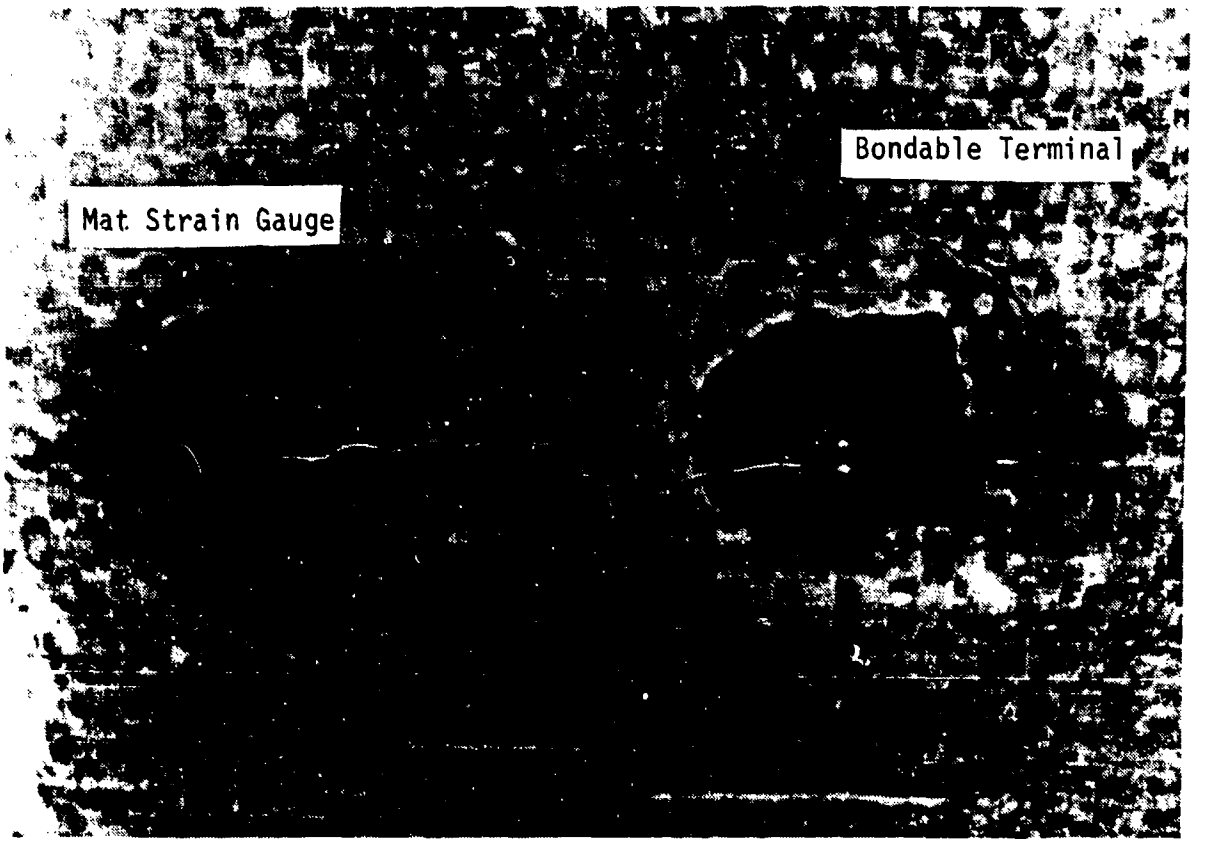

Figure A-15. Strain Gauge and Terminal Glued to Mat and Connected by Wire Lead

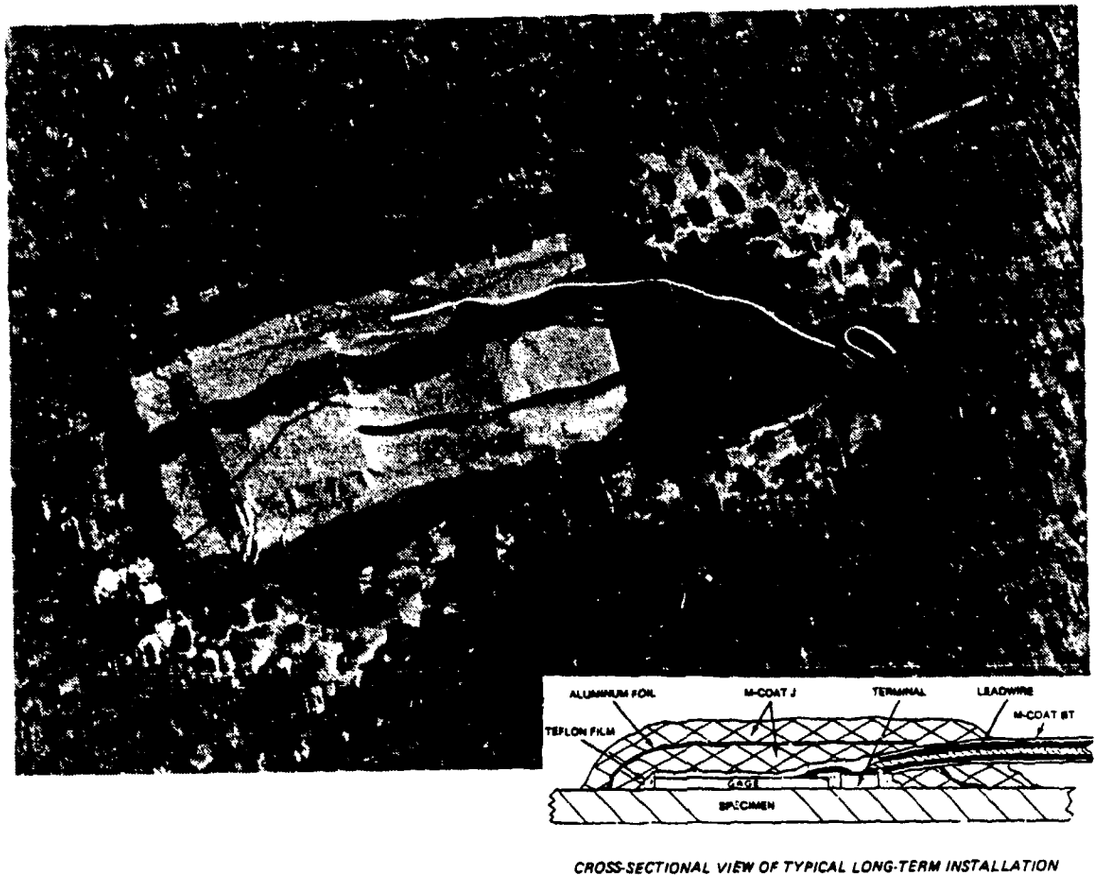

Figure A-16. Gauge Area Coated with M-Coat F and Aluminum Foil Tape

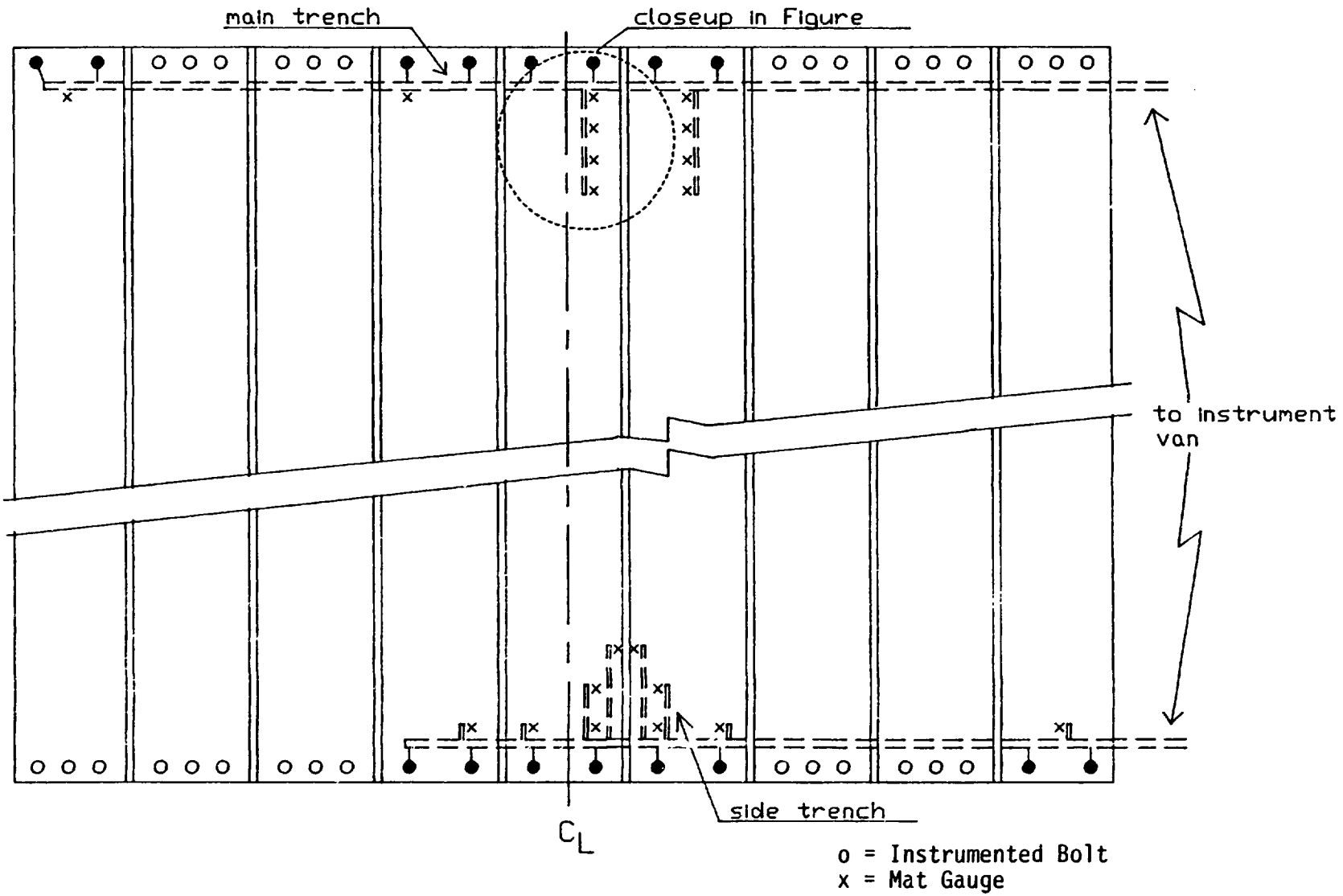

Figure A-17. Layout of Instrumentation Wire Trenches Under Mat

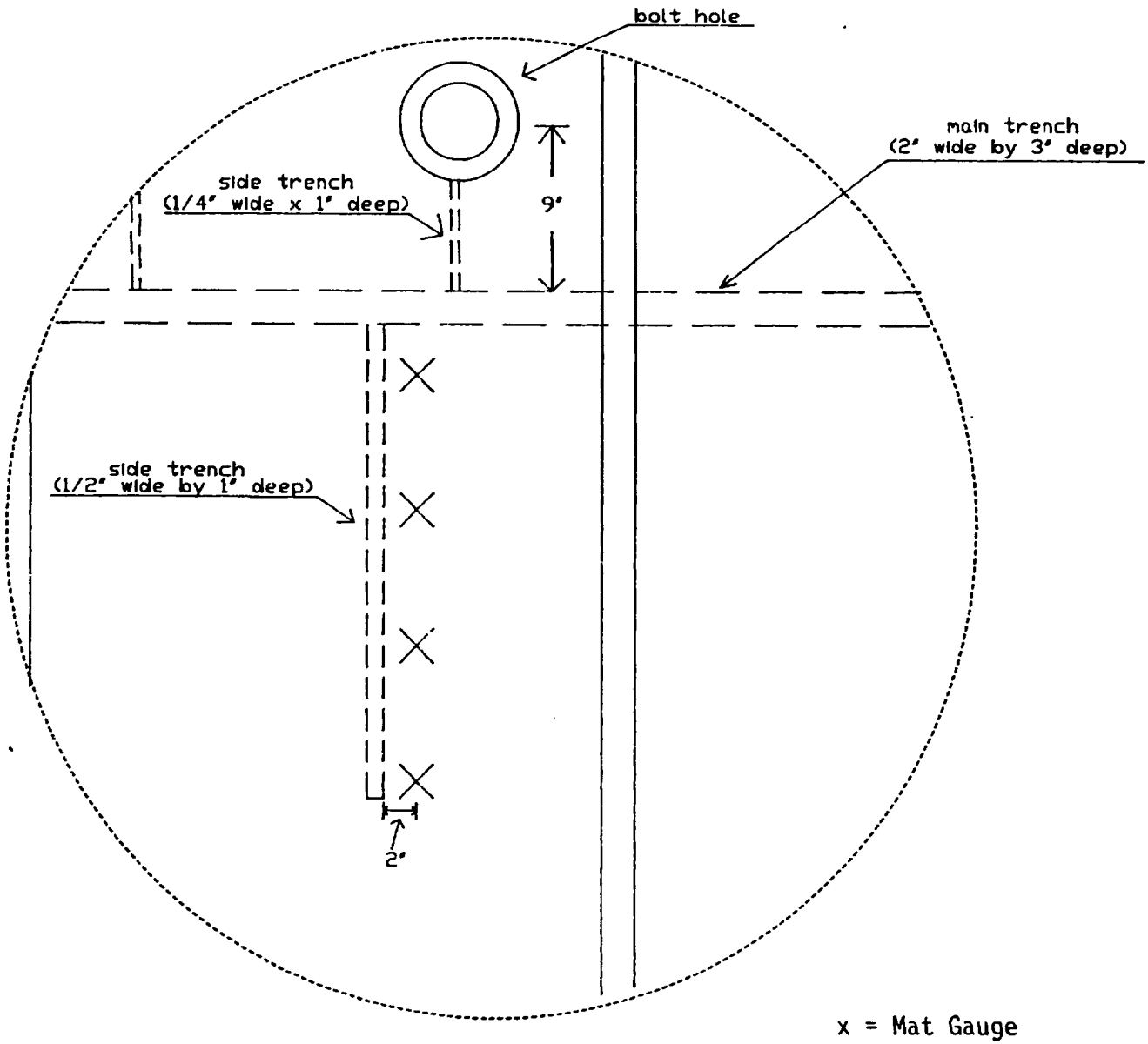

Figure A-18. Instrumentation Wire Trench Dimensions

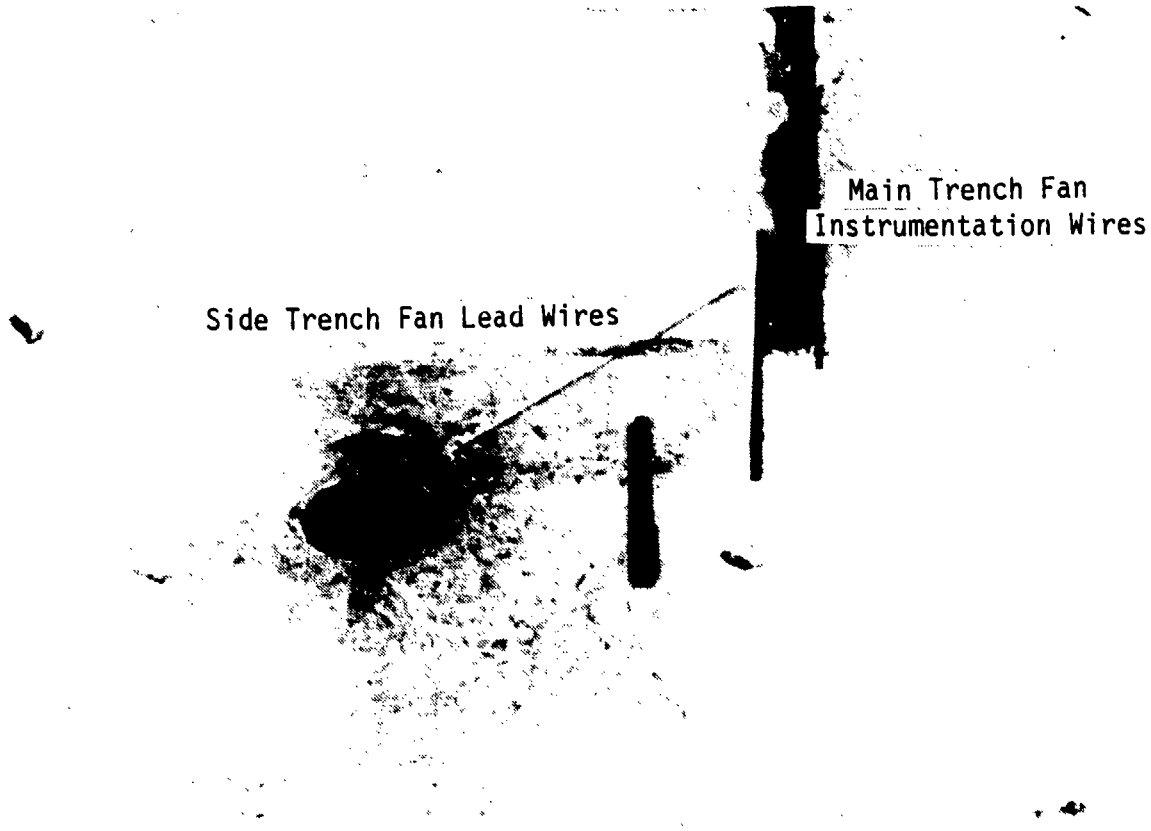

Figure A-19. Anchor Bolt Hole with Side Trench Fan Lead Wires and Main Trench Fan Instrumentation Wires

(The reverse of this page is blank.)

APPENDIX B

UNFILTERED, HORIZONTAL ANCHOR BOLT LOADS

FOR EVENT 187

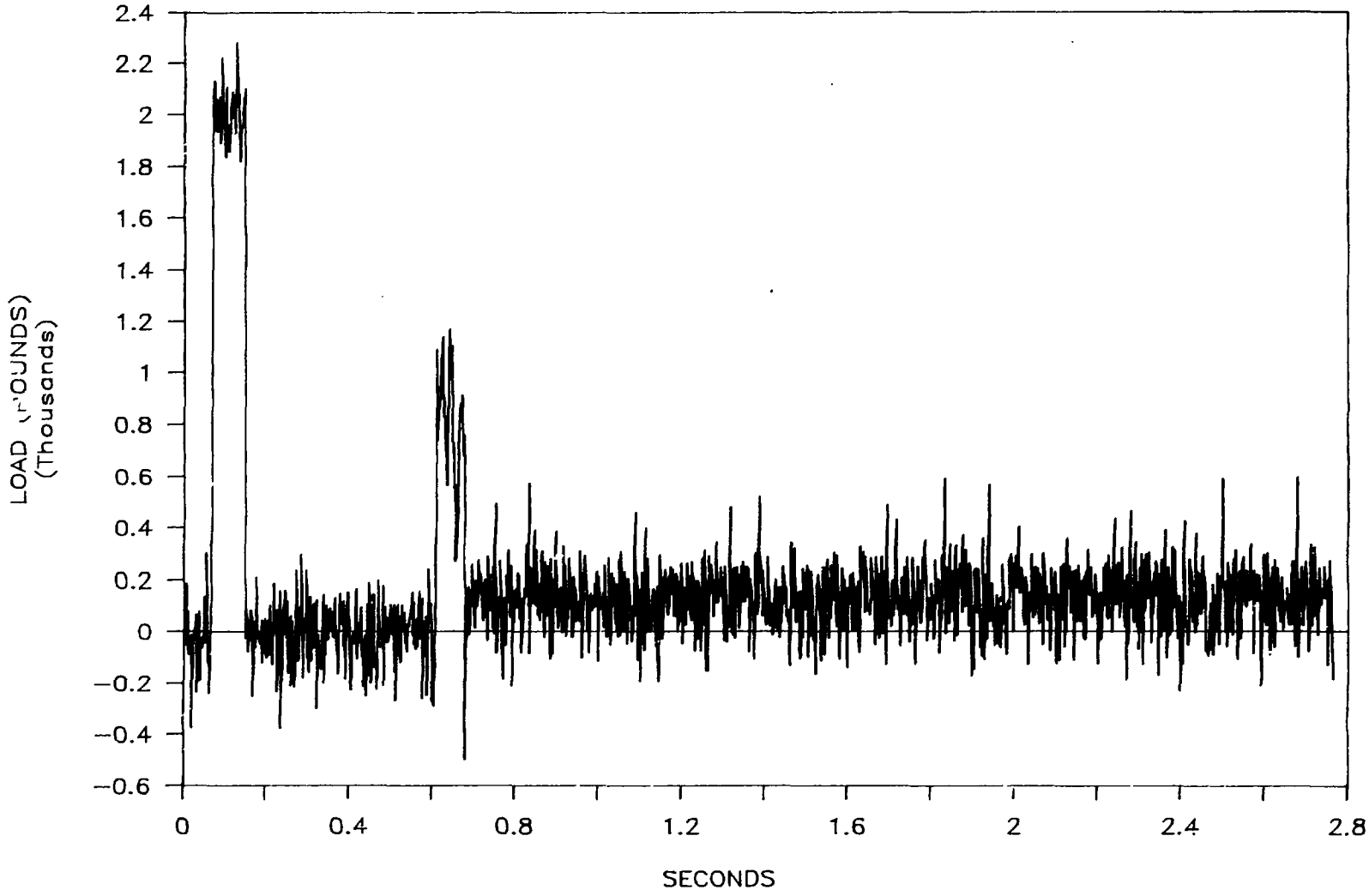

Figure B-1. Bolt 1, In-Plane Horizontal Anchor Bolt Load, Event 187, F-15 East Taxi (Hard Braking)

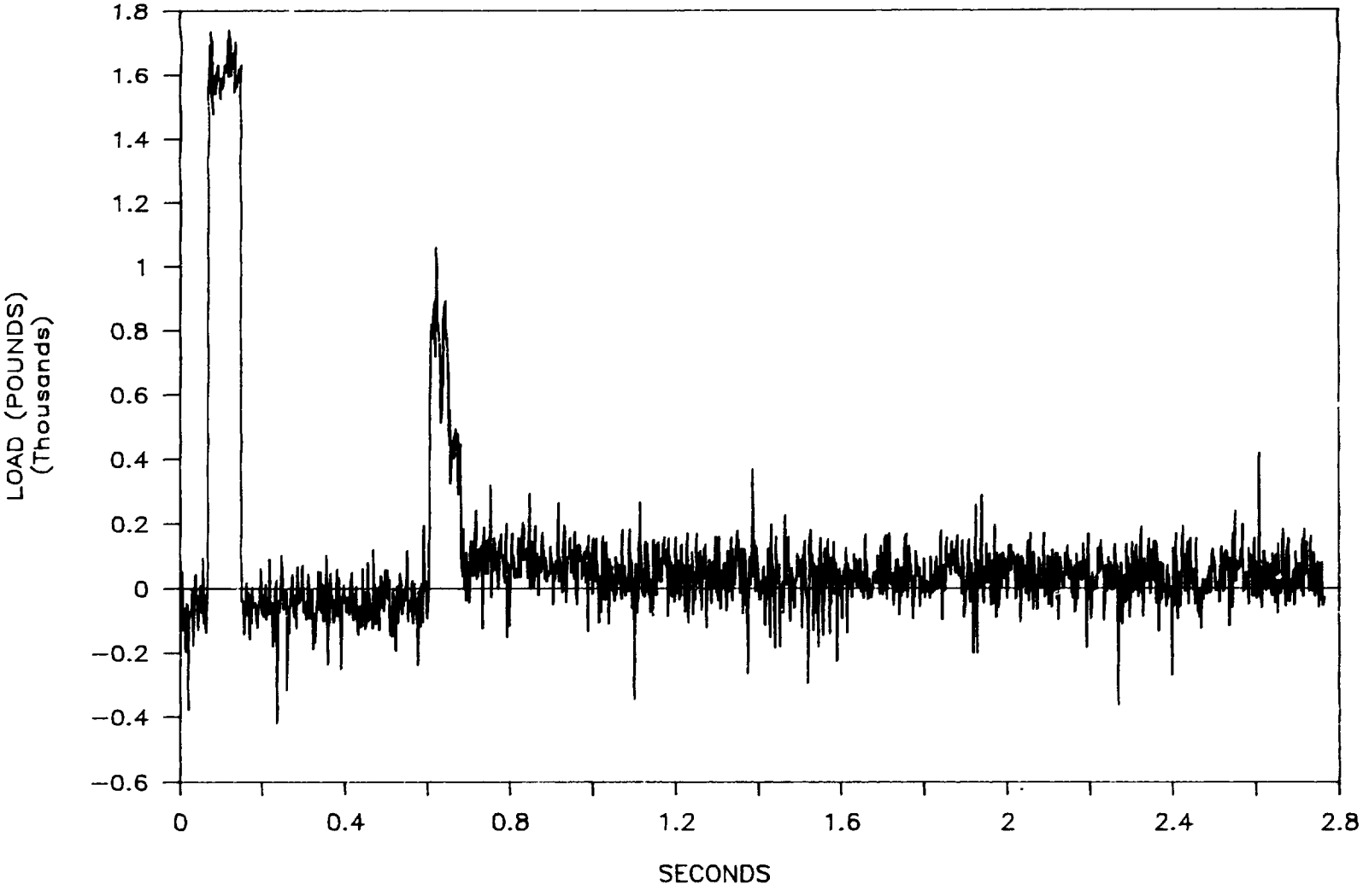

Figure B-2. Bolt 2, In-Plane Horizontal Anchor Bolt Load, Event 187, F-15 East Taxi (Hard Braking)

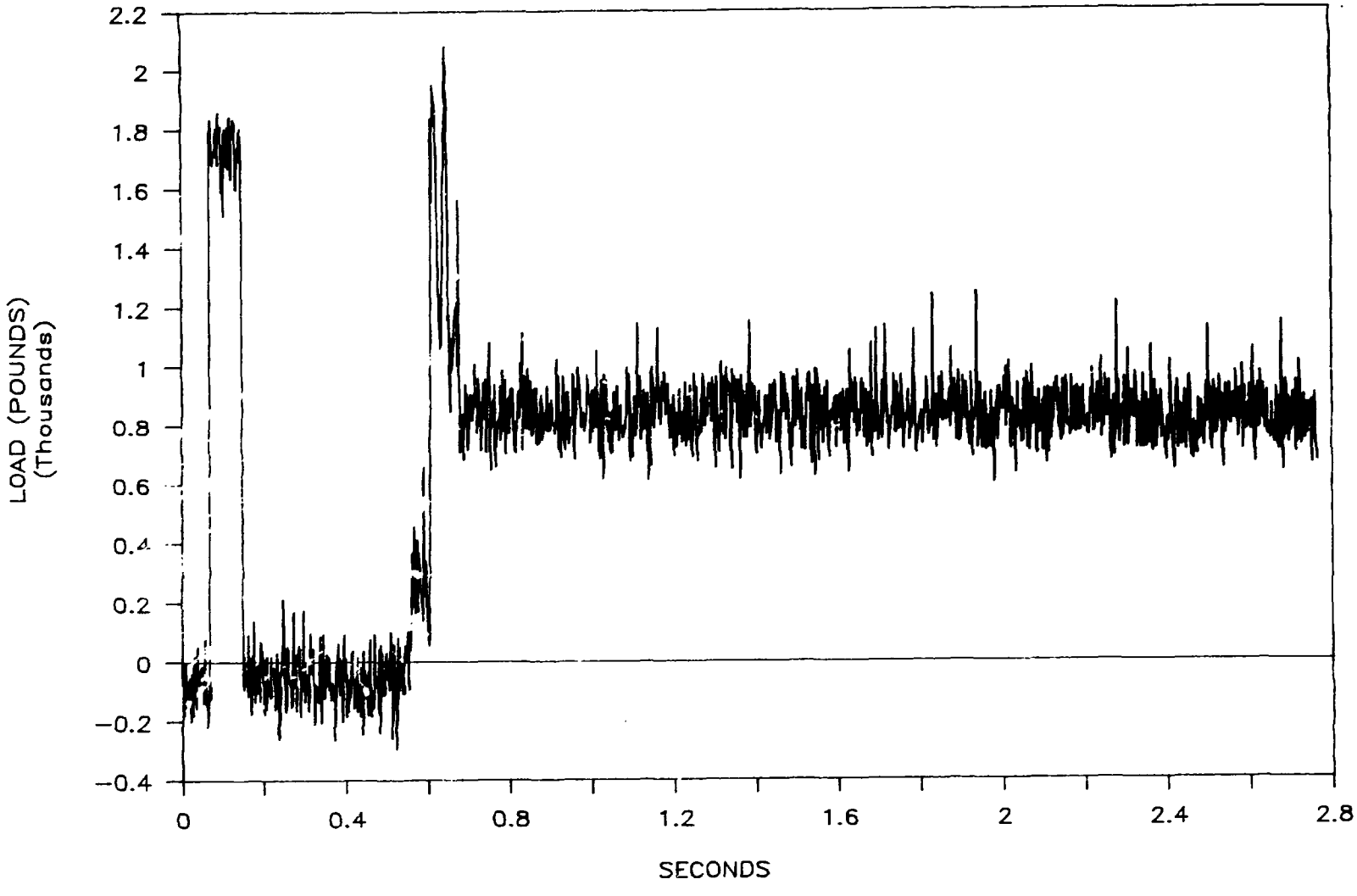

Figure B-3. Bolt 4, In-Plane Horizontal Anchor Bolt Load, Event 187, F-15 East Taxi (Hard Braking)

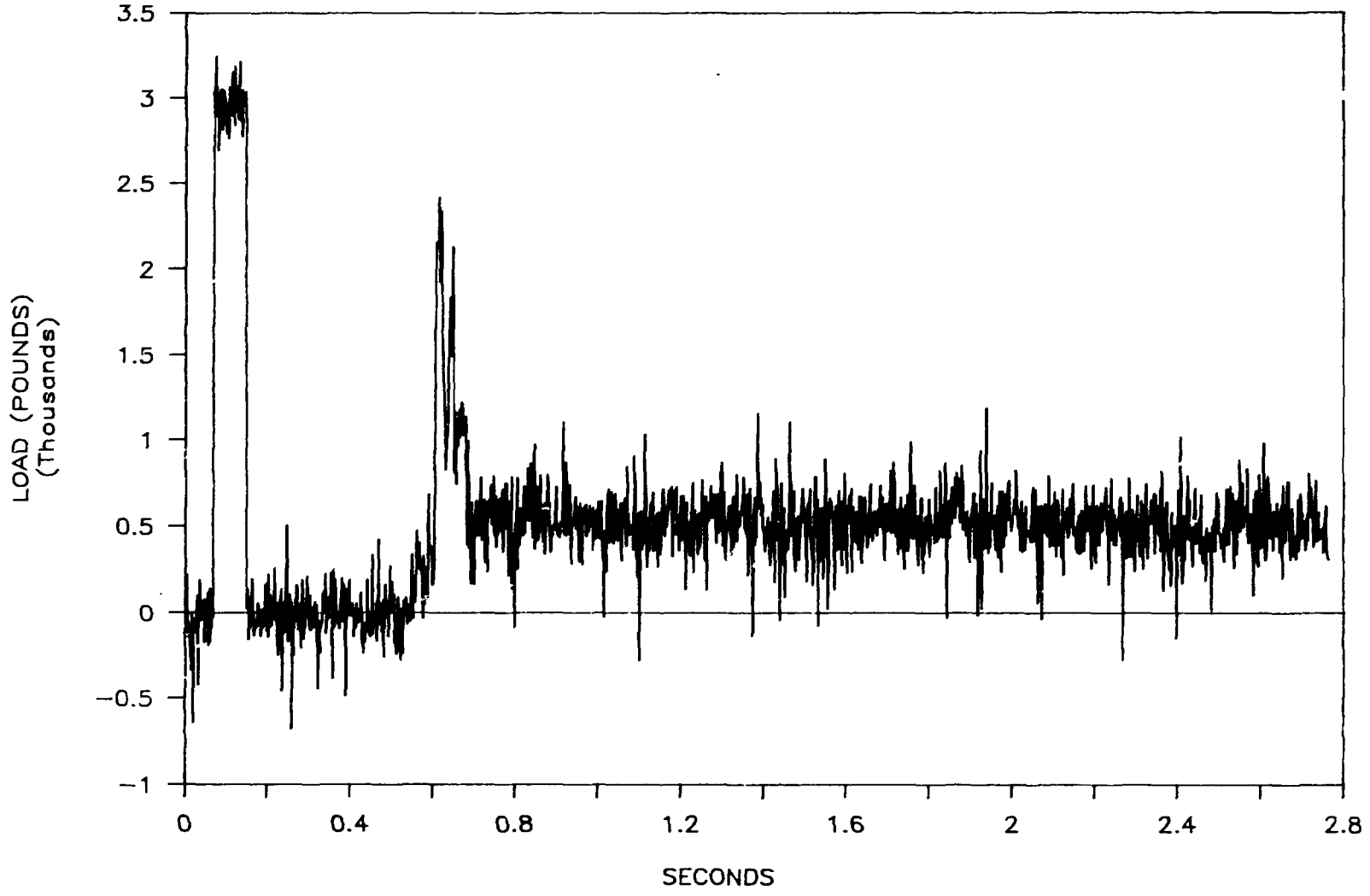

Figure B-4. Bolt 5, In-Plane Horizontal Anchor Bolt Load, Event 187, F-15 East Taxi (Hard Braking)

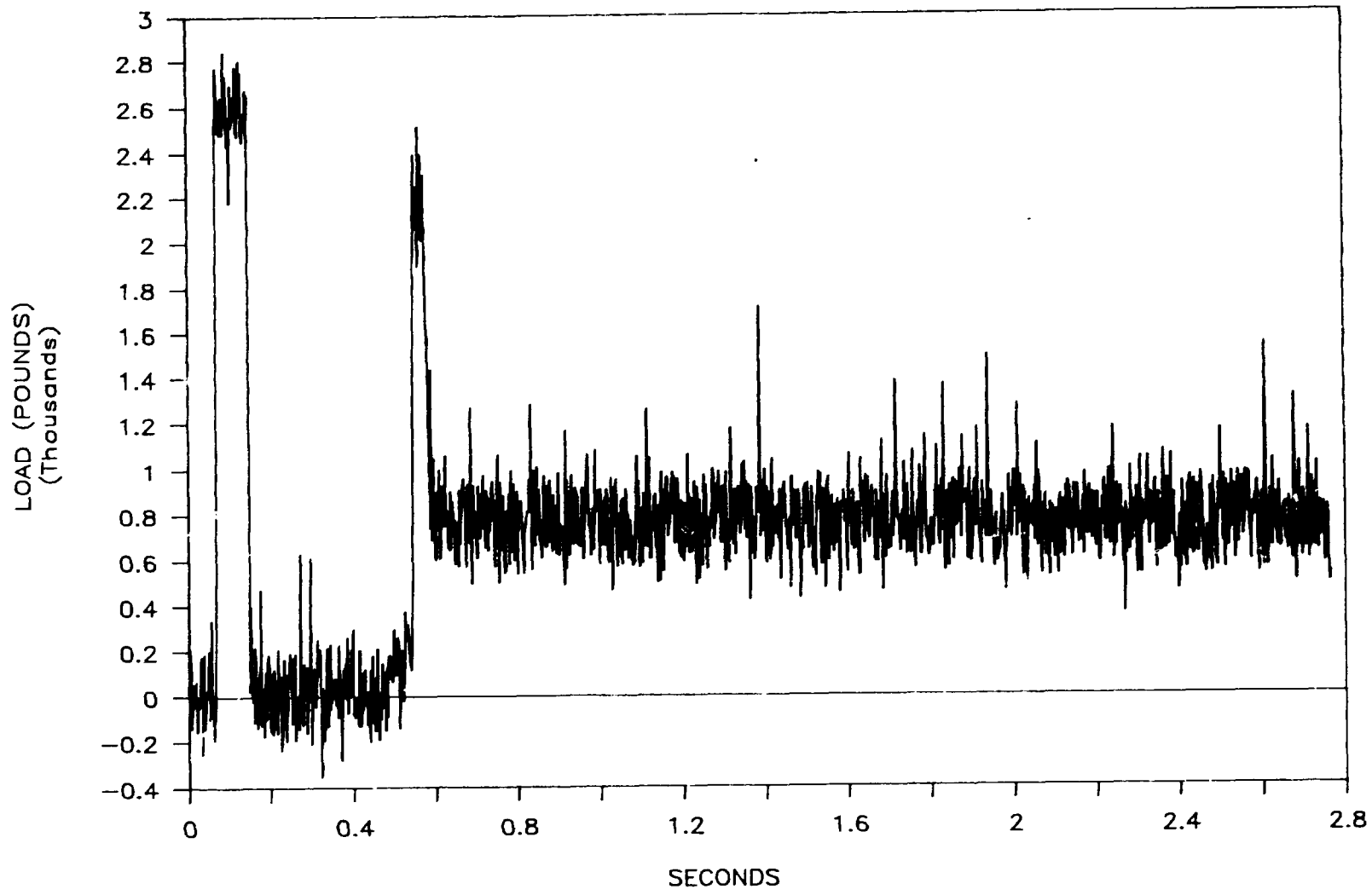

Figure B-5. Bolt 6, In-Plane Horizontal Anchor Bolt Load, Event 187, F-15 East Taxi (Hard Braking)

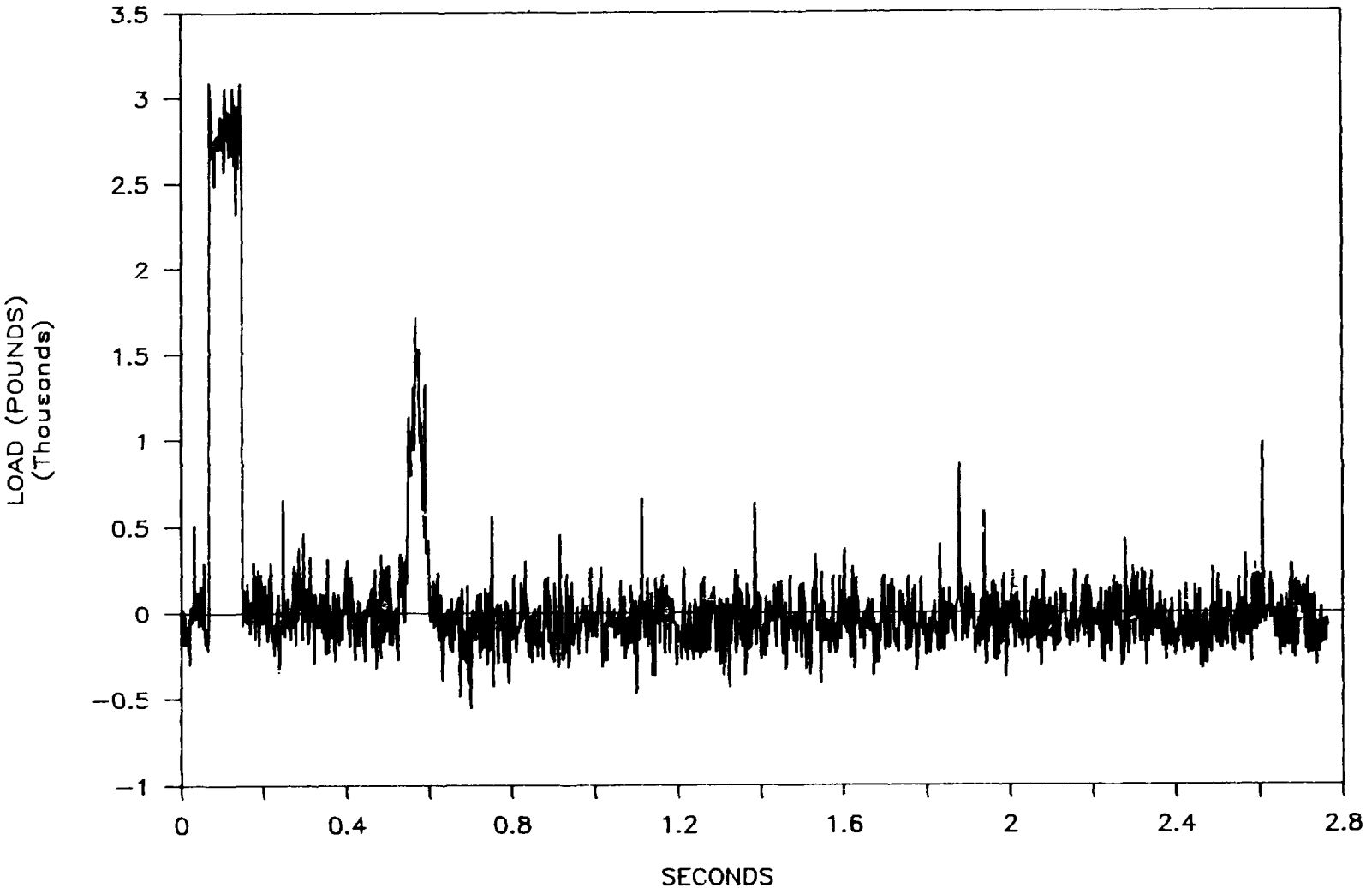

Figure B-6. Bolt 8, In-Plane Horizontal Anchor Bolt Load, Event 187, F-15 East Taxi (Hard Braking)

(The reverse of this page is blank.)

APPENDIX C

MAT AND CONCRETE AND MAT AND CRUSHED STONE

STATIC FRICTION COEFFICIENT TESTS

In support of the mat analysis effort, static friction coefficient tests were conducted between a mat section and concrete, and also between a mat section and crushed stone. The purpose of the test was to provide estimates for the static friction coefficient for the mat when supported by concrete and by crushed stone.

The tests were conducted at the Small Crater Test Facility using the test setup shown in Figure C-1. As shown in Figure C-1, the mat test specimen was a polyester mat section, approximately 8 inches wide by 14 inches long. The test series consisted of four events: two on crushed stone and two on concrete with a textured finish. At each location, care was taken to ensure that loose material on the surfaces was removed before placing the mat section. The mat sections were loaded vertically by calibrated weights. Four vertical load increments were used: 40.2, 80.4, 145, and 190 pounds. At each load increment, a gradually increasing lateral load was applied to the weighted mat section until incipient sliding was generated. The lateral load was measured by a 400-pound spring scale, which was checked for accuracy using calibrated weights. Measurement accuracy of the scale was approximately +/- 1 pound. The maximum lateral load resisted by the weighted mat section was recorded for each vertical load value.

Tables C-1 and C-2 show the results from the crushed stone and concrete surfaces, respectively. The average static coefficient of friction measured between the mat section and the crushed stone surface is 0.14. The static coefficient of friction between the mat section and the textured finished concrete is 0.37. For both surfaces, the static coefficient of friction measured with a vertical load of 40.2 pounds, was similar to that documented with a vertical load of 190 pounds. This simple test indicates that the static coefficient of friction between the mat and the textured concrete is more than twice that measured for the mat on crushed stone. Not shown in the tables is the reduction of friction resistance following incipient sliding, which was, on average, approximately one-half the maximum friction resistance.

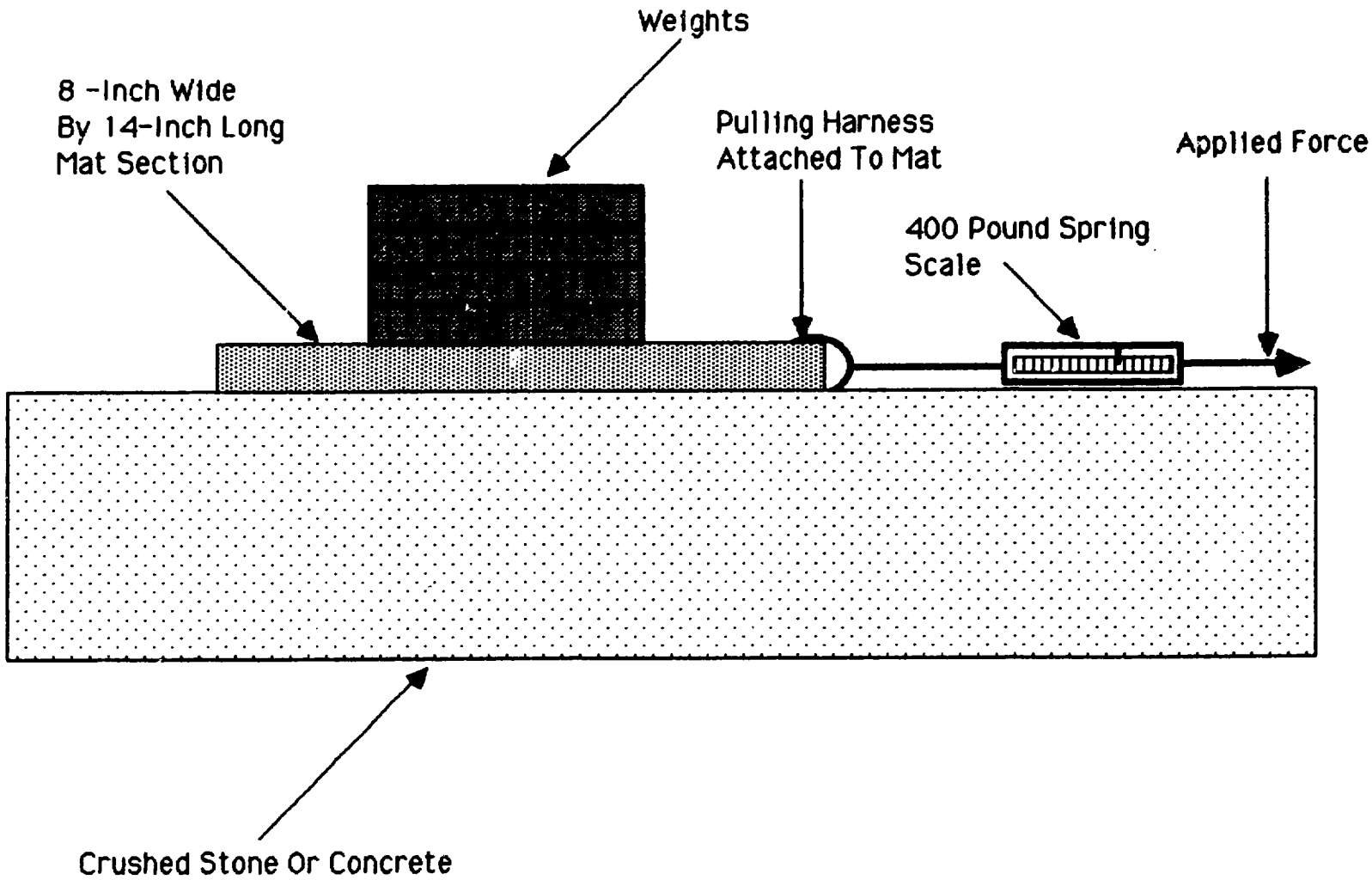

Figure C-1. Friction Test Configuration

TABLE C-1. STATIC COEFFICIENT OF FRICTION TEST RESULTS, MAT SECTION ON CRUSHED STONE

Location	Vertical Load (lb)	Maximum Horizontal Resistance (lb)	Static Coefficient of Friction
1	40.2	6	0.15
1	40.2	3.5	0.09
1	40.2	3.5	0.09
1	80.4	9.5	0.12
1	80.4	8.5	0.11
1	80.4	5.5	0.07
1	145	25	0.17
1	190	28.5	0.15
2	40.2	5	0.12
2	40.2	5.5	0.14
2	40.2	4	0.10
2	80.4	9.5	0.12
2	80.4	10	0.12
2	80.4	10	0.12
2	145	23	0.16
2	145	23	0.16
2	145	23	0.16
2	190	26.5	0.14

Average Static Coefficient of Friction = 0.14

TABLE C-2. STATIC COEFFICIENT OF FRICTION TEST RESULTS, MAT SECTION ON CONCRETE WITH TEXTURED FINISH

Location*	Vertical Load (lb)	Maximum Horizontal Resistance (lb)	Static Coefficient of Friction
1	40.2	14.5	0.36
1	40.2	14.5	0.36
1	40.2	11.5	0.29
1	80.4	30	0.37
1	80.4	30	0.37
1	80.4	31.5	0.39
1	145	60	0.41
1	190	70	0.37
2	40.2	14	0.35
2	40.2	12	0.30
2	40.2	14	0.35
2	80.4	29	0.36
2	80.4	30	0.37
2	80.4	29	0.36
2	145	57	0.39
2	190	72	0.38

Average Static Coefficient of Friction = 0.37

*Direction of horizontal load for Location 1 was against the grain of the textured finish of the concrete surface.

Direction of horizontal load for Location 2 was with the grain of the concrete surface textured finish.

REFERENCES

1. Fertal, Martin J., Analysis of Fiber Reinforced Mat System for Rapid Runway Repair, BDM/MCL-86-0035-TR, The BDM Corporation, McLean, Virginia, 1986.

2. Measurements Group, "Strain Gage Installation and Protection in Field Environments," Instruction Bulletin TT-607, 1983.

3. Measurements Group, "Surface Preparation for Strain Gage Bonding," Instruction Bulletin B-129-4, 1976.

4. Measurements Group, "Strain Gage Applications with M-Bond AE-10115 and M-Bond GA-2 Adhesive Systems," Instruction Bulletin B-137-11, 1979.

5. Measurements Group, "M-Coat F Application Instruction," Instruction Bulletin B-134-1, 1978

6. Measurements Group, "Strain Gage Selection: Criteria, Procedures, Recommendations," Technical Note TN-505, 1983.

7. Draft Letter Report from LAW Engineering, Phase II Mat Material Testing, May, 1988.

8. ADINA - A Finite Element Program for Automatic Dymnamic Incremental Nonlinear Analysis, Report AE 84-1, ADINA Engineering, December 1984.

9. ADINA-IN - A Program for Generating Input Data Using ADINA, Report AE 84-4, ADINA Engineering, December 1984.

10. ADINA-PLOT - A Program for Display of Input and Output Data Using ADINA, Report AE-84-3, ADINA Engineering, December 1984.

11. Kapur, K. C. and Lamberson, L.R., Reliability in Engineering Design, John Wiley and Sons, NY, 1977.

INITIAL DISTRIBUTION LIST

HQ USAF/LEE	1	HQ USCENTAF/LGDE	1
HQ USAF/LEEX	1	AD/YQ	1
HQ USAF/XOORB	1	AD/AFATL/DL (TECH LIB)	1
HQ AFESC/DEO	1	AFWL/NTE	1
HQ AFESC/TST (LIBRARY)	1	AFWAL/FIES/CDIC	1
HQ AFESC/RDC/RDCP	1	AFWAL/FIEM	1
HQ PACAF/DEO	1	DTIC/DDA	1
HQ PACAF/DOUP	1	USAFTAWC/TC	2
HQ TAC/DED	1	USA CORPS OF ENG SCHOOL/ATZA-CDO	1
HQ TAC/DRP	1	WATERWAYS EXPERIMENT STATION/GF	1
1HQ TAC/DEMM	1	20 NAVAL CONST REGIMENT 20NCR/R24	1
HQ USAFE/DEM/DES	1	COMCBLANT	1
SAF/AQPN	1	USN CIV ENG LAB/L03AB	1